

AD-A031 950

FRANKLIN INST RESEARCH LABS PHILADELPHIA PA

F/G 13/9

DEVELOPMENT OF COMPLIANT-MOUNTED GAS-BEARINGS FOR A SMALL HIGH---ETC(U)

SEP 76 W SHAPIRO, R COLSHER

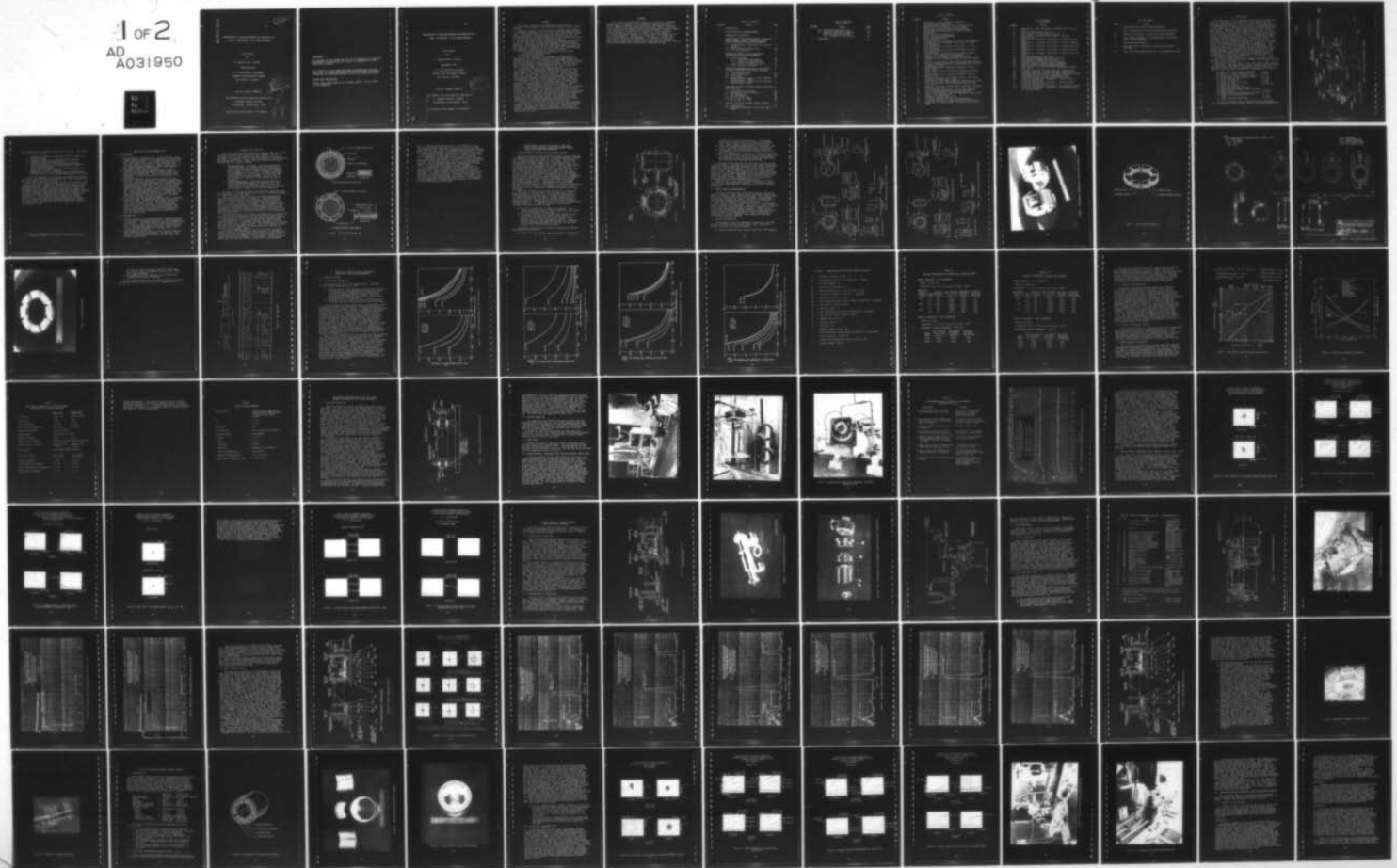
DAAK02-72-C-0571

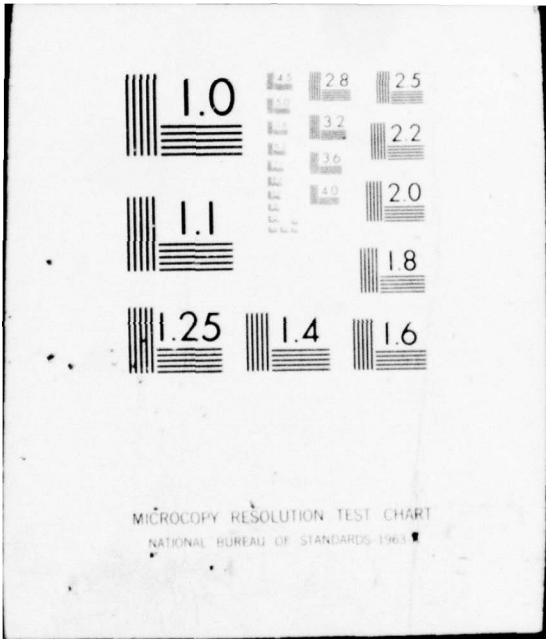
UNCLASSIFIED

FIRL-I-C3425

NL

1 of 2
AD
A031950





MICROCOPY RESOLUTION TEST CHART
NATIONAL BUREAU OF STANDARDS-1963-A

ADA031950

12

AD

DEVELOPMENT OF COMPLIANT-MOUNTED GAS-BEARINGS FOR
A SMALL, HIGH-SPEED, 10 KW TURBOALTERNATOR

Final Report

By

W. Shapiro and R. Colsher

September 1976

U. S. Army Mobility Equipment
Research and Development Command
Fort Belvoir, Virginia

Contract DAAK02-72-~~C~~0571

The Franklin Institute Research Laboratories
Benjamin Franklin Parkway
Philadelphia, Pennsylvania 19103

Distribution of This Report is Unlimited

R D D C
RECEIVED
NOV 12 1976

Handwritten signatures and date: 11/17/76

DISCLAIMER

The findings in this report are not to be construed as an official Department of the Army position, unless so designated by other authorized documents.

The citation of trade names and names of manufacturers in this report are not to be construed as official Government indorsement or approval of commerical products or services referenced herein.

DISPOSITION INSTRUCTIONS

Destroy this report when it is no longer needed. Do not return to the originator.

AD

DEVELOPMENT OF COMPLIANT-MOUNTED GAS-BEARINGS FOR
A SMALL, HIGH-SPEED, 10 KW TURBOALTERNATOR

Final Report

By

W. Shapiro and R. Colsher

September 1976

U. S. Army Mobility Equipment
Research and Development Command
Fort Belvoir, Virginia

Contract DAAK02-72-~~C~~-0571

The Franklin Institute Research Laboratories
Benjamin Franklin Parkway
Philadelphia, Pennsylvania 19103

Distribution of This Report is Unlimited

DDC
RECEIVED
NOV 12 1976
RECEIVED
C

ADD TO FILE	
NTIS	<input checked="" type="checkbox"/>
ERIC	<input type="checkbox"/>
EDRS	<input type="checkbox"/>
ADDITIONAL	
BY	
DATE	
A	

SUMMARY

This report describes the design and test of an air-lubricated rotor-bearing system for small turbo-alternator applications.

Compliant-mounted journal and thrust bearings were analyzed and designed to support a 12 lb, 93,500 rpm 10 KW turboalternator rotor. Slow-speed component tests were conducted at FIRL. Lift-off was achieved at low speed (400 rpm) and high load (5 psi). At least 40 start-stops were completed on each bearing with negligible starting torque, and no evidence of wear.

A test rig that closely simulated the geometry of an actual 10 KW rotor was built by the Solar Division of International Harvester. Simulator testing was conducted at Solar's facility. Four tests were attempted but sustained high-speed operation was not achieved. Failure occurred at the wheel end journal bearing. The failure was traceable to two potential causes:

- 1) Inadvertant blockage of cooling-air to the region by an instrumentation tube
- 2) Possible rotor whirl.

The journal bearings were redesigned to improve whirl characteristics, facilitate installation and manufacture and improve the ability of the bearings to accommodate thermal distortions produced by viscous heat generation. The major revisions were incorporation of a beam spring to support the top shoe of the journal bearings, and modifications of the elastomer geometry to reduce the pitch restraint of the pads.

In addition a high-speed component test rig was built by FIRL, whose rotor resembled that of the Solar simulator. The maximum speed of the unit was 76,000 rpm and the new bearings were tested to this speed without incident. Smooth operation ensued and maximum orbit sizes were approximately 0.0005 inches. The originally designed bearings were also tested at FIRL and subsynchronous rotor whirl was evidenced at about 65,000 rpm.

Subsequent testing of the spring-mounted, compliant-pivot bearings were accomplished on the Solar simulator. Sustained operation, in which thermal equilibrium was reached, was achieved at approximately 62,000 rpm. In attempting to accelerate beyond this speed a wheel-end journal bearing failure occurred. The data did not suggest any bearing induced reasons for the failure. It is believed that the built-up Solar rotor experienced a mass shift due to thermal gradients that caused high unbalance. Even though large excursions of the shaft occurred (> 0.020 inches) the only damage was rubbing to the wheel-end journal bearing and rotor, demonstrating the capability of the spring-mount design to withstand large shock and vibrations.

Since speeds up to 76,000 rpm were realized during bearing testing, without any evidence of difficulty, the spring-mounted compliant bearings show definite promise for high-speed turbo-machinery applications. Further development is required to qualify the 10 KW gas-bearing turboalternator for an operating speed of 93,500 rpm.

FOREWORD

This report was prepared for the U.S. Army Mobility Equipment Research and Development Command (MERADCOM) under Contract No. DAAK02-72-0571 by members of the Mechanical Engineering Laboratory of The Franklin Institute Research Laboratories (FIRL). Technical data provided by the Solar Division of International Harvester Company under Subcontract No. 24839 are included. W. Shapiro acted as program manager for FIRL, and R. Colsher as project engineer. L. Blinman was project manager for Solar, and T. Psychogios was the Solar lead engineer. Messers D. D. Faehn and F. D. Jordan were the technical monitors for MERADCOM. F. Kramberger of FIRL was principally involved with manufacture and test of the bearings at FIRL, and for providing consultation at Solar during simulator testing. Theoretical support was provided by M. Jaskowiak of FIRL.

TABLE OF CONTENTS

<u>SECTION</u>	<u>TITLE</u>	<u>PAGE</u>
1	INTRODUCTION	1
2	CONCLUSIONS AND RECOMMENDATIONS	4
3	BEARING TYPE SELECTION	5
4	DESCRIPTION OF THE SPRING-MOUNTED, COMPLIANT-PIVOT JOURNAL BEARING, COMPLIANT-MOUNTED THRUST BEARING AND ROTOR CONFIGURATION	8
	4.1 Spring-Mounted, Compliant-Pivot Journal Bearing	8
	4.2 Thrust Bearing Configuration	10
	4.3 Rotor Configuration	10
5	JOURNAL AND THRUST BEARING ANALYTICAL PERFORMANCE AND DESIGN PARAMETERS	19
	5.1 Journal Bearings	19
	5.1.1 Fluid-Film Performance	19
	5.1.2 Stability Considerations	27
	5.1.3 Design of Compliant Mounts	27
	5.2 Thrust Bearing Performance	27
6	HIGH-SPEED COMPONENT TESTING OF THE SPRING-MOUNTED, COMPLIANT-PIVOT JOURNAL BEARINGS	33
	6.1 FIRL High-Speed Rig	33
	6.2 Initial Check-out	35
	6.3 Start-Stops	35
	6.4 Spring-Mounted, Compliant-Pivot Bearing Testing (April, 1976)	35
	6.5 Spring-Mounted, Compliant-Pivot Bearing Testing (July, 1976)	41
7	SIMULATOR TESTING OF SPRING-MOUNTED COMPLIANT-PIVOT BEARINGS	49
	7.1 Description of Test Rig	49
	7.2 Description of Installation	49
	7.3 Instrumentation	59
	7.4 Initial Check-out	59
	7.5 Run 1 (May 18, 1976)	59
	7.6 Run 2 (May 19, 1976)	60
8	ORIGINAL COMPLIANT MOUNTED JOURNAL BEARING	73
	8.1 Configuration	73
	8.2 High-Speed Component Rig Testing (April, 1976)	73

TABLE OF CONTENTS
(continued)

<u>SECTION</u>	<u>TITLE</u>	<u>PAGE</u>
8.3	Slow-Speed Component Tests	77
8.4	Simulator Testing of Original Compliant-Mounted Bearings	84
	8.4.1 Summary of Test Results	84
9	REFERENCES	92

LIST OF FIGURES

<u>Number</u>	<u>Title</u>
1	Gas-Bearing, Turbo-alternator Simulator
2	Compliant-Mounted Bearings
3	Spring-Mounted, Compliant-Pivot Journal Bearing
4	Wheel-End Journal Bearing, Design Drawing
5	Starter-End Journal Bearing, Design Drawing
6	Spring-Mounted, Compliant-Pivot Journal Bearing Assemblies
7	Thrust Bearing Configuration
8	Thrust Bearing Design Drawings
9	Thrust Bearing Assembly
10	Rotor Dimensions
11	Tilting-Pad Load Coefficient vs. Pivot Film Thickness
12	Tilting-Pad Friction Moment Coefficient vs. Pivot Film Thickness
13	Tilting-Pad Pitch Stiffness Coefficient vs. Pivot Film Thickness
14	Tilting-Pad Radial Stiffness Coefficient vs. Pivot Film Thickness
15	Stability Map, Compliant-Mounted Journal Bearing
16	Thrust Bearing Theoretical Performance
17	Schematic of High-Speed Gas Bearing Test Rig
18	Overview of FIRL, High-Speed Test Rig with Instrumentation
19	Close-up of High-Speed, Gas Bearing Component Test Rig
20	Journal Bearing Installation, High-Speed, Gas-Bearing Component Test Rig
21	Thermocouple Data - High-Speed Component Testing - April, 1976
22	Typical Shaft Orbits, High-Speed Component Testing - April, 1976
23	Frequency Spectrum, High-Speed Component Testing, April, 1976
24	Frequency Spectrum, Low Frequency Range, High-Speed Component Testing, April, 1976
25	Shaft Orbits, High-Speed Component Testing, July, 1976
26	Frequency Spectrum, High-Speed Component Testing, July, 1976
27	Frequency Spectrum, Reduced Range, High-Speed Component Testing, July, 1976
28	Solar Simulator Crosssection and Cooling Passages
29	Solar 10 KW Simulator Rotor and Gas Bearings
30	Solar 10 KW Simulator, Housing Components, Capacitance Probes and Thermocouples
31	Schematic of Solar Test Loops
32	10 KW Gas Bearing Test Rig, Instrumentation
33	10 KW Gas Bearing Test Rig, Test Cell Installation
34	Amplitude vs. Start-up Speed, Simulator Test, May 18, 1976

LIST OF FIGURES
(continued)

<u>Number</u>	<u>Title</u>
35	Amplitude vs. Shut-down Speed, Simulator Test, May 18, 1976
36	Recorded Temperatures, Run No. 1
37	Orbit Traces, 10 KW Simulator Testing
38	Amplitude vs. Frequency, Data Point 4, Outboard Vertical Probe
39	Amplitude vs. Frequency, Data Point 4, Middle Vertical Probe
40	Amplitude vs. Frequency, Data Point 4, Inboard Vertical Probe
41	Amplitude vs. Frequency, Data Point 5, Outboard Vertical Probe
42	Amplitude vs. Frequency, Data Point 5, Middle Vertical Probe
43	Amplitude vs. Frequency, Data Point 5, Inboard Vertical Probe
44	Recorded Temperatures, Run No. 2
45	Photograph of Damaged Aft Journal Bearing
46	Photograph of Damaged Shaft Section
47	Configuration of Original Journal Bearing
48	Compliant Mounted Journal Bearing Components
49	Compliant Mounted Journal Bearing Assembly
50	Orbit Traces - Original Bearings, High-Speed Component Test Rig
51	Frequency Spectrum, Original Bearings, Inboard End
52	Frequency Spectrum, Original Bearings, Outboard End
53	Frequency Spectrum, Original Bearings, Horizontal Probes
54	Slow-Speed Journal Bearing, Component Test Rig
55	Slow-Speed Thrust Bearing Component Test Rig
56	10 KW Gas Bearing Rig - Teardown 1 - Thrust Bearing Failure, Aft Bearing
57	10 KW Gas Bearing Rig - Teardown 1, Thrust Bearing Failure, Forward Bearing
58	10 KW Gas Bearing Rig - Teardown 3, Aft Bearing Journal
59	10 KW Gas Bearing Rig - Teardown 3, Thrust Bearing and Aft Radial Bearing

LIST OF TABLES

<u>Number</u>	<u>Title</u>
I	Nomenclature for Journal Bearing Analysis
II	Computed Performance of Starter-End Journal Bearings
III	Computed Performance of Wheel-End Journal Bearings
IV	Final Design Parameters of Spring-Mounted, Compliant-Pivot Journal Bearings
V	Thrust Bearing Geometry
VI	Instrumentation, High-Speed, Gas-Bearing Component Test Rig
VII	Solar 10 KW Gas Bearing Test Rig - Instrumentation List

1. INTRODUCTION

The application of air bearings to high-speed turbomachinery offers the potential of increased life and mean time between overhauls, elimination of a lube-oil system, reduced drag and high temperature capability. The purpose of the program described in this report was to fabricate and test an air-lubricated main rotor-bearing system for typical small military turbo-alternator applications. The Army 10 KW turboalternator, built by the Solar Division of International Harvester was the unit to which the gas bearings were applied. Figure 1 is the basic configuration of the rotor-bearing system. It is a cross-section of the simulator built by Solar and closely resembles the actual 10 KW, gas-turbine driven ball-bearing unit. For purposes of the simulator, the gas turbine was replaced by an air turbine drive, and a dummy wheel was used to simulate the compressor. As shown on Fig. 1 the turbine and compressor are overhung at the aft end of the unit in the conventional back to back manner. The simulated alternator rotor assembly is supported between the two journal bearings. The double acting thrust bearing is located between the aft journal bearing and the alternator rotor. At the starter or forward end of the unit are located labyrinth sealed chambers that can be pressurized to apply thrust loads to the rotor in either direction.

To enable assembly, the rotor is made in several sections, joined by curvic couplings and held together with tie-bolts through the mid-axis of the rotor.

The journal bearing diameters were dictated by rotor dynamic considerations. They were sized so that the first bending critical would be at least 20% above the operating speed of the unit. Pertinent specifications and geometric parameters are as follows:

- Wheel end journal bearing diameter = 1.8 in
- Wheel end journal bearing length = 1.8 in
- Starter end journal bearing diameter = 1.4 in
- Starter end journal bearing length = 1.4 in
- Thrust bearing O.D. = 3.0 in
- Thrust bearing I.D. = 2.0 in
- Weight of rotating assembly = 13 lbs
- Operating speed = 93,500 rpm
- Lubricant = ambient air
- Life = 10,000 hours (minimum)
- Number of start-stops = 3000 (minimum)
- Bearing span = 9.92 in
- Wheel end journal bearing static load = 8.6 lbs
- Starter end journal bearing static load = 3.4 lbs
- Thrust bearing normal load = 10 lbs

The overall program that was conducted can be separated into a number of distinct phases, some of which were designed and

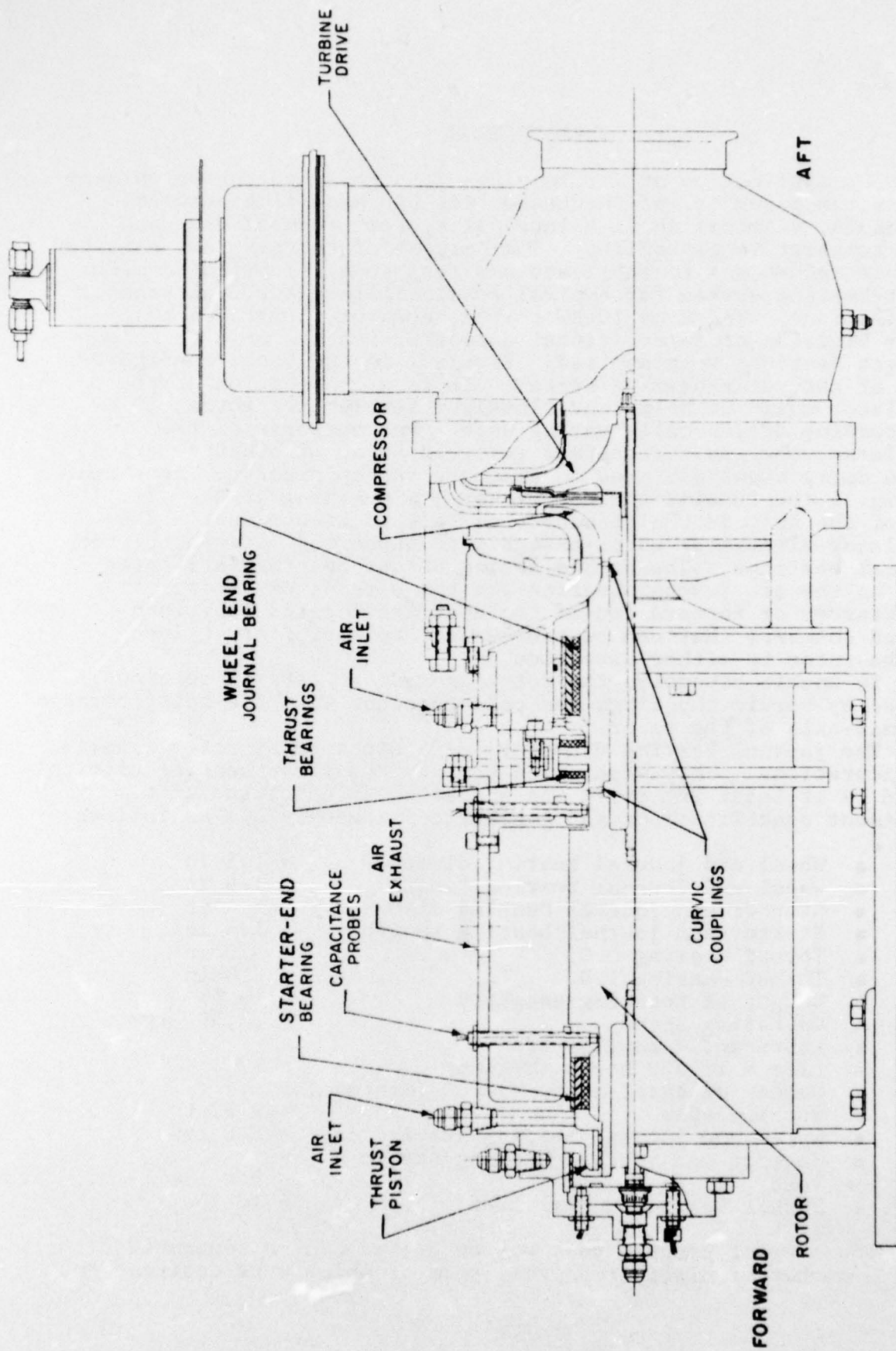


Figure 1. Gas-Bearing, Turbo-alternator Simulator

some of which were dictated by the course of events. The phases are identified as follows:

1. Analysis and design of compliant-mounted journal and thrust bearings
2. Component testing of compliant-mounted bearings
3. Simulator design and manufacture
4. Simulator testing of compliant-mounted bearings
5. Design and manufacture of spring-mounted, compliant-pivot journal bearings
6. High-speed component testing of spring-mounted, compliant pivot journal bearings
7. Simulator testing of spring-mounted, compliant-pivot journal bearings, and compliant-mounted thrust bearings.

Solar's involvement in the program was primarily concerned with the design and construction of the full scale simulator and the testing done with this simulator.

The order of discussion of these phases is by priority with respect to the final results of the program and thus is not in chronological order. Emphasis is placed on the spring-mounted compliant bearings, because they were the most successful and recommended type for this high-speed application. Results of the pure compliant-mounted bearings which were originally designed have been previously reported upon in the Interim Report (1)*. Information was also published by the Society of Automotive Engineers (2). In this final report, some of the testing done on the original compliant mounted bearings is discussed, but the analysis, theoretical performance and design aspects have been omitted because they have been adequately covered in the references cited.

* Parenthetic numerals designate references in Section 9.

2. CONCLUSIONS AND RECOMMENDATIONS

2.1 CONCLUSIONS

- Spring-mounted, compliant-pivot journal bearings demonstrated definite potential for application to small high-speed turboalternators. In an FIRL high-speed bearing rig, rotor speeds of 76,000 rpm were achieved with excellent bearing performance. Higher speeds could not be attained because maximum capacity of the impulse air-turbine drive had been reached.
- Compliant mounted thrust bearings proved entirely satisfactory through the highest speeds to which they were tested (65,000 rpm). Initial difficulties were traceable to improper mounting of the bearings in the simulator.
- Full-speed operation on the Solar simulator was not achieved. The most successful running was accomplished with the spring-mounted bearings with an operating speed of approximately 65,000 rpm. Test data did not reveal impending bearing difficulties. It is speculated that thermal heating of the rotor resulted in a mass shift that caused a high unbalance that precipitated the failure. The bearing exhibited ability to accommodate large rotor excursions because when failure occurred rotor vibrations exceeded 0.020 inches, and only the wheel-end journal bearing sustained damage.
- Some start-stop performance was accomplished by component testing at FIRL. Break-away torques were negligible under unit loads of 5 psi for the journal bearing and 7 psi for the thrust bearing. These loadings are considered heavy for gas-bearing start-up conditions. After 40 start-stop cycles with loaded bearings, the wear of pad surfaces was negligible indicating that the selected material combination can be expected to meet the design goal.

2.2 RECOMMENDATIONS

- Further testing of the spring-mounted, compliant bearing is recommended to qualify them for full speed operation (93,500 rpm). The FIRL high-speed rig drive system should be modified to enable full speed journal bearing operation. The rig should also be revised to permit installation of the double-sided thrust bearing used in the turboalternator simulator.
- Investigation into the precise reason for the simulator test failure should be continued. Specifically, the effects of axial thermal gradients on rotor mass shift should be determined.

3. BEARING TYPE SELECTION

The 10 KW turboalternator requires a bearing that can operate at ultra-high speeds with relatively light loading. To our knowledge, the 1.8 inch diameter journal running at 93,500 rpm represents the highest surface speed requirements of any documented gas-bearing application. These conditions impose two serious problems for the journal bearings:

1. Whirl Stability - High speed, low-load operation is a condition that can readily excite subsynchronous whirl of gas-bearing supported rotors. Hydrodynamic gas bearings are prone to whirl instability because of low damping of the gas-film. The most successful counter-measure to the prevention of whirl has been the tilting-pad journal bearing. Thus, for the 10 KW application, some type of tilting-pad bearing is essential.
2. Thermal Distortions - High speed viscous shearing of the fluid-film can generate significant heat, even though a gas film is employed. Thus, the bearing configuration should have breathing ability to accommodate geometric changes due to thermal expansions.

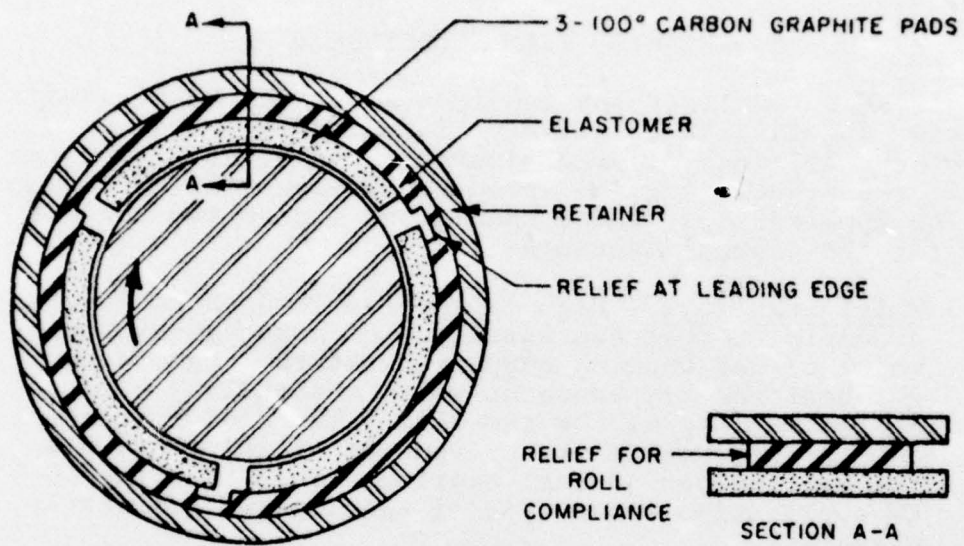
In addition, the bearing must have good life characteristics and ruggedness since one application of the 10 KW turboalternator is as portable army field unit.

After screening several candidate bearing configurations, compliant-mounted bearings were selected. Compliant-mounted journal and thrust bearings are schematically represented in Figure 2. They consist of rigid pads mounted on a compliant substrate which is usually an elastomer. The deformation properties of the elastomer permit the separate pads to pitch so that the necessary converging wedge for hydrodynamic lubrication is automatically formed by rotation of the journal or thrust runner. They behave similarly to tilting-pad bearings in this respect and thus are whirl free.

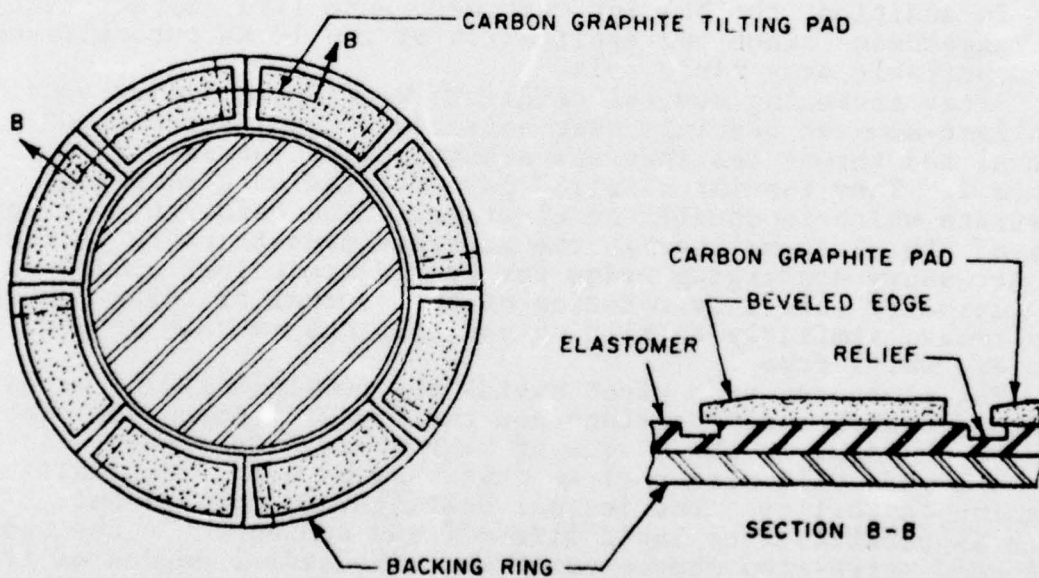
The elastomer type pivot avoids the complexities of mechanical ball and socket configurations and the fretting corrosion problems which occur in the pivots of high-speed tilting-pad bearings.

The pads will also roll so that they have inherent self-aligning capability. The journal bearings can move radially which is beneficial to rapid lift-off and consequently the bearings have good start-stop characteristics. The radial degree of freedom also helps in flushing out trapped particles that may be lodged in the clearance region.

The thrust bearing pads can pitch so that the converging wedge necessary for hydrodynamic film generation is automatically formed. The pads can also move axially and this ability assists in equalizing the load among the several pads. If one pad is loaded more than its neighbors, it will deflect axially a greater amount and the load will then be transmitted to the adjacent



a) Compliant Mounted Journal Bearing



b) Compliant Mounted Thrust Bearing

Figure 2. Compliant Mounted Bearings

pads. For high speed applications, it is essential to use separate pads since they will not thermally distort as much as a complete disc. Thus, the compliant-mounted thrust bearing offers all the advantages of the common self-equalized, tilting-pad bearings without their complexity and length requirements.

The inherent damping capabilities of compliant pads offer another advantage as they help suppress rotor vibrations.

Temperature limitations of the elastomers are the most restricting factor with respect to the use of compliant-mounted bearings. Prior experience with similar 10 KW ball-bearing units is that the bearing compartment temperatures are below 200°F, and thus within the range of most elastomers.

It is important to recognize that the coefficient of thermal expansion of an elastomer is approximately 10 times that of steel. Thus, from pure considerations of thermal expansion, the tendency would be for the pads to clamp against the shaft. As long as the film stiffness exceeds that of the elastomer or other pad mounting, this danger is avoided, and the pitch roll and radial motion capabilities of the elastomer are very beneficial in permitting the bearing to accommodate thermal expansions and distortions.

4. DESCRIPTION OF THE SPRING-MOUNTED, COMPLIANT-PIVOT JOURNAL BEARING, COMPLIANT-MOUNTED THRUST BEARING AND ROTOR CONFIGURATION

4.1 SPRING-MOUNTED, COMPLIANT-PIVOT JOURNAL BEARING

The final design of the compliantly mounted journal bearings is schematically shown on Figure 3. A bearing assembly consists of a bearing retainer and three 100° arc pads. The pads are made of carbon-graphite bonded to a steel outer shell. The pad material is a dense carbon with a lubricating binder. It is manufactured by Pure Carbon Corp. of St. Mary's, Pennsylvania; the carbon material designation is P6452. This material demonstrated excellent start-stop and high-speed rub characteristics over the course of this project. Note that the top shoe of the latest configuration is mounted to a beam spring. In the original version of the bearing, all pads were solidly mounted to the bearing shell. The uncertainties of the expansion and stiffness values of the neoprene elastomer of the original configuration were thought to have caused some difficulties experienced during testing. The spring allows centrifugal and thermal expansions to be accommodated in a predictable and well-controlled manner. The spring also alleviates manufacture of close tolerance installation clearances which was a major disadvantage of the completely contained pad design previously employed.

Note that between the elastomer and the pad a corrugated heat exchanger is incorporated. Air flowing through this exchanger removes the heat of viscous friction and precludes it from overheating the elastomer. Thermal computations as presented in References (1) and (2) dictated the necessity of the heat exchanger. Bearing design was based upon two major considerations: (1) preventing rotor whirl and (2) accommodating thermal expansions. To improve stability the following rationale went into the final design:

- The pitch inertia of the pads was minimized. The bearing pads were made as light as possible, especially at the leading and trailing edges.
- The pitch stiffness of the rubber was reduced as much as possible to allow the pads to pitch freely. A design goal for the pitch stiffness of the rubber was 1/5 to 1/10 of the film pitch stiffness. The angular extent of the elastomer was kept to a minimum and the elastomer thickness was selected so that the proper radial stiffness was obtained.

The thermal criteria was satisfied by applying the following concepts to the design:

- One of the three bearing pads incorporated a mechanical

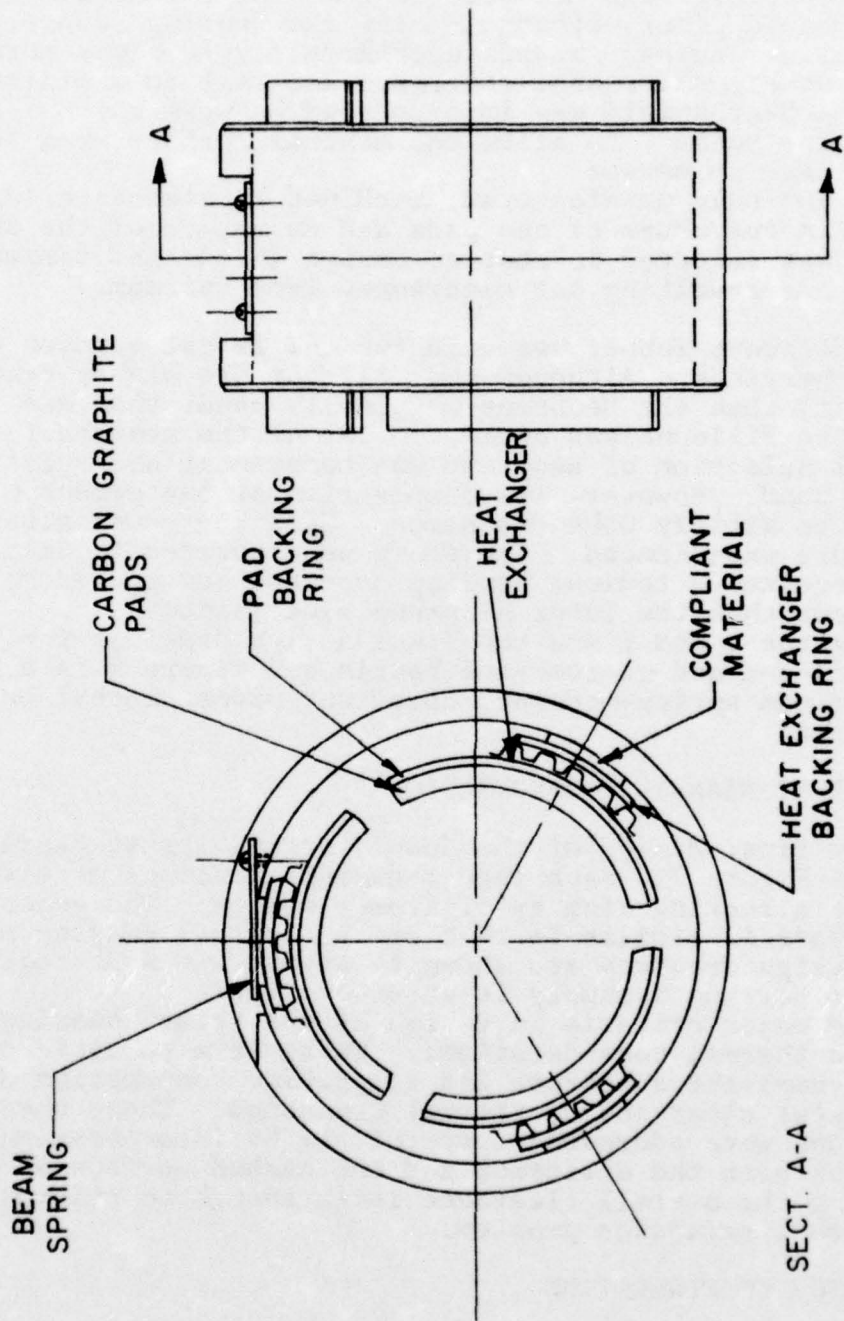


Figure 3. Spring-Mounted Compliant-Pivot Journal Bearing

- spring with a "soft" spring constant. The spring stiffness was selected so that large thermal growth could occur without loading the bearing severely.
- Since rubber expands approximately 10 times more than steel, the rubber thickness was kept to a minimum.
 - A heat shield was incorporated between the pad and the rubber, to allow the maximum surface area for the heat to escape.
 - The cold manufactured, machined in clearance (difference in curvature of the pads and curvature of the shaft) was selected so that at design speeds and temperatures the resulting hot clearances were optimum.

A Silicone rubber was used for the latest version of the journal bearings. Although the Silicone has higher temperature capability than the Neoprene originally used, that was not the reason the Silicone was applied. One of the reasons for the original selection of Neoprene was because it was relatively easy to bond. However, the composition of the cement had been changed to satisfy OSHA standards. With the newer glue erratic bonds were experienced. Therefore we converted to Silicone, which requires a tedious bonding process, but proved more consistent than the later Neoprene glue joints.

Figures 4 and 5 are the final design drawings for both the wheel-end and starter-end bearings. Figure 6 is a photograph of the spring-mounted, compliant-pivot journal bearing assemblies.

4.2 THRUST BEARING CONFIGURATION

The final design of the double acting thrust bearing is shown in Figure 7. Each thrust element consists of eight pads fixed to a backing ring by elastomer mounts. The construction of the pads is similar to that of the journal bearing pads. Final design drawings are shown in Figure 8. A photograph of a thrust bearing assembly is shown on Figure 9.

The major criteria in design of the thrust bearings were based on thermal considerations. These were to avoid overheating of the compliant substrate and to prevent consumption of the total axial clearance by thermal expansion. These thermal conditions were addressed respectively by incorporating a heat shield between the elastomer and the carbon surface and by selecting the overall clearance large enough to eliminate the thermal expansion problem.

4.3 ROTOR CONFIGURATION

The simulator rotor was designed to incorporate the same overall dimensions as the actual 10 KW rotor. The major features of this rotor are as follows:

- Bearing diameters were sized so that the first bending

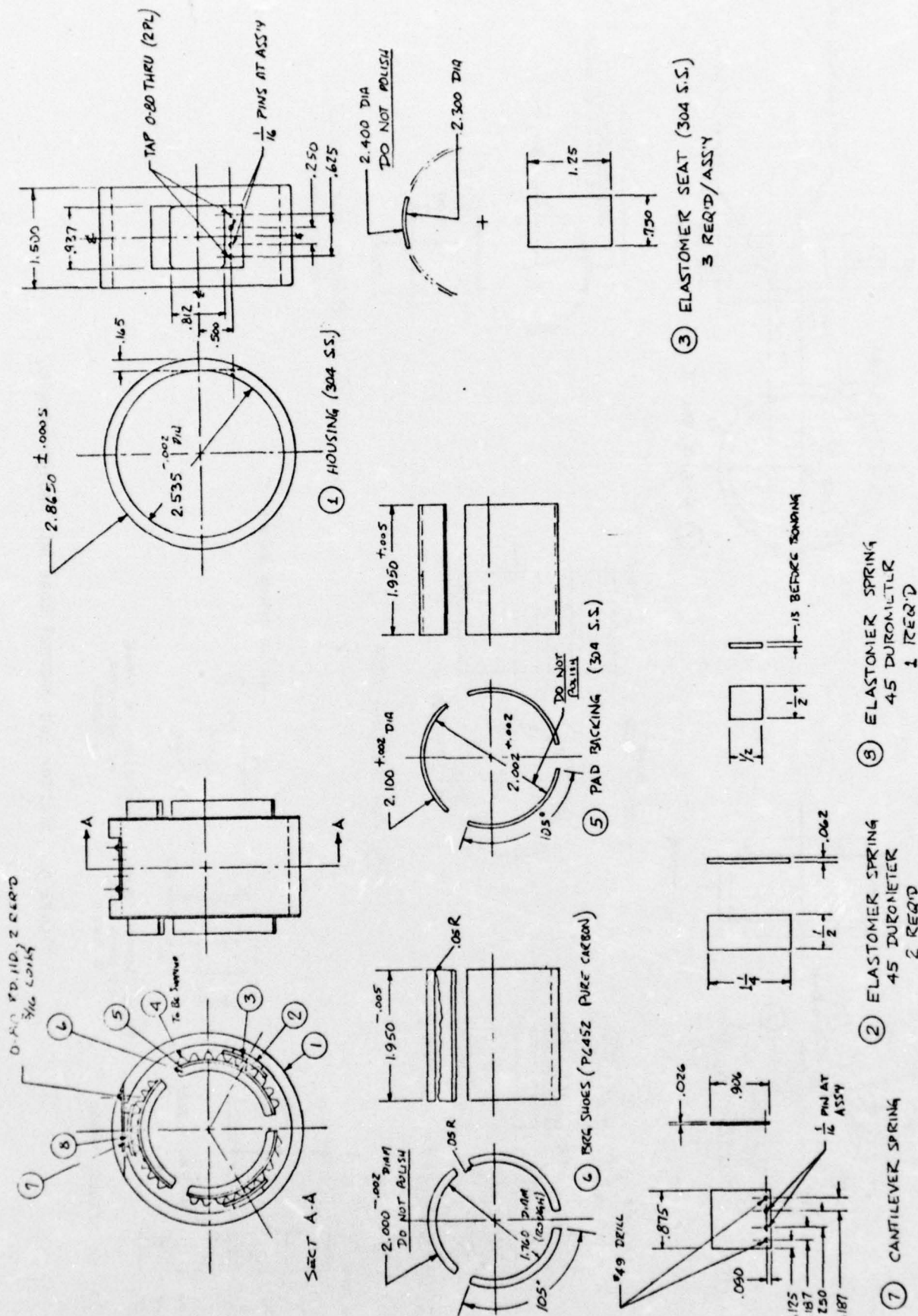
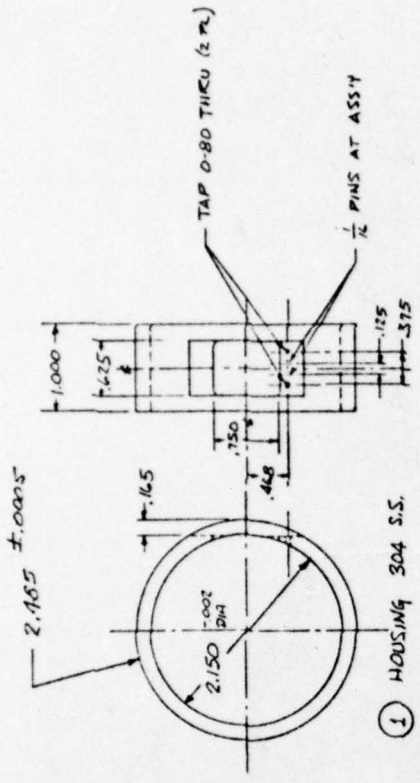
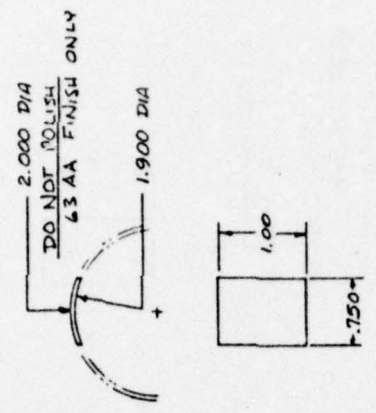


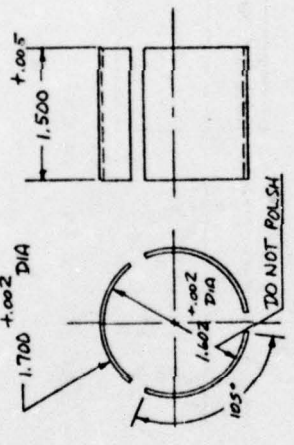
Figure 4. Wheel End Journal Bearing, Design Drawing



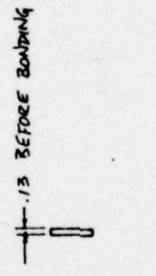
① HOUSING 304 S.S.



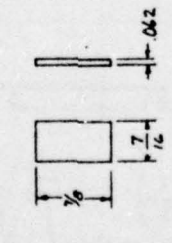
③ ELASTOMER SEAT (304 S.S.)
3 REQ'D/ASSY



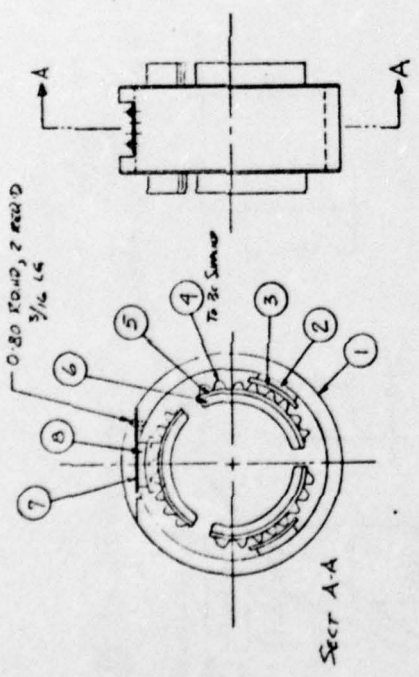
⑤ PAD BACKING (304 S.S.)



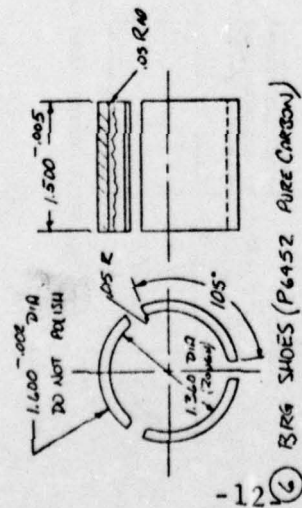
⑧ ELASTOMER SPRING
45 DURCHMETER
1 REQ'D



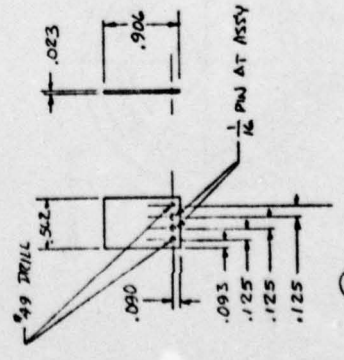
② ELASTOMER SPRING
45 DURCHMETER
2 REQ'D



SECT A-A



④ BRG SHOES (P6452 PURE CARBON)



⑦ CANTILEVER SPRING

Figure 5. Starter End Journal Bearing, Design Drawing

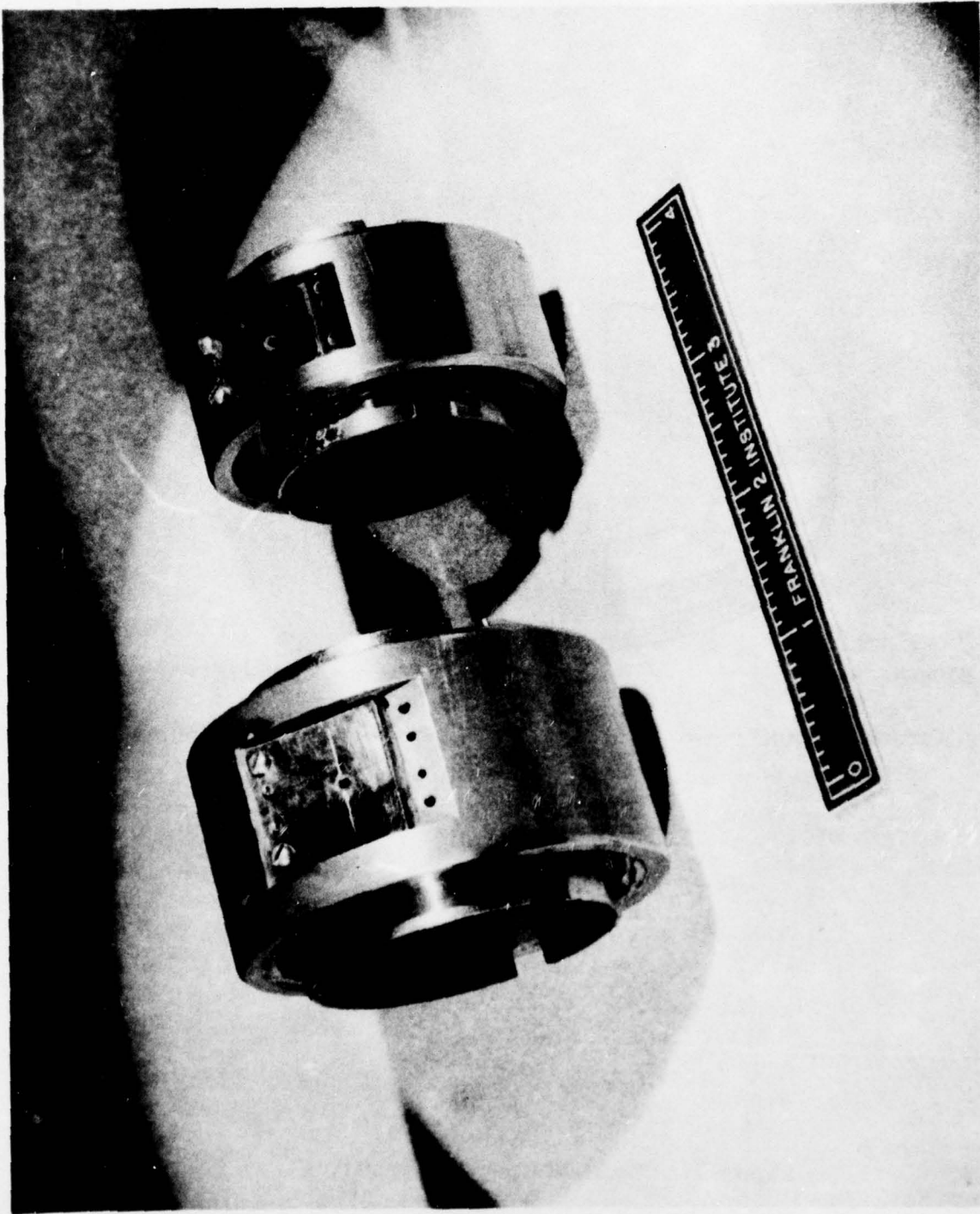


Figure 6. Spring-Mounted, Compliant-Pivot Journal Bearing Assemblies

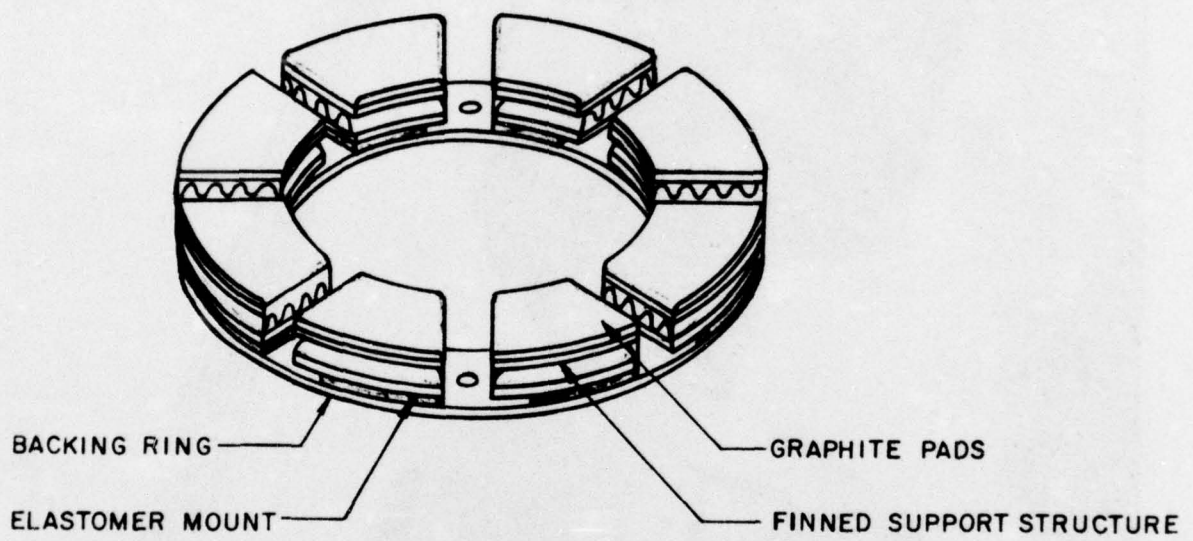


Figure 7. Thrust Bearing Configuration

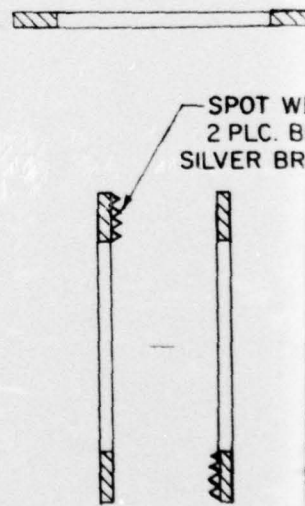
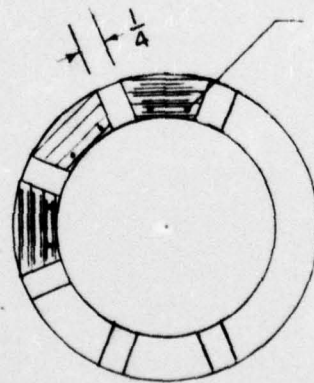
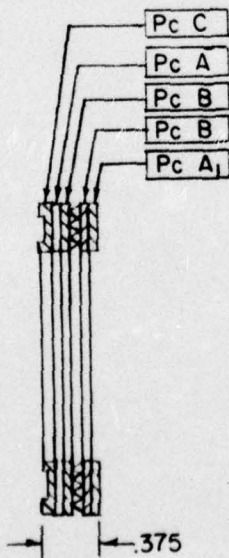
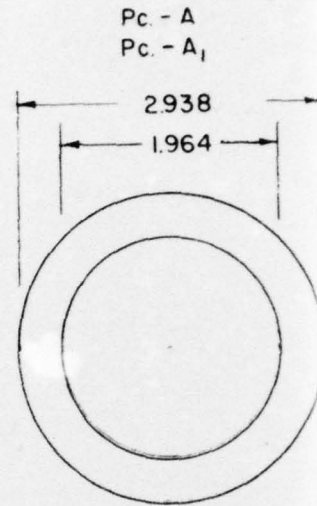
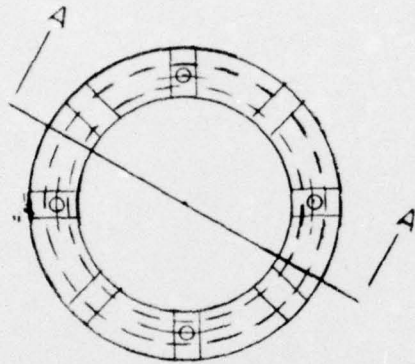
NOTE :

USE CORBORUNDUM TYPE GRINDING WHEEL TO GRIND CARBON

I.D. - C - 46 - L4VGC

O.D. - C - 60 - 34VE

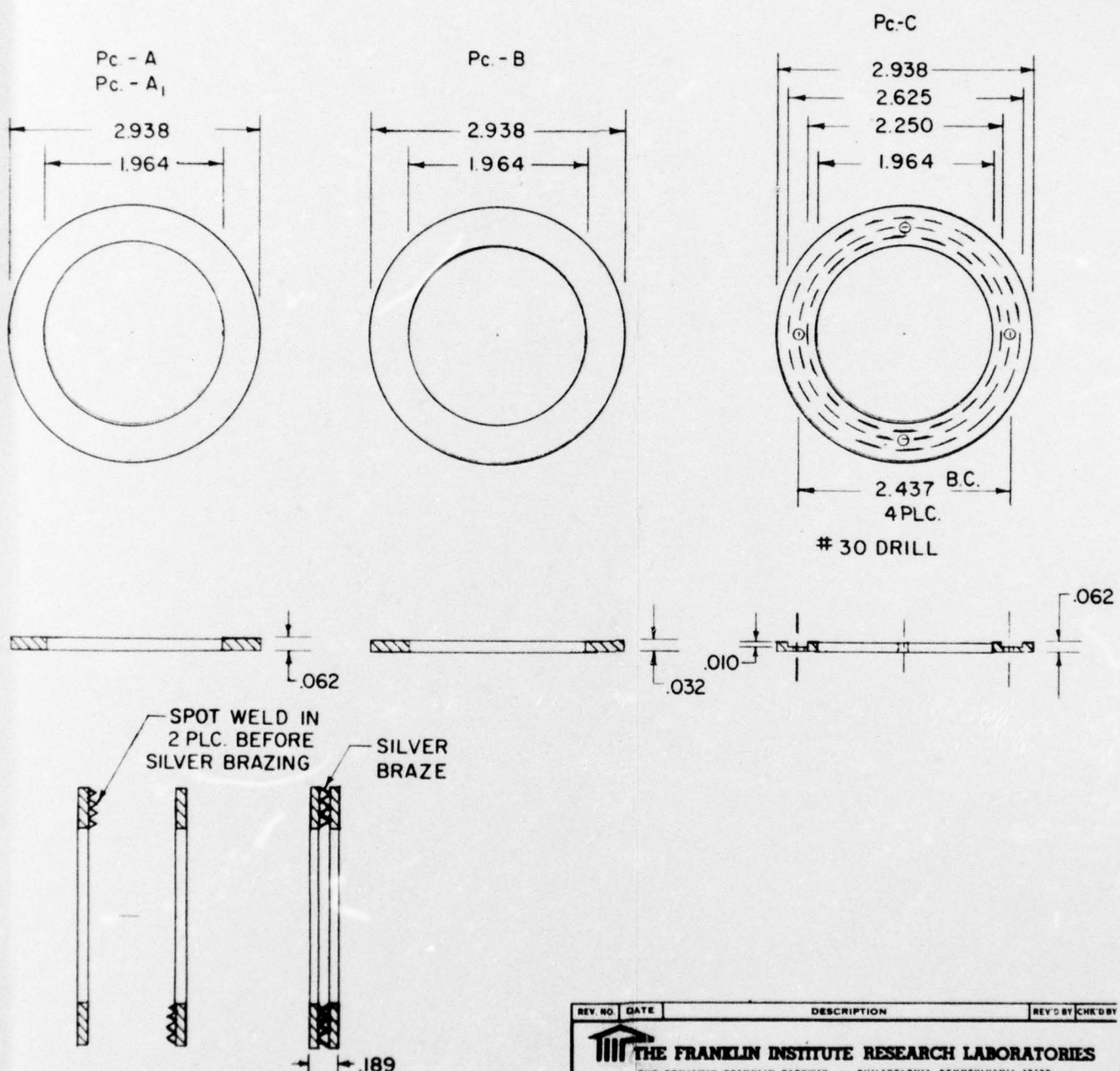
6000 F.P.M.



HEAT SHIELD
FINISH TO SIZE AF

D CARBON

- 1 - Pc. A - ELASTOMER
- 1 - Pc. A₁ - CARBON GRADE 6452
- 2 - Pc. B - 304 STAINLESS STEEL
- 1 - Pc. C - 304 STAINLESS STEEL



HEAT SHIELD
FINISH TO SIZE AFTER BRAZING


REV. NO.	DATE	DESCRIPTION	REV'D BY	CHEK'D BY
 THE FRANKLIN INSTITUTE RESEARCH LABORATORIES THE BENJAMIN FRANKLIN PARKWAY • PHILADELPHIA, PENNSYLVANIA 19103				
TITLE 32G - C 3425 - 01				
TOLERANCES UNLESS OTHERWISE NOTED DIM. 0.00" ± .01 DIM. 0.000" ± .002 PRACTICAL DIM. ± 1/64 ANGLES ± 30'		DRAWN	DATE	SCALE
		CHECKED	DATE	APPVD. DATE
		DWG. NO.		REFERENCE
<small>ALL DIMENSIONS SHARP EDGES</small>				

Figure 8. Thrust Bearing, Design Drawings

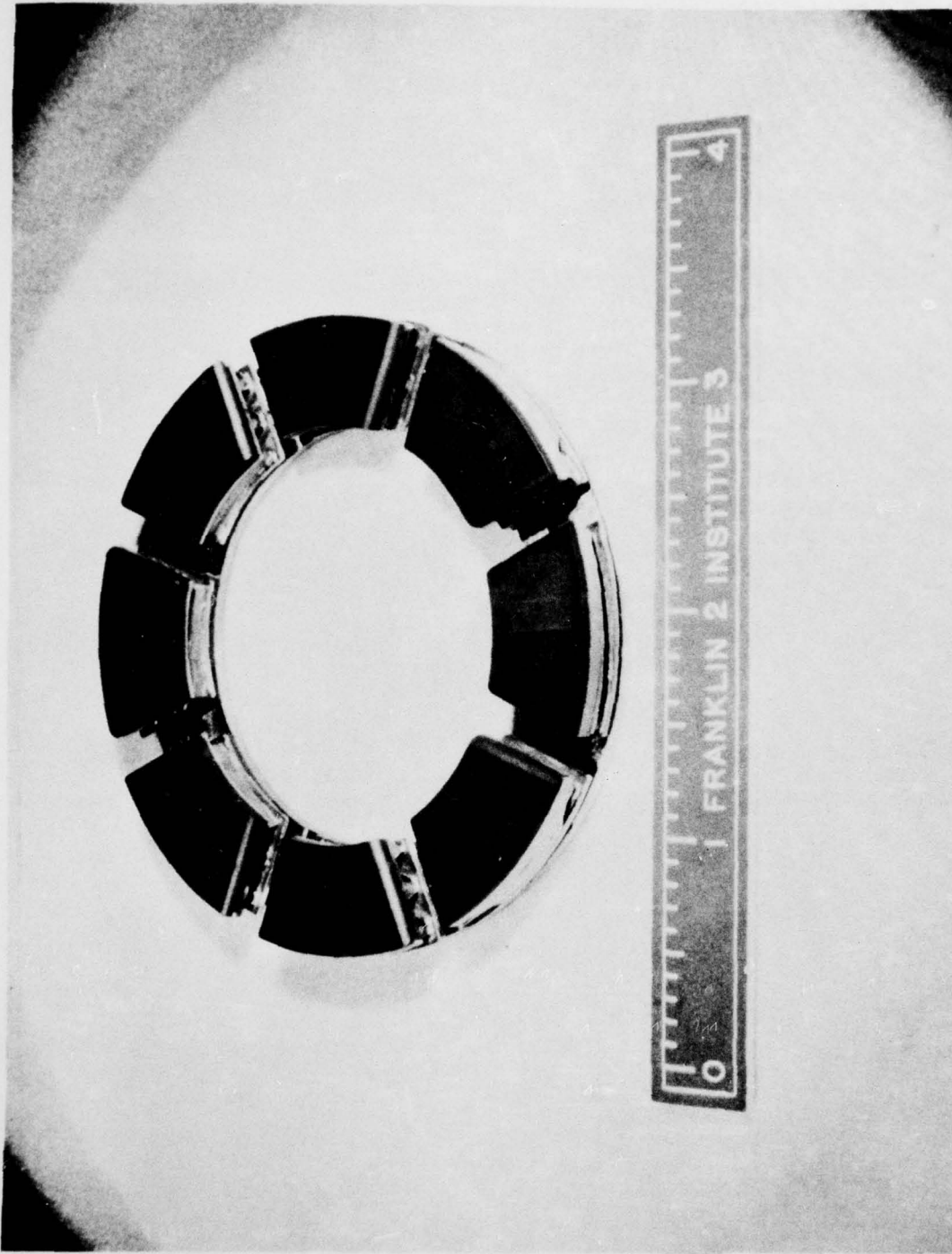
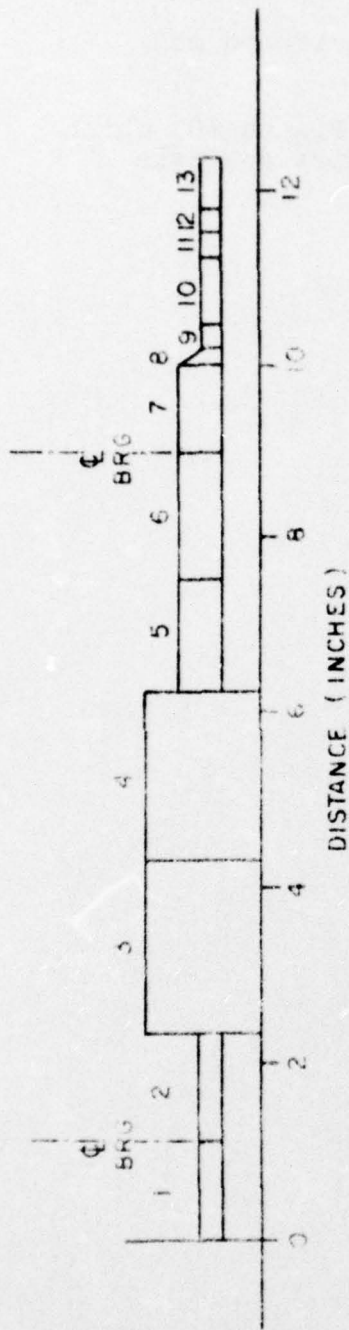


Figure 9. Thrust Bearing Assembly

critical was above the design speed of 93,500 rpm. The overall critical dimensions of the actual 10 KW rotor were maintained.

- For assembly purposes the rotor was sectioned and assembled using curvic couplings.

The dimensions of the rotor are shown on Figure 10, which is the model that was used for the rotor dynamics analysis (1), (2).



Element	1	2	3	4	5	6	7	8	9	10	11	12	13
Length (in)	1.15	1.20	1.91	1.91	1.34	1.437	0.906	0.28	0.25	0.755	0.31	0.25	0.537
O.D. (in)	1.4	1.4	2.56	2.56	1.8	1.8	1.8	1.8	1.26	1.26	1.26	1.26	1.26
I.D. (in)	0.9	0.9	0	0	0.80	0.8	0.8	0.8	0.8	0.8	0.8	0.8	0.8
Station	1	2	2	4	5	6	7	8	9	10	11	12	13
Disk	(Piston)	-	(Alternator)	(Alternator)	(Alternator)	(Thrust Runner)	(Thrust Runner)	(Impeller)	(Impeller)	(Impeller)	(Impeller)	(Impeller)	(Turbine)
I_p (lb-in ²)	0.07	-	1.14	2.28	1.14	0.56	-	-	-	0.667	-	-	1.19
I_T (lb-in ²)	0.04	-	0.992	1.91	0.992	0.28	-	-	-	0.58	-	-	0.77
W (lb)	0.09	-	0.02	-	-	0.40	-	-	-	0.935	-	-	1.65

Figure 10. Rotor Dimensions

5. JOURNAL AND THRUST BEARING ANALYTICAL PERFORMANCE AND DESIGN PARAMETERS

5.1 JOURNAL BEARINGS

5.1.1 Fluid-Film Performance

The design criteria for the spring-mounted, compliant-pivot journal bearings were as follows:

- a) Impose as small a spring pre-load and spring stiffness as practical so as to minimize individual pad loads, and readily permit expansion of the bearing pivot circle to accommodate thermal growths. Thus, the selected spring stiffness and pre-load did not affect the loading on the bottom pads.
- b) Minimize the pitch restraint of the compliant pivots to enhance the anti-whirl capabilities of the bearing.

With the above criteria, design data on frictionless pivot tilting pad bearings are sufficient to establish analytical performance of the bearings. Figures 11 through 14 are individual pad performance curves, which present the important non-dimensional parameters as a function of film thickness over the presumed pivot position. Nomenclature is shown on Table I. It can be shown that for an equally spaced three-pad bearing, in which the spring preload is insignificant, the vertical load on the bearing, directed between the pads opposite the spring, is equal to the radial load on an individual pad. Since gravity is the major load and is directed between the two bottom pads, this condition applies. Thus the analysis of the bearing in essence reduces to the analysis of a single pad. The general procedure is to first compute the compressibility parameter, Λ , from the given geometric and operating parameters, and then compute performance from the information available in Figures 11 through 14.

Table II lists performance of the starter-end journal bearing as a function of the radial clearance and Table III indicates similar information for the wheel-end bearing. The radial clearances considered under normal operation are those occurring after the machine has reached thermal equilibrium and thermal expansions have taken place. Because it is difficult to estimate the final clearance precisely, and there is a tolerance range on the cold clearance, a range of clearances were considered. Two loads were also considered, the first being the gravity load and the second being an excessively heavy load that might result from degraded unbalance conditions. Tables II and III also provide information on start-up operation where machined-in radial clearances are very large because the machine is in a cold condition.

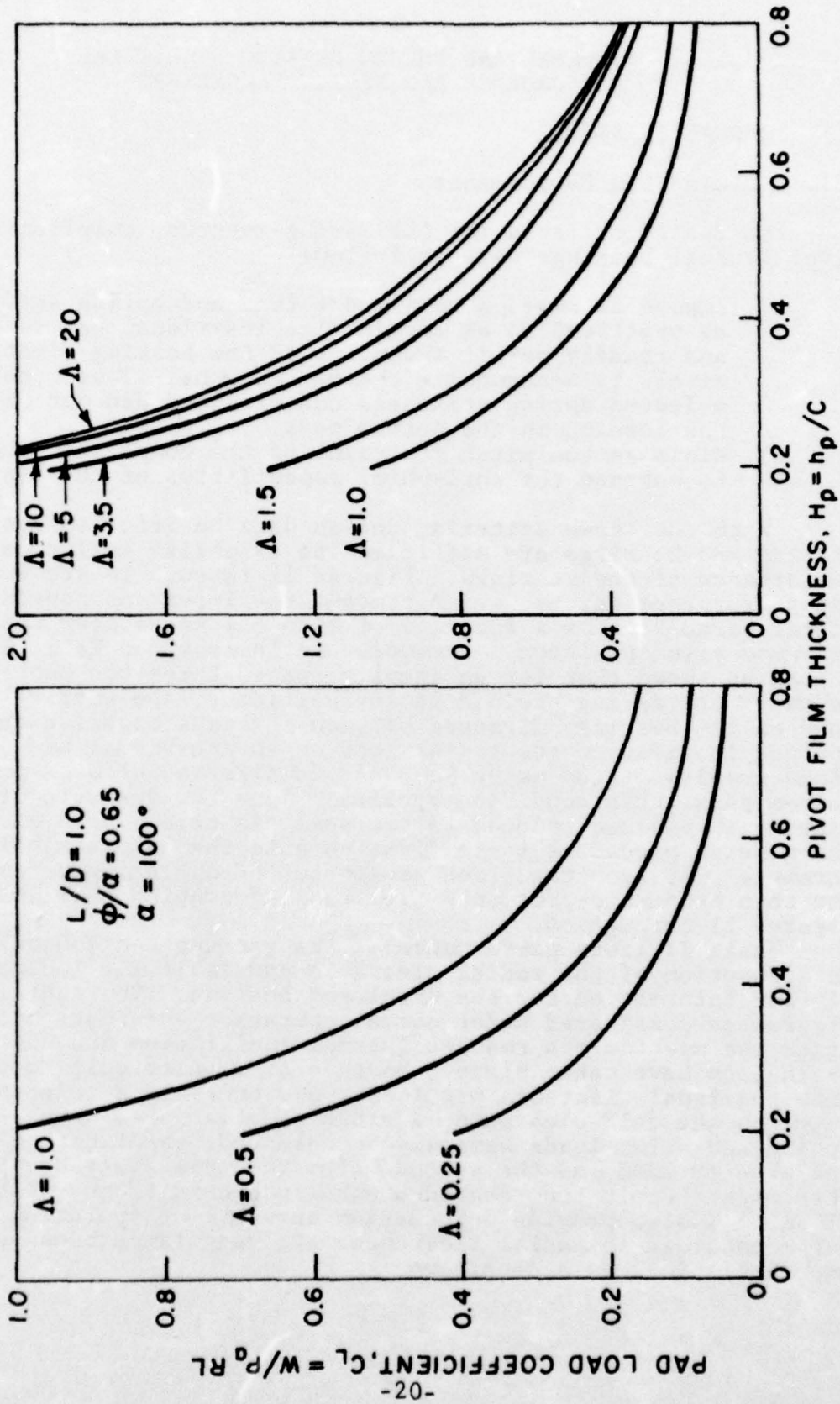


Figure 11. Tilting Pad Load Coefficient vs. Pivot Film Thickness

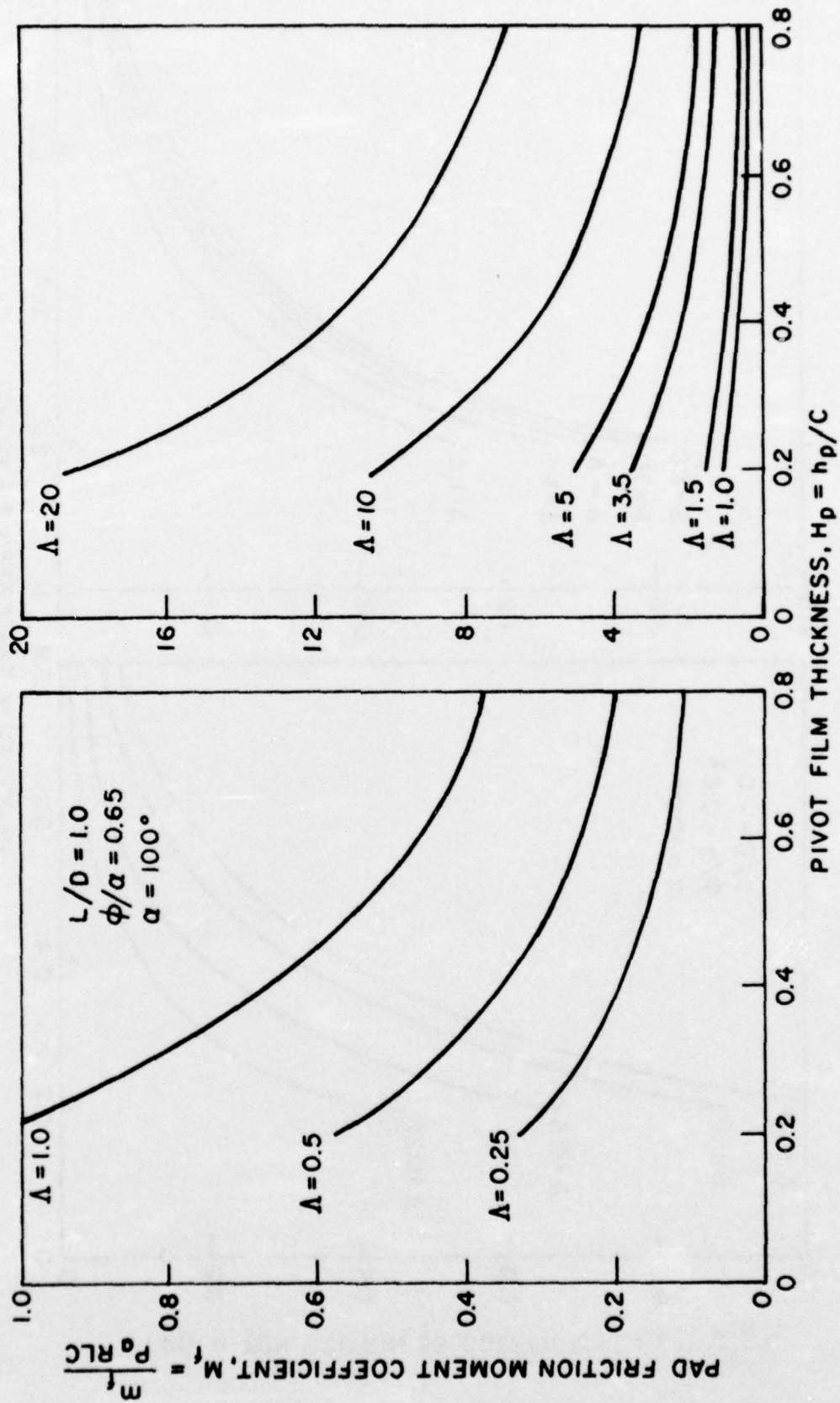


Figure 12. Tilting Pad Friction Moment Coefficient vs. Pivot Film Thickness

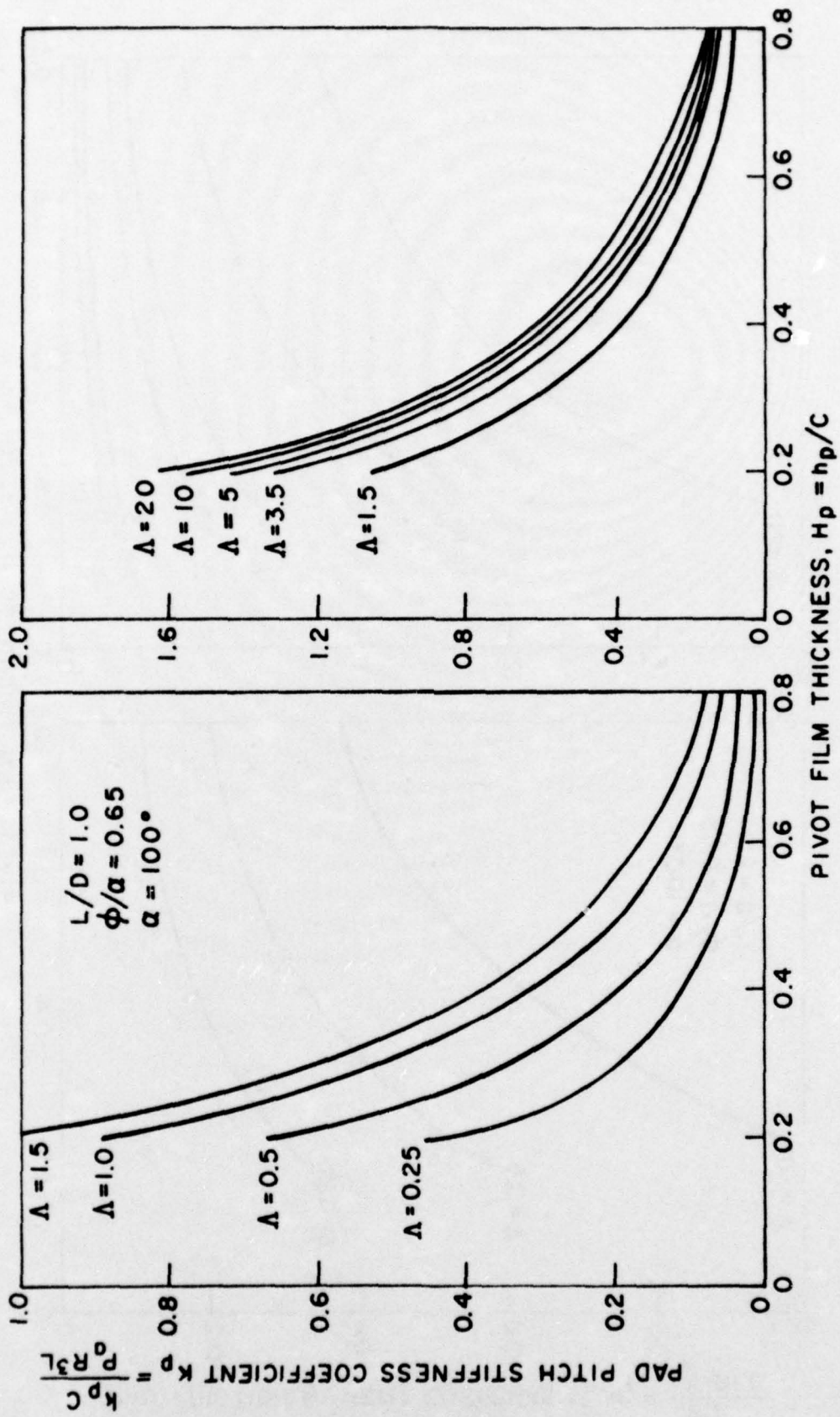


Figure 13. Tilting Pad Pitch Stiffness Coefficient vs. Pivot Film Thickness

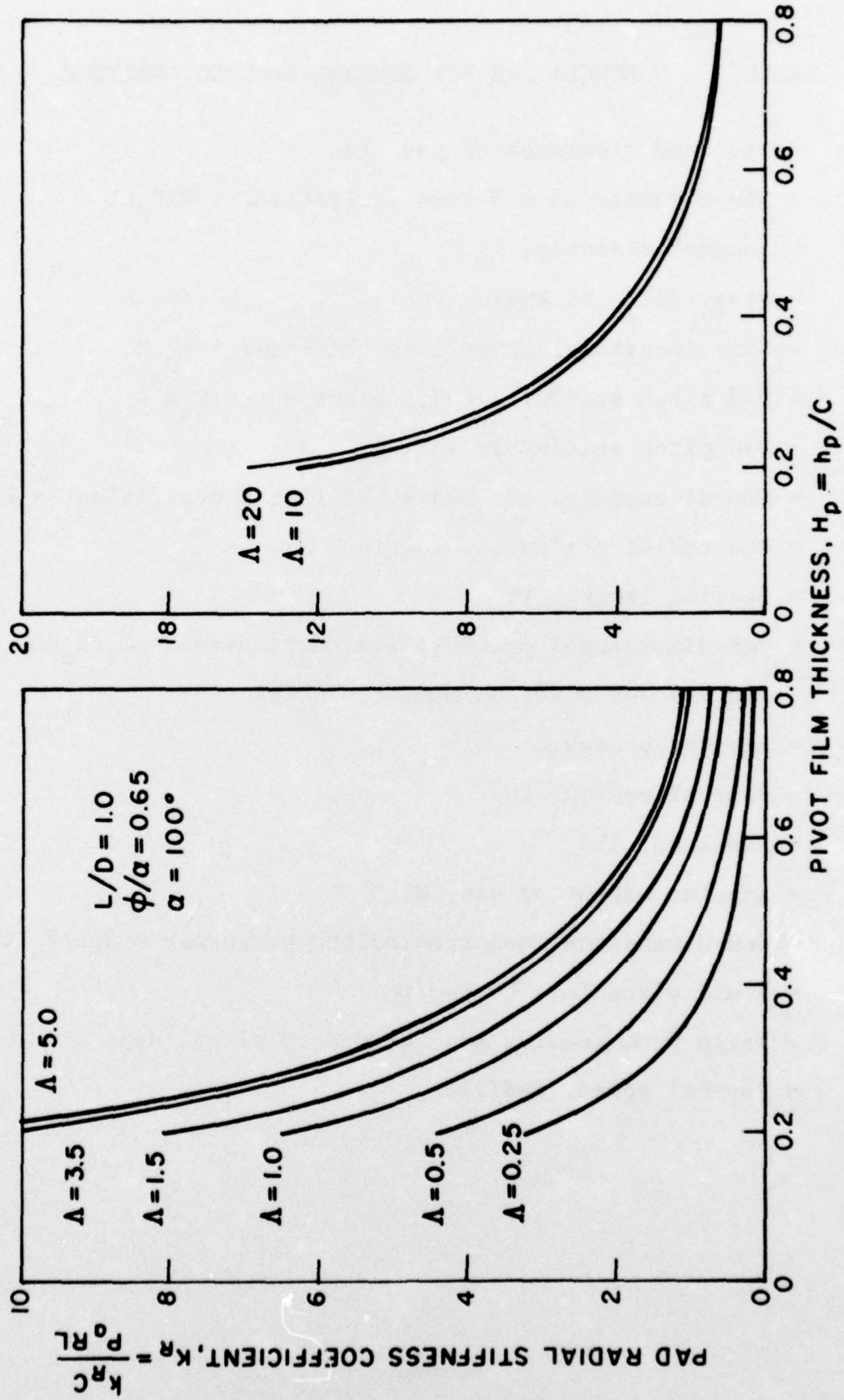


Figure 14. Tilting Pad Radial Stiffness Coefficient vs. Pivot Film Thickness

TABLE I - NOMENCLATURE FOR JOURNAL BEARING ANALYSIS

C	= Machined clearance of pad, in.
C_L	= Non-dimensional pad load coefficient = $W/P_a RL$
D	= Journal diameter, in.
h_p	= Pivot film thickness, in.
H_p	= Non-dimensional pivot film thickness = h_p/C
K_p	= Pad pitch stiffness coefficient = $k_p C/P_a R^3 L$
k_p	= Pad pitch stiffness, in-lbs
K_R	= Non-dimensional pad radial stiffness coefficient = $k_R C/P_a RL$
k_R	= Pad radial stiffness, lbs/in
L	= Bearing length, in.
M_f	= Non-dimensional pad friction coefficient = $M_f/P_a RLC$
m_f	= Pad viscous friction moment, in-lbs
P_a	= Ambient pressure, psia
R	= Journal radius, in.
W	= Pad load, lbs
α	= Angular extent of pad, deg.
Λ	= Non-dimensional compressibility parameter = $6\mu\omega/P_a (C/R)^2$
μ	= Fluid viscosity, lb-sec/in ²
ϕ	= Angle from leading edge of pad to pivot, deg.
ω	= Journal speed, rad/sec

TABLE II

COMPUTED PERFORMANCE OF STARTER-END JOURNAL BEARING

NORMAL OPERATION - HOT CLEARANCES

SPEED = 93,000 rpm

VISCOSITY = 3.0×10^{-9} lb-sec/in² @ temp = 250°F

Operating Radial Clearance (in.)	Load (lb)	Bearing Power Loss (HP)	Min. Pad Rad. Pivot Clear. (in.)	Pad Radial Stiffness (lb/in)	Pad Pitch Stiffness (in-lb/rad)
.0025	3.4	.080	.00138	6910	353
	8.0	.095	.00075	20700	1270
.0020	3.4	.085	.00144	6120	423
	8.0	.103	.00084	19080	1235
.0015	3.4	.092	.00160	6000	282
	8.0	.117	.00114	15840	894

START-UP OPERATION - COLD CLEARANCES

LOAD = 6.4 lbs

VISCOSITY = 3.0×10^{-9} lb-sec/in² @ temp = 250°F

MACHINED IN RADIAL CLEARANCE = .00325 in.

Speed (rpm)	Min. Pad Rad. Pivot Clear. (in.)	Pad Radial Stiffness (lb/in)	Pad Pitch Stiffness (in-lb/rad)
42000	.00059	16800	1080
84000	.00094	12400	890

TABLE III

COMPUTED PERFORMANCE OF WHEEL-END BEARINGS

NORMAL OPERATION - HOT CLEARANCES

SPEED = 93,500 rpm

VISCOSITY = 3.0×10^{-9} lb-sec/in² @ temp = 250°F

Machined In Clearance (in.)	Load (lbs)	Bearing Power Loss (HP)	Min. Pad Rad. Pivot Clear. (in.)	Pad Radial Stiffness (lb/in)	Pad Pitch Stiffness (in-lb/rad)
.003	8.6	.169	.00135	13100	1480
	17.0	.229	.00083	29770	3570
.0025	8.6	.181	.00138	14290	1659
	17.0	.243	.00088	34290	3627
.002	8.6	.205	.00140	13700	1544
	17.0	.275	.00090	32750	3135

START-UP OPERATION - COLD CLEARANCES

LOAD = 11.6 lbs

VISCOSITY = 3.0×10^{-9} lb-sec/in² @ temp = 250°F

MACHINED-IN RADIAL CLEARANCE = .004 in.

Speed (rpm)	Min. Pad Radial Pivot Clear. (in.)	Pad Radial Stiffness (lb/in)	Pad Pitch Stiffness (in-lb/rad)
22500	.0004	16600	2400
45000	.0007	22800	2411
90000	.0011	16800	1977

The results of Tables II and III indicate that the anticipated bearing operation is quite good. Even at very heavy load, minimum film thickness exceeds 0.5 mils. The pitch stiffness of the fluid-film exceeds that of the elastomer with adequate margin to ensure that the pads will pitch properly. For cold operation in which geometric clearances are far from optimum, the minimum film thicknesses are quite acceptable even at low-speed conditions which would be obtained very quickly.

5.1.2 Stability Considerations

High speed tilting-pad bearing systems may be subject to two types of instabilities. The first is rotor whirl because the pitch resistances or inertias of the pads are excessive, introducing a lag in the pitch motions of the pads. The second is pad flutter due to improper inertia characteristics and insufficient damping in the pivot. Information exists (3) that enables pad inertias to be selected to avoid both flutter and whirl problems provided pivot resistance is negligible. Using information from reference (3), a stability map was generated and is shown on Figure 15. It is a plot of the pad pitch inertia coefficient \bar{I}_p vs. the shaft mass coefficient \bar{M}_s . \bar{I}_p is a parameter related to the pad pitch inertia, and \bar{M}_s is a parameter relating to the quantity of mass that the bearing supports. The stability limit is shown by the dashed line. The actual performance of the bearing is shown by the solid line. The only variable that is changing is the shaft speed Ω , thus the curve represents the effects of speed on stability. The actual shaft speed is shown on the upper portion of the graph. The curve indicates that the new design is stable over the operating range of the machine.

5.1.3 Design of Compliant Mounts

The initial design of the compliant mounts was accomplished by the formulas presented in references (1) and (2). Since these formulas only provide qualitative direction, it was necessary to test each pad in its assembled bearing, and adjust the elastomer dimensions accordingly to achieve the target values of elastomer radial and pitch stiffness. Table IV lists the final geometric parameters for the journal bearings.

5.2 THRUST BEARING PERFORMANCE

The analytical procedures for determining thrust bearing performance are described in references (1) and (2). Figure 16 is a plot of thrust bearing performance as a function of axial clearance. It depicts performance of a single bearing, but since a large total axial clearance was finally selected there is very little influence of one thrust bearing upon the other and Figure 16 accurately represents the double-sided thrust

$$I_p \text{ (pad pitch inertia)} = .92 \times 10^{-4} \text{ lb-in-sec}^2$$

$$C \text{ (pad machined clearance)} = .0025 \text{ in.}$$

$$P_a \text{ (ambient pressure)} = 14.7 \text{ psi}$$

$$R \text{ (journal radius)} = .9 \text{ in.}$$

$$L \text{ (bearing length)} = 1.8 \text{ in.}$$

$$M_S \text{ (shaft mass)} = 8.6 \text{ lbs.}$$

$$\Omega = \text{shaft speed (rad/sec)}$$

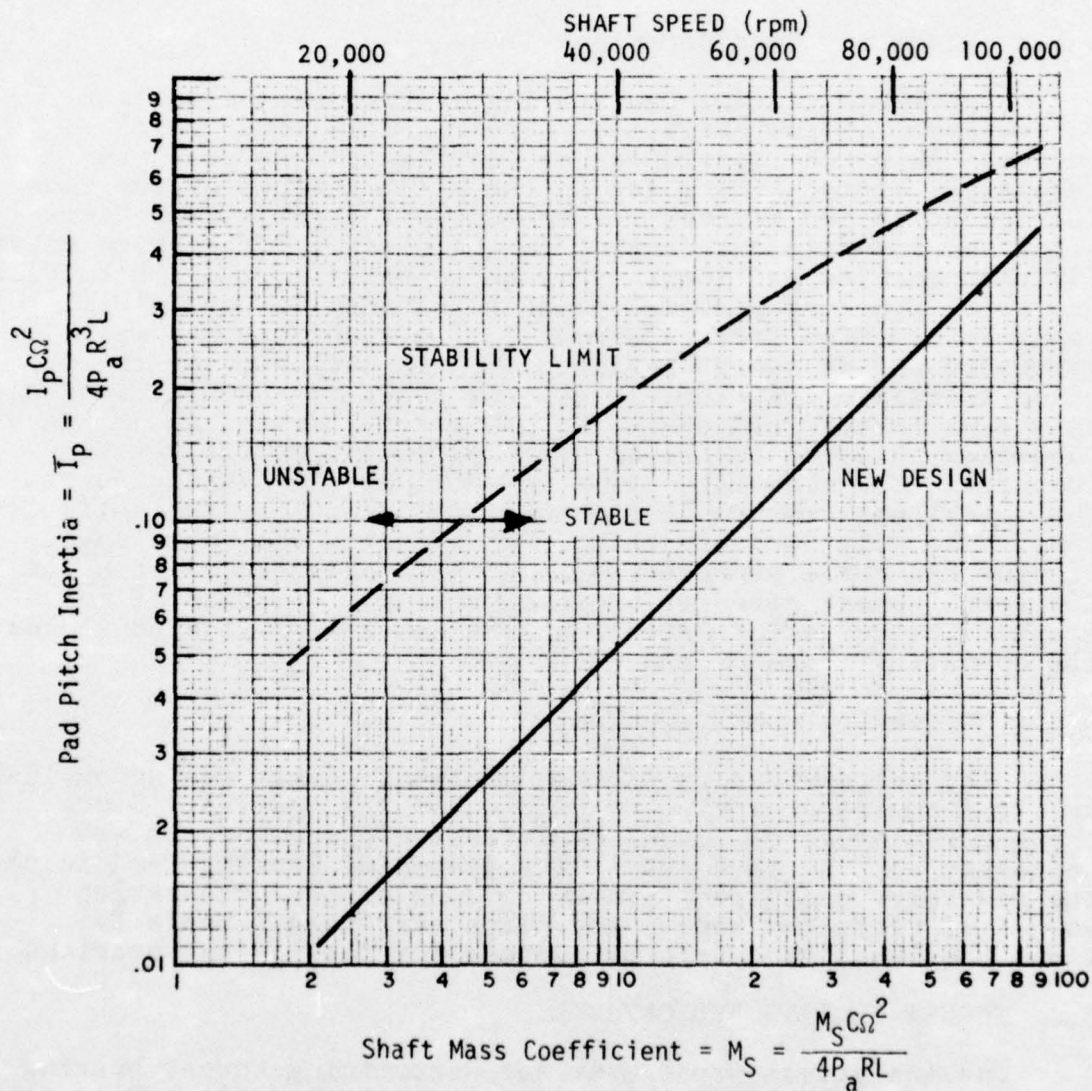


Figure 15. Stability Map, Compliant-Mounted Journal Bearing

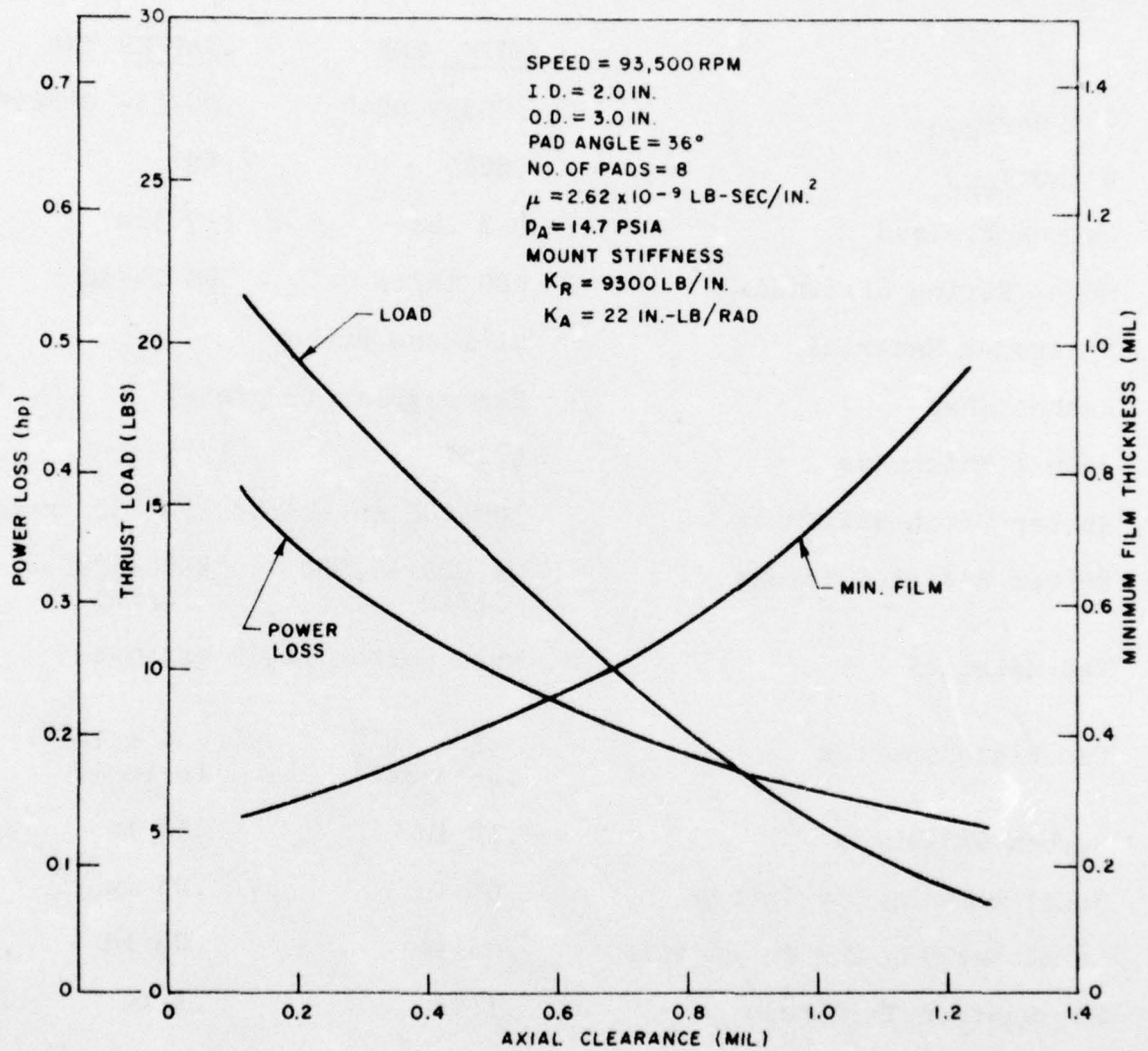


Figure 16. Thrust Bearing Theoretical Performance

TABLE IV

FINAL DESIGN PARAMETERS OF SPRING-MOUNTED,
COMPLIANT PIVOT JOURNAL BEARINGS

	<u>WHEEL END</u>	<u>STARTER END</u>
C (cold) _{rad}	.0035-.004"	.00275-.00325"
C (hot) _{rad}	.0025	.002
Set-up Preload	0-2 lbs.	0-2 lbs.
Mech. Spring Stiffness	600 lb/in	500 lb/in
Elastomer Material	Silicone Rubber	
Rubber Shape	Rectangular (1 piece)	
Rubber Thickness	1/16"	1/16"
Rubber Pitch Stiffness	300-500 in-lb/rad	150-250 in-lb/rad
Rubber Radial Stiffness	20,000-30,000 lb/in	8000-12,000 lb/in
Pad Material	Pure Carbon P6452 graphite	
Pad Pitch Inertia	.92 x 10 ⁻⁴ lb-in-sec ²	.44 x 10 ⁻⁴ lb-in-sec ²
Carbon Thickness	.12 in	.12 in
Steel Backing for Carbon	.05 in	.05 in
Steel Backing for Corrugation	.05 in	.05 in
Corrugation Thickness	.1 in	.1 in

bearing performance. The elastomer characteristics for the thrust bearing were determined in a manner similar to that of the journal bearing, i.e., a combined theoretical and empirical approach. On Table V are listed the values of relevant geometry and elastomer stiffness parameters.

TABLE V
THRUST BEARING GEOMETRY

Configuration	= Double-acting compliantly mounted thrust bearing with 8 pads for each thrust element
O.D.	= 3.0 in.
I.D.	= 2.0 in.
Pad angle	= 40°
Pad material	= Pure carbon P6452 graphite
Elastomer mount	= Rectangular
Length	= 0.53 in.
Width	= 0.5 in.
Thickness	= 0.0625
Material	= Neoprene, 45 durometer
Axial stiffness/pad	= 9300 lb/in.
Angular stiffness/pad	= 22.4 in-lb/rad
Total axial clearance (cold)	= .008-.012 in.

6. HIGH SPEED COMPONENT TESTING OF THE SPRING MOUNTED, COMPLIANT-PIVOT JOURNAL BEARINGS

6.1 FIRL HIGH SPEED RIG

The Solar simulator closely resembled the actual turbo-alternator. As such, it had several disadvantages as a bearing check-out and test device. Once the bearings were installed, they were completely hidden from visual observation, and their performance was determined only via remote instrumentation. It was not possible to inspect the bearings after a run without a major tear down, which was expensive and time consuming. Because of the relatively low torque available from the simulator drive turbine, it was necessary to start with high turbine flow, and once the rotor became airborne high speeds were attained very quickly. At start-up throttle control was difficult. Also, the rig required thrust balancing at start-up, via the thrusting chambers at the starter end. This was necessary because the simulator incorporated a dummy wheel for the compressor, which in its normal configuration would have provided aerodynamic thrust balancing. This requirement of remotely controlled thrust balance further complicated start-up and operation of the simulator.

To facilitate the study of the high-speed performance of the bearings in a more rigorous fashion, and to provide a means for bearing checkout prior to full simulator testing, FIRL designed and built a high-speed journal bearing test rig. The production of this rig was funded by a separate project in which gas-bearing studies were being undertaken. Since prior testing of the original bearings at Solar had indicated satisfactory operation of the thrust bearings, the rig was designed solely for checkout of the journal bearings.

Figure 17 is a schematic of the FIRL high-speed test rig. The rotor was designed to simulate the weight distribution of the Solar 10 KW simulator rotor, with identical journal bearing diameters for the starter and wheel end bearings. The rig basically consists of a base plate, two bearing pedestals, the rotor and the nozzle assembly. The test bearings are inserted in the pedestals. The rotor is slightly tilted towards the wheel-end bearing so that a light load is imposed upon the single thrust bearing used in the rig.

The rotor is driven by a four-nozzle impulse turbine, which consists of the nozzle ring and turbine buckets machined into the rotor. The rig was designed for easy access to the bearings and provided for insertion of extensive instrumentation. Figure 17 indicates the instrumentation that was applied to the rig.

A limitation of the rig, with respect to the turboalternator application, is that the maximum speed available from the rig is approximately 76,000 rpm. To achieve this speed required modification to the original nozzles. Extensive changes would

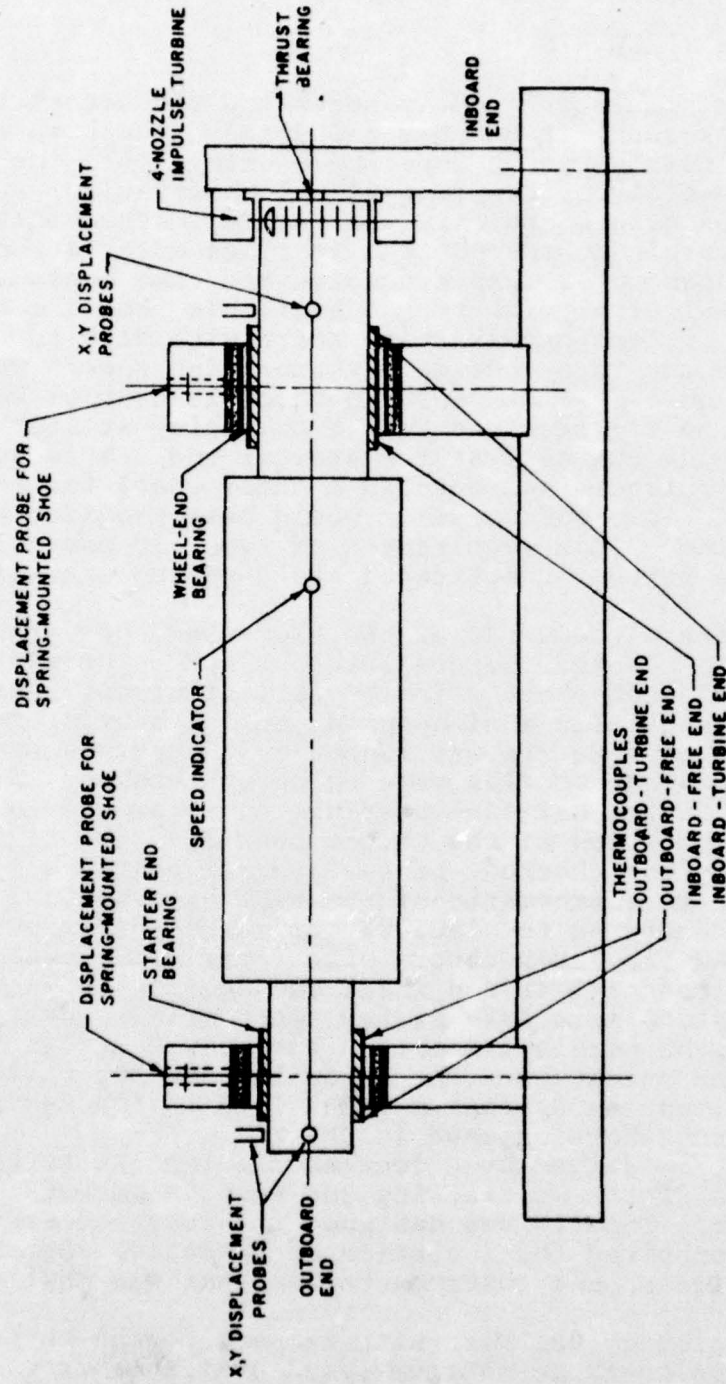


Figure 17. Schematic of High-Speed Gas Bearing Test Rig

be necessary to both the wheel and nozzles to achieve a 93,500 rpm capability. A picture of the experimental set-up illustrating the test rig and the instrumentation is shown in Figure 18. Figures 19 and 20 are close-up photographs of the test rig. Table VI is a list of the instrumentation used for the testing. Inductance probes were used to measure shaft vibration and capacitance probes were used to measure the displacements of the spring loaded shoes. Thermocouples were imbedded in the bearing pads between the carbon and steel interface. All vibration signals were recorded on a 14-channel tape recorder and the temperature data was continuously printed during testing. The test rotor was balanced to .0003 in-oz.

6.2 INITIAL CHECK OUT

The purpose of this initial test was to verify the rig. There was some difficulty with the thrust bearing, which was a hydrostatic porous bearing. It experienced pneumatic hammer type instability. Modifications were made to its design which made the rig acceptable for use although axial vibrations were not entirely eliminated.

During this initial testing the top rotor speed was 73,500 rpm. At that time, this speed was the maximum obtainable from the air turbine drive. There were no critical speeds observed during run-up or shut-down.

6.3 START-STOPS

During the course of testing 20 start-stops were accomplished without any noticeable wear. It was necessary to turn the rotor by hand in order to start. This was due to the low starting torque capability of our test rig and the spring pre-load and the loaded pad start-up friction.

6.4 SPRING-MOUNTED, COMPLIANT-PIVOT BEARING TESTING (APRIL 1976)

A one-hour endurance test was conducted to determine the bearing performance for an extended period of time. The rotor speed fluctuated between 70,000 rpm and 72,000 rpm during this testing. Figure 21 shows the temperature as a function of time at the locations specified on Figure 17. The thermocouples were located on the pad which carried the highest load, therefore, they recorded the highest temperature values. The inboard bearing remained very cool during the testing due to the turbine air flow. However, there was a 40°F temperature gradient axially across this bearing and performance was still acceptable. On the outboard bearing the temperature was 100°F hotter than the inboard bearing. Due to the flexibility of the rubber and spring, resulting thermal distortions did not present any problems. Also, there was no external cooling for this bearing. It took approximately 12 minutes to reach thermal equilibrium.

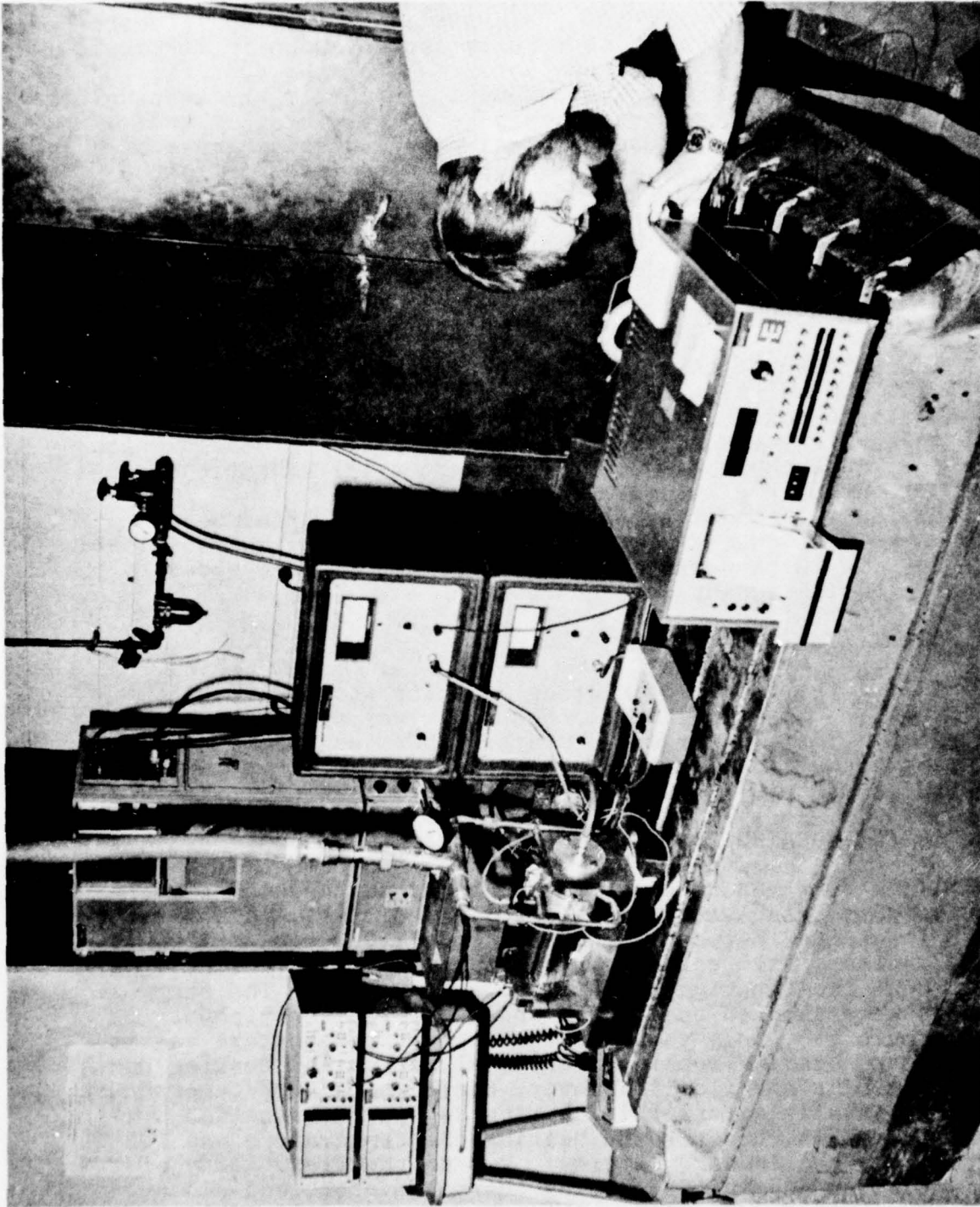


Figure 18. Overview of FIRL High-Speed Test Rig with Instrumentation

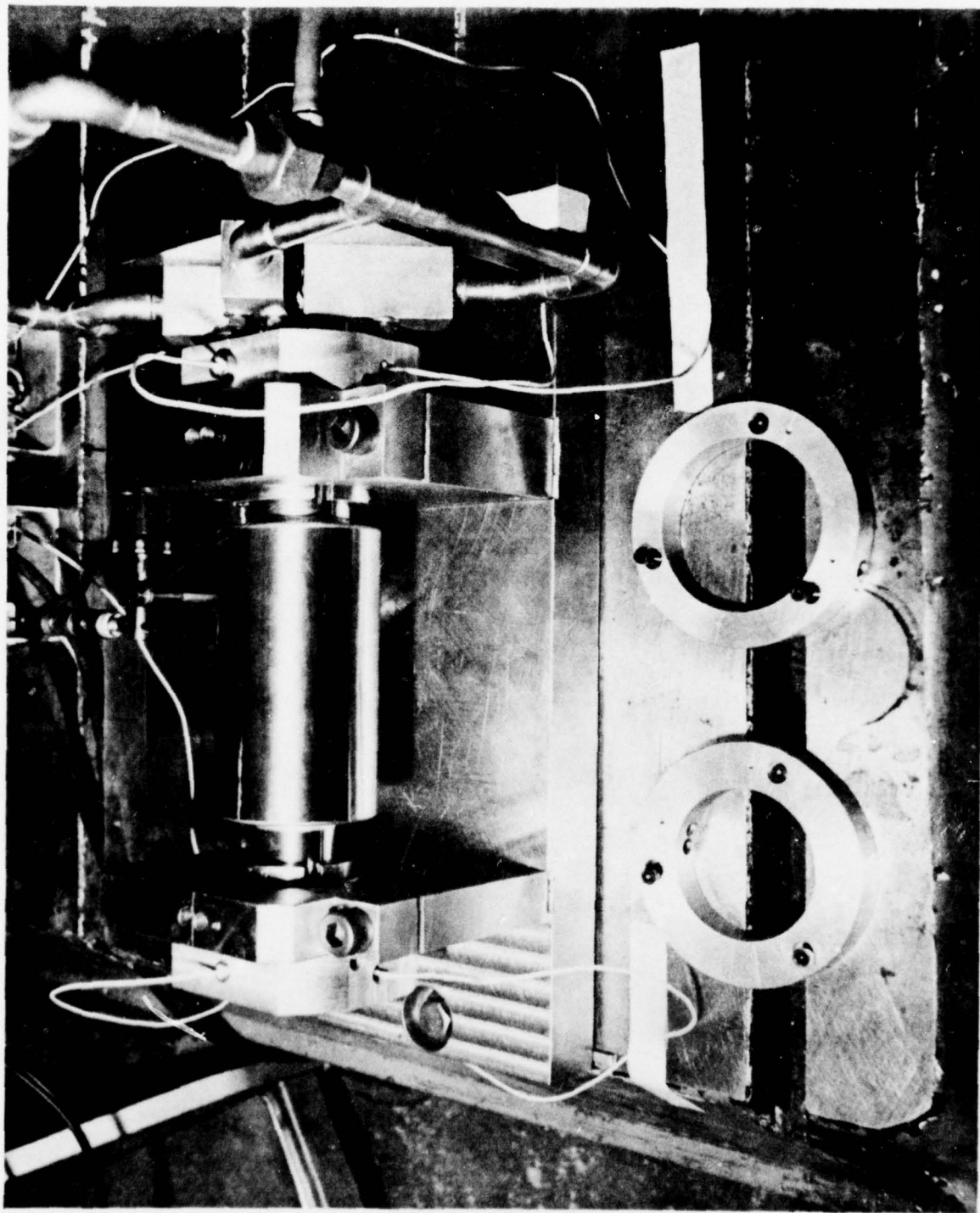


Figure 19. Close-up of High-Speed, Gas Bearing, Component Test Rig

Figure 20. Journal Bearing Installation, High-Speed, Gas-Bearing
Component Test Rig

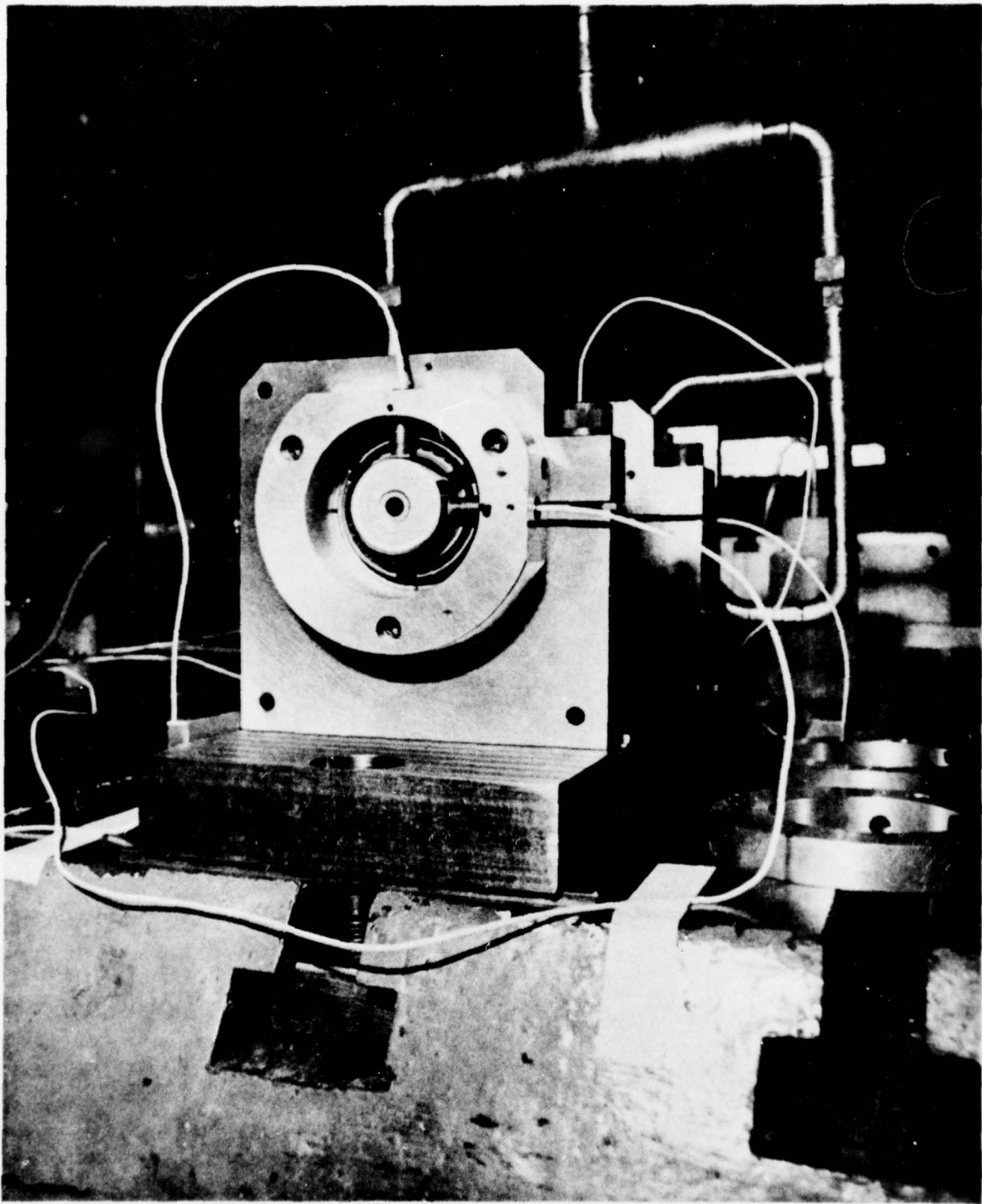


Figure 20. Journal Bearing Installation, High-Speed, Gas-Bearing Component Test Rig

TABLE VI
 INSTRUMENTATION FOR HIGH-SPEED, GAS-BEARING
 COMPONENT TEST RIG

<u>Instrument</u>	<u>Purpose</u>
1) Sangamo Model 3652 14-channel, F.M. Tape Recorder, S/N 4284	To record vibration and speed data on tape for subsequent playback and interpretation
2) Two Tektronix Model R5030 Dual Beam Oscilloscopes, S/N B010136 and S/N B010145	To visually observe shaft orbits or X and Y vibrations at each bearing station
3) Moviport Model D711 Electronic Tachometer	To record rotor speed
4) Esterline Angul Model D-2020 Digital Data Acquisition System	To record on strip charts thermocouple temperatures
5) Bentley Nevada Type 300 Relative Displacement Proximity Probes and Model 3500-2388 Proximiters (4 each)	To monitor time dependent shaft displacements
6) Capacitance Probes and Wayne-Kerr Model DM 100B Distance Meter	To measure vibrations of spring-mounted pads
7) Saicor Model SAI-51B Real Time Analyzer-Digital Integration	To establish frequency spectral density from playback of tape data
8) Tektronix Model C-12 Oscilloscope Camera	To photograph orbits, vibration spectrum, frequency density etc. during playback through tape recorder

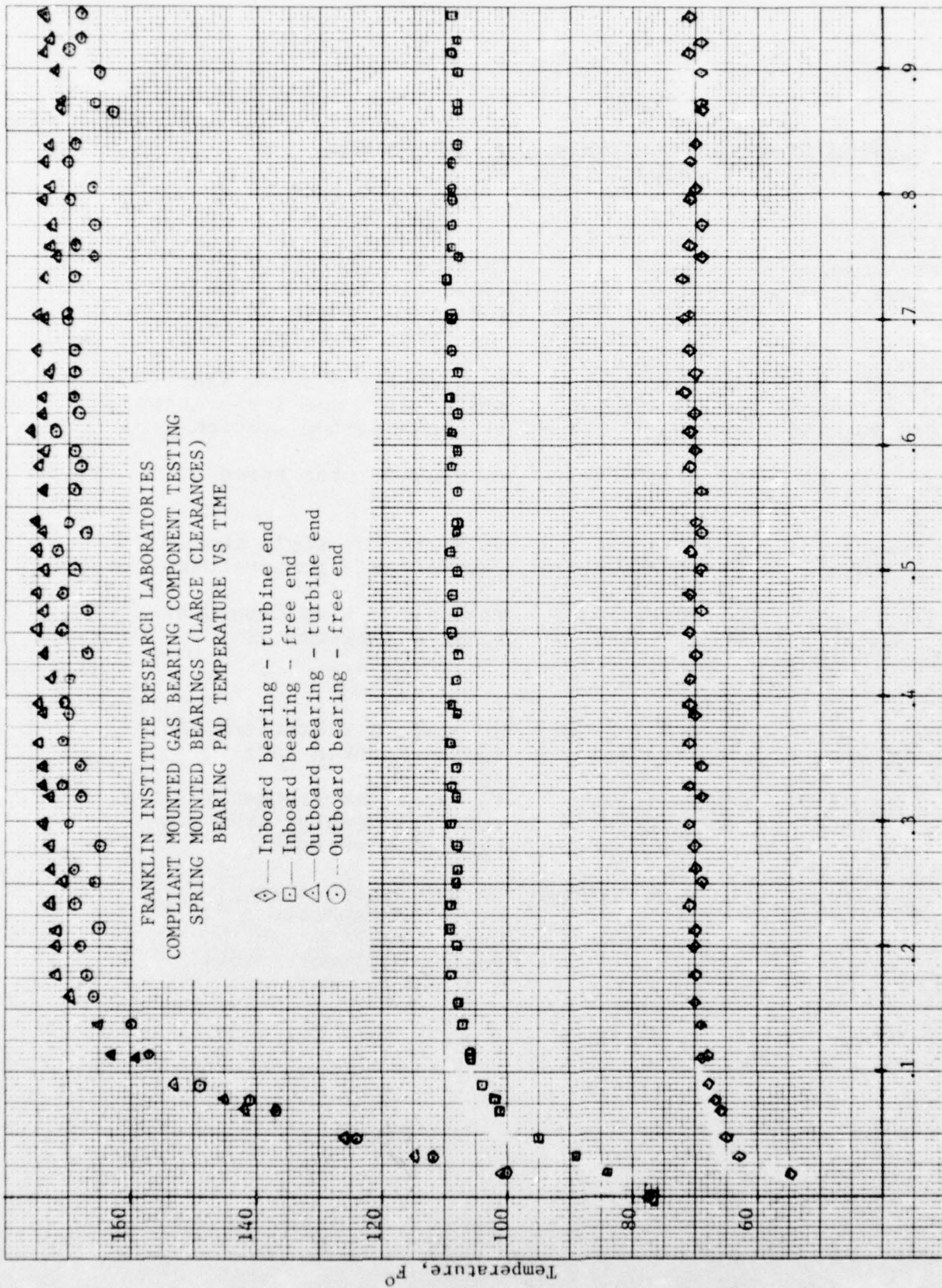


Figure 21. Thermocouple Data, High-Speed Component Testing, April, 1976

The shaft orbits at both inboard and outboard ends were very stable during the testing with the exception of the thrust bearing induced vibration which would periodically appear. Figure 22 illustrates typical orbits. The outboard end has larger motion because of the thrust bearing vibration. Peak to peak amplitudes at this end without the thrust bearing vibration is approximately .5 mils. With the thrust bearing vibration, the peak amplitude is .75 mils. The peak amplitudes for the inboard bearing with or without the thrust bearing motion is .5 mils. There was little change in orbit size or shape during the testing, even during the thermal transient at the beginning of the endurance test.

A real time frequency analyzer was used to determine the frequencies present during the testing. The results are shown on Figures 23 and 24. These figures show amplitude as a function of frequency. They indicate the frequencies present in the rotor system and their relative importance to the vibration level of the rotor. Examining Figure 23, the shaft speed is the dominant frequency for the outboard end with a relatively low 2nd and 3rd harmonic present. There also is present, at this end a large subsynchronous frequency at 1200 cpm. This frequency is due to the thrust bearing motion. At the inboard end the 2nd harmonic is quite prevalent. It is believed that this is also caused to a certain extent by the thrust bearing. The subsynchronous frequencies at the inboard end have very low amplitude. Figure 24 shows in more detail the low frequency range. At the outboard end the subsynchronous frequency of 1200 cpm has a relatively large amplitude associated with it, while the subsynchronous frequency at the inboard end did not substantially influence the vibration level of the rotor.

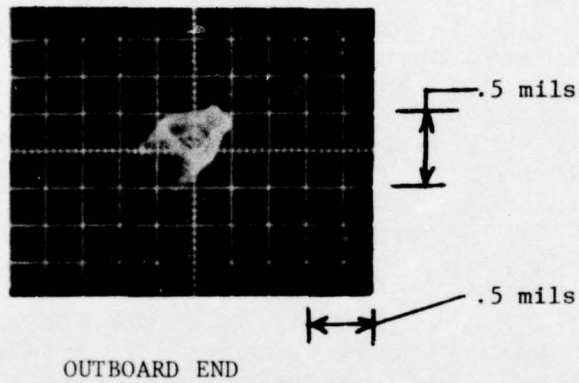
In summary, the revised journal bearing designs behaved very well through the maximum speed range attainable on the FIRL rig.

6.5 SPRING-MOUNTED, COMPLIANT-PIVOT, BEARING TESTING (JULY, 1976)

Upon completion of the simulator testing at Solar reported on in Section 8, a new set of bearings was assembled with the same design parameters as those bearings that were tested previously at FIRL and at Solar. The test rig was modified slightly to see if the speed could be increased. Also, the thrust bearing used for the test rig was changed to a compliant mounted hydrodynamic bearing. This change was made to eliminate the axial vibration caused by the movement observed during the April testing.

The maximum obtainable speed for the test rig after minor modification to the nozzles was 76,000 rpm. In July 1976, a half hour test was conducted at this speed. Figure 25 illustrates orbit plots of both end of the rotor. As indicated in the April testing the orbits remained very small. Peak to peak amplitudes were approximately .6 mils at both ends.

FRANKLIN INSTITUTE RESEARCH LABORATORIES
COMPLIANT MOUNTED GAS BEARING COMPONENT TESTING
SPRING MOUNTED BEARINGS (LARGE CLEARANCE)
ONE HOUR ENDURANCE TEST-ORBIT ANALYSIS



SHAFT SPEED - 70,000 RPM

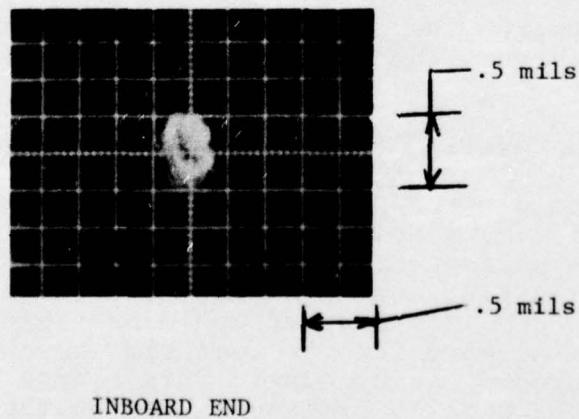


Figure 22. Typical Shaft Orbits. High-Speed Component Testing, April, 1976

FRANKLIN INSTITUTE RESEARCH LABORATORIES
 COMPLIANT MOUNTED GAS BEARING COMPONENT TESTING
 SPRING MOUNTED BEARINGS (LARGE CLEARANCE)
 FREQUENCY SPECTRUM ANALYSIS
 ONE HOUR ENDURANCE TEST

SHAFT SPEED = 70,000 RPM

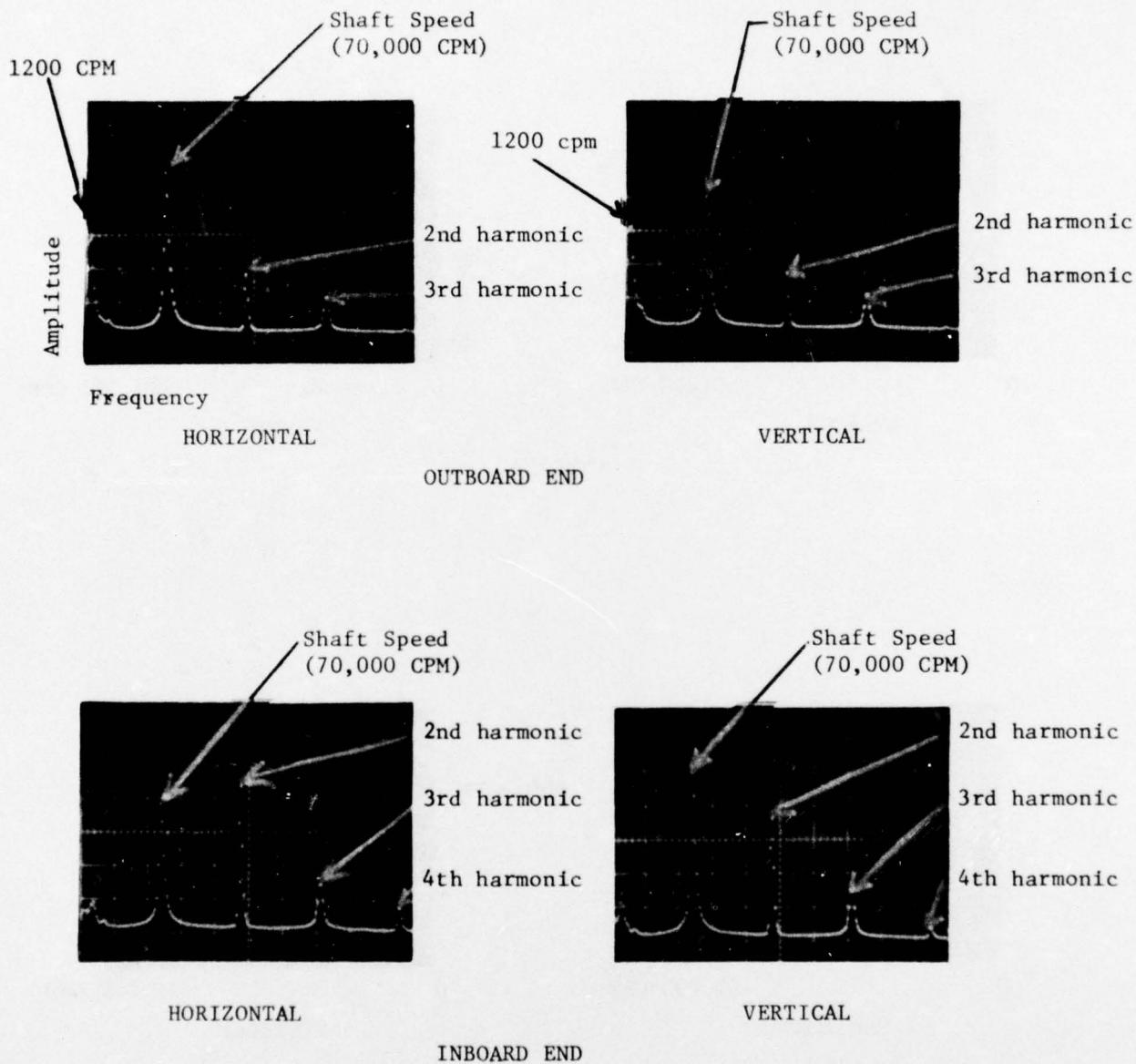


Figure 23. Frequency Spectrum, High Speed Component Testing, April, 1976

FRANKLIN INSTITUTE RESEARCH LABORATORIES
COMPLIANT MOUNTED GAS BEARING COMPONENT TESTING
SPRING MOUNTED BEARINGS (LARGE CLEARANCE)
FREQUENCY SPECTRUM ANALYSIS (LOW FREQUENCY RANGE)
ONE HOUR ENDURANCE TEST

SHAFT SPEED = 70,000 RPM

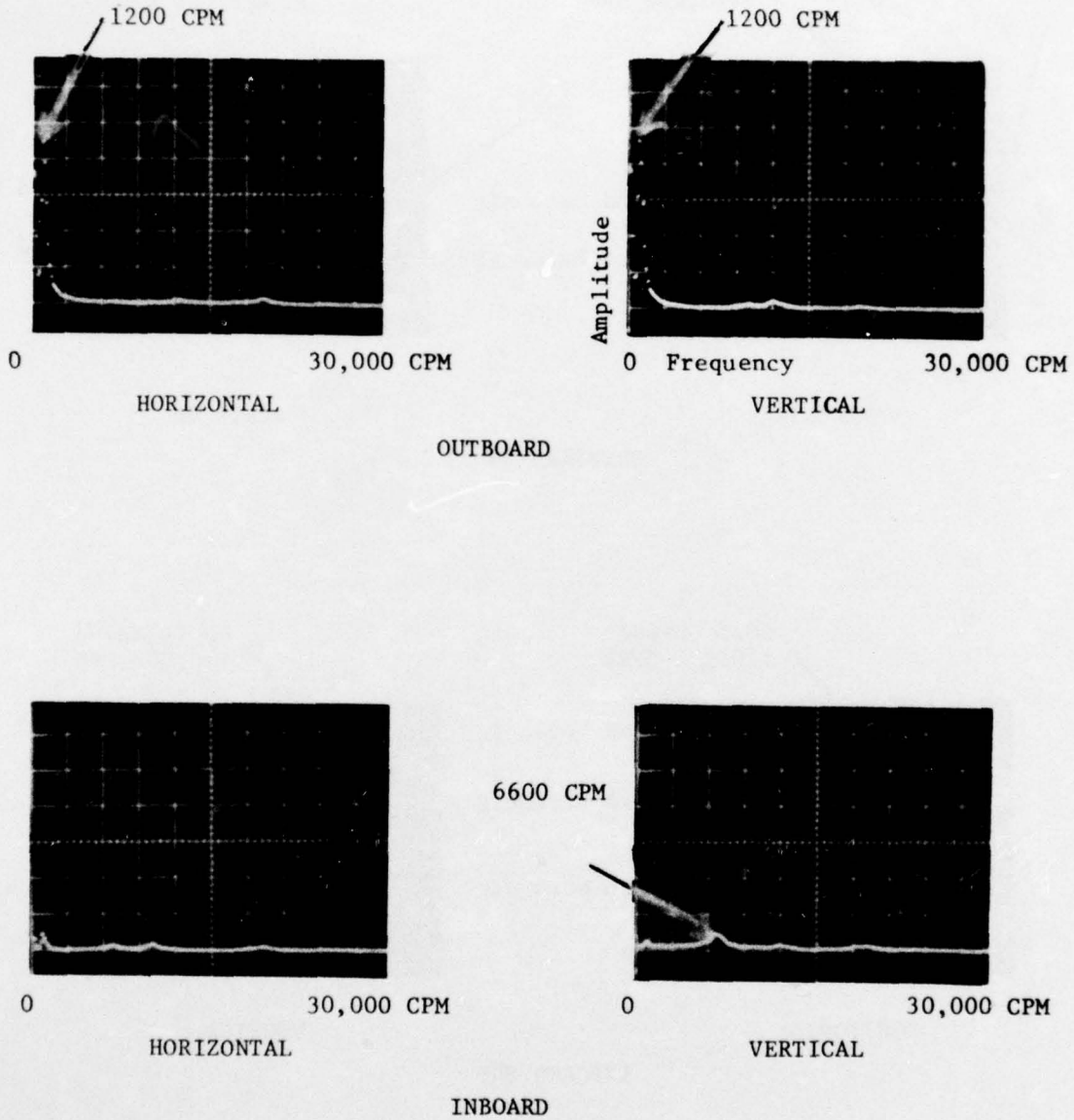
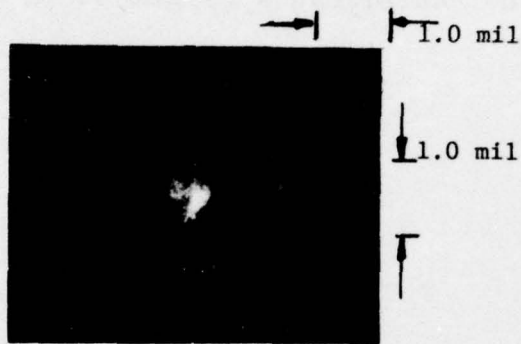


Figure 24. Frequency Spectrum, Low-Frequency Range,
High-Speed Component Testing, April, 1976

FRANKLIN INSTITUTE RESEARCH LABORATORIES
COMPLIANT MOUNTED GAS BEARING COMPONENT TESTING
SPRING MOUNTED BEARINGS (LARGE CLEARANCE)

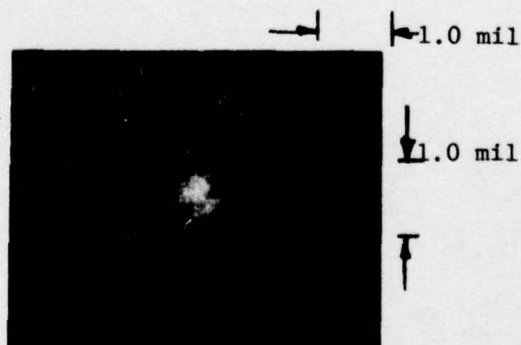
JULY 2, 1976 TESTING

ORBIT ANALYSIS



Outboard End

SHAFT SPEED - 76000 RPM



Inboard End

Figure 25. Shaft Orbits, High-Speed Component Testing, July, 1976

The vibration caused by the thrust bearing observed during the April testing was completely eliminated. Figures 26 and 27 are frequency plots which indicate relative amplitude as a function of the frequency present in the system. The predominant frequency occurs at the running speed. There is a frequency (Figure 27) that fluctuated between 45,000 cpm and 65,000 cpm. It had a relatively low amplitude and was related to the impulse turbine (throttling the turbine at operating speed removed this frequency). The bearing remained stable and the orbit levels remained the same throughout the test. There was no indication of any vibration problem during any of the testing at FIRL using the redesigned spring-mounted bearings.

FRANKLIN INSTITUTE RESEARCH LABORATORIES
COMPLIANT MOUNTED GAS BEARING COMPONENT TESTING
SPRING MOUNTED BEARINGS (LARGE CLEARANCE)

JULY 2, 1976 TESTING

FREQUENCY SPECTRUM ANALYSIS

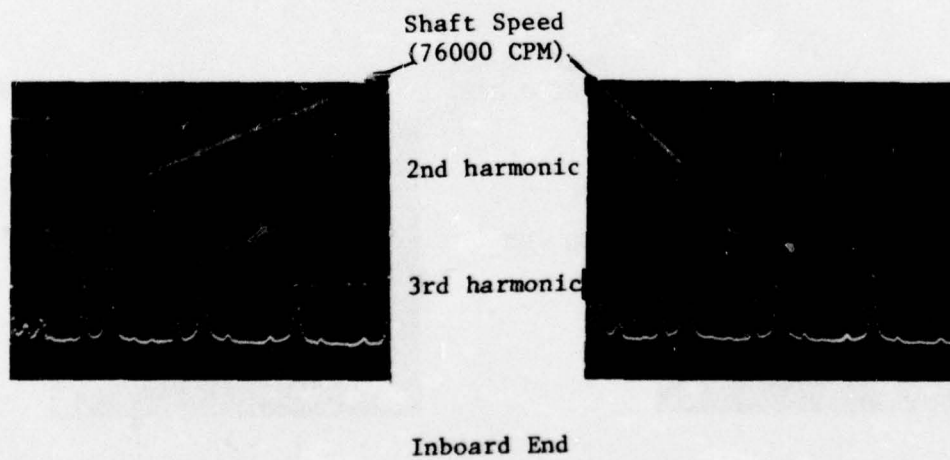
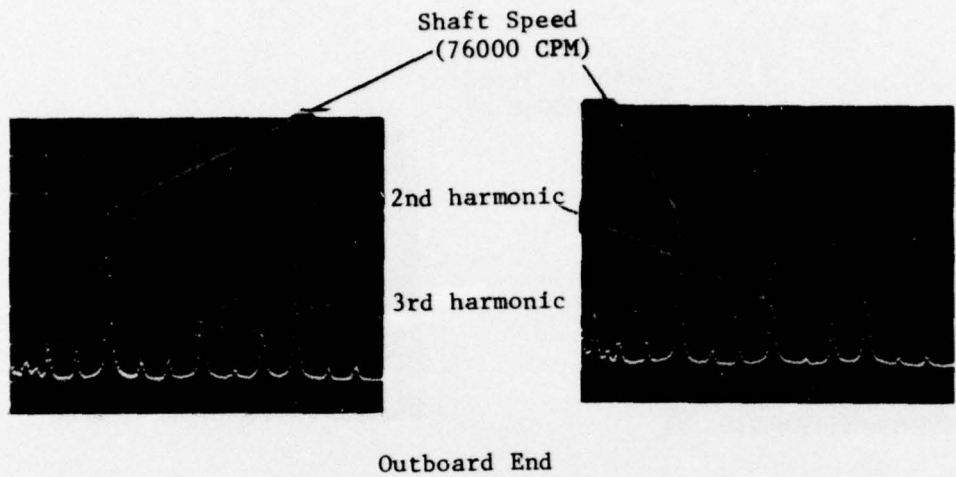


Figure 26. Frequency Spectrum, High Speed Component Testing, July, 1976

FRANKLIN INSTITUTE RESEARCH LABORATORIES
COMPLIANT MOUNTED GAS BEARING COMPONENT TESTING
SPRING MOUNTED BEARINGS (LARGE CLEARANCE)

JULY 2, 1976 TESTING

FREQUENCY SPECTRUM ANALYSIS
LOW FREQUENCY RANGE

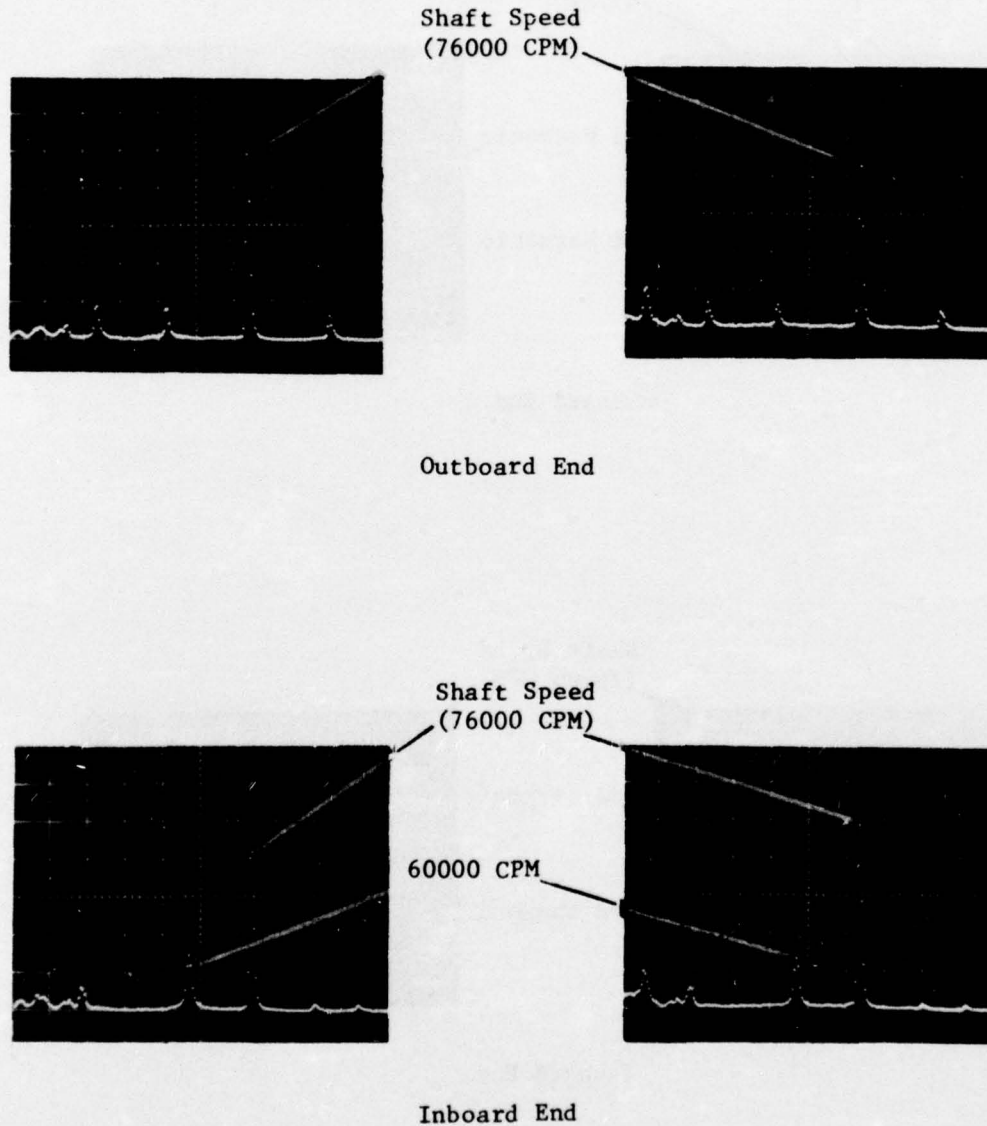


Figure 27. Frequency Spectrum, Reduced Range, High-Speed Component Testing, July, 1976

7. SIMULATOR TESTING OF SPRING-MOUNTED COMPLIANT-PIVOT BEARINGS

This section describes the final tests conducted at Solar using the spring-mounted journal bearings. The testing of the original compliant-mounted bearings at Solar is reported on in Section 8 of this report.

7.1 DESCRIPTION OF TEST RIG

Figure 28 shows an extended layout of the bearing test rig. The rotor system simulates closely the masses and inertias of the 10 KW turboalternator components. It includes a modified 10 KW turbine and simulated alternator and compressor rotors. The alternator rotor is supported between two journal bearings with the compressor and turbine rotors overhung from the aft end in the conventional back to back manner. The double acting thrust bearing is located between the aft journal bearing and the alternator rotor. The rotating assembly also includes a thrust piston outboard of the forward journal bearing. Thus, thrust loads on the bearing can be adjusted. Note that curvic couplings are used at all major rotor interfaces.

The latest version of the bearing cooling flow passages is shown on Figure 28. Three bearing air supplies are provided. One inlet is located at the starter end and this air supply exhausts through the alternator case. The starter end thrust bearing is fed through a separate inlet connection and exhaust through the exit passage between the double sided thrust bearing. The wheel end bearing supply passes through the wheel end journal bearing and thrust bearing and exhausts in the air outlet between the thrust bearings.

The X'd sections on the diagram indicate the original air inlets that were subsequently blocked and replaced. The original design allowed flow circuits that could bypass the bearings. The cross-section, Figure 28 also shows the location of the three planes where proximity probes were mounted for monitoring rotor vibrations. Photographs of the simulator rotor, bearings, housing and some of the instrumentation are shown on Figures 29 and 30.

7.2 DESCRIPTION OF INSTALLATION

The test rig was installed in Solar's test cell complex, cell 6, building 30. A schematic diagram is shown in Figure 31. The test was set up for completely manual operation except for overspeed shutdown and one bearing overtemperature shutdown. All data were manually taken.

Bearing air was supplied by the in-house low pressure system (90 psi) via a 20-micron filter. Each of the three rig supplies was measured and controlled separately. This

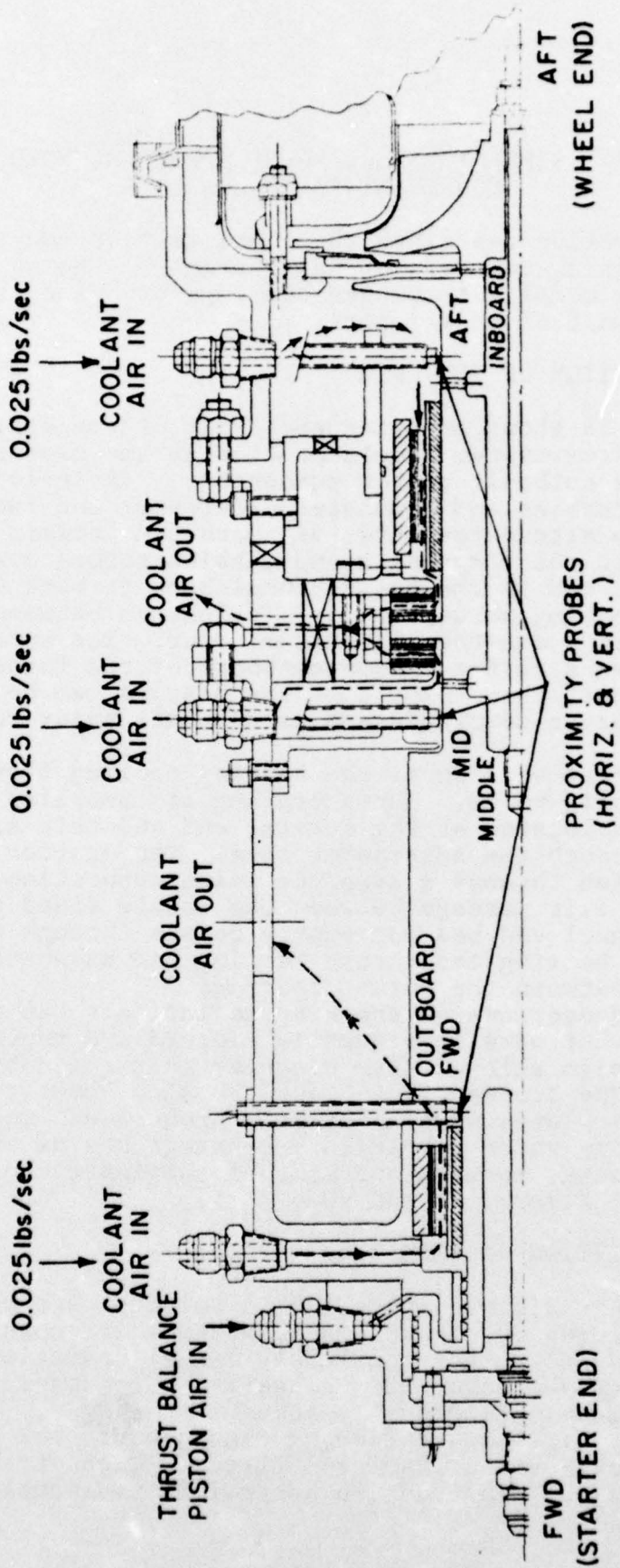
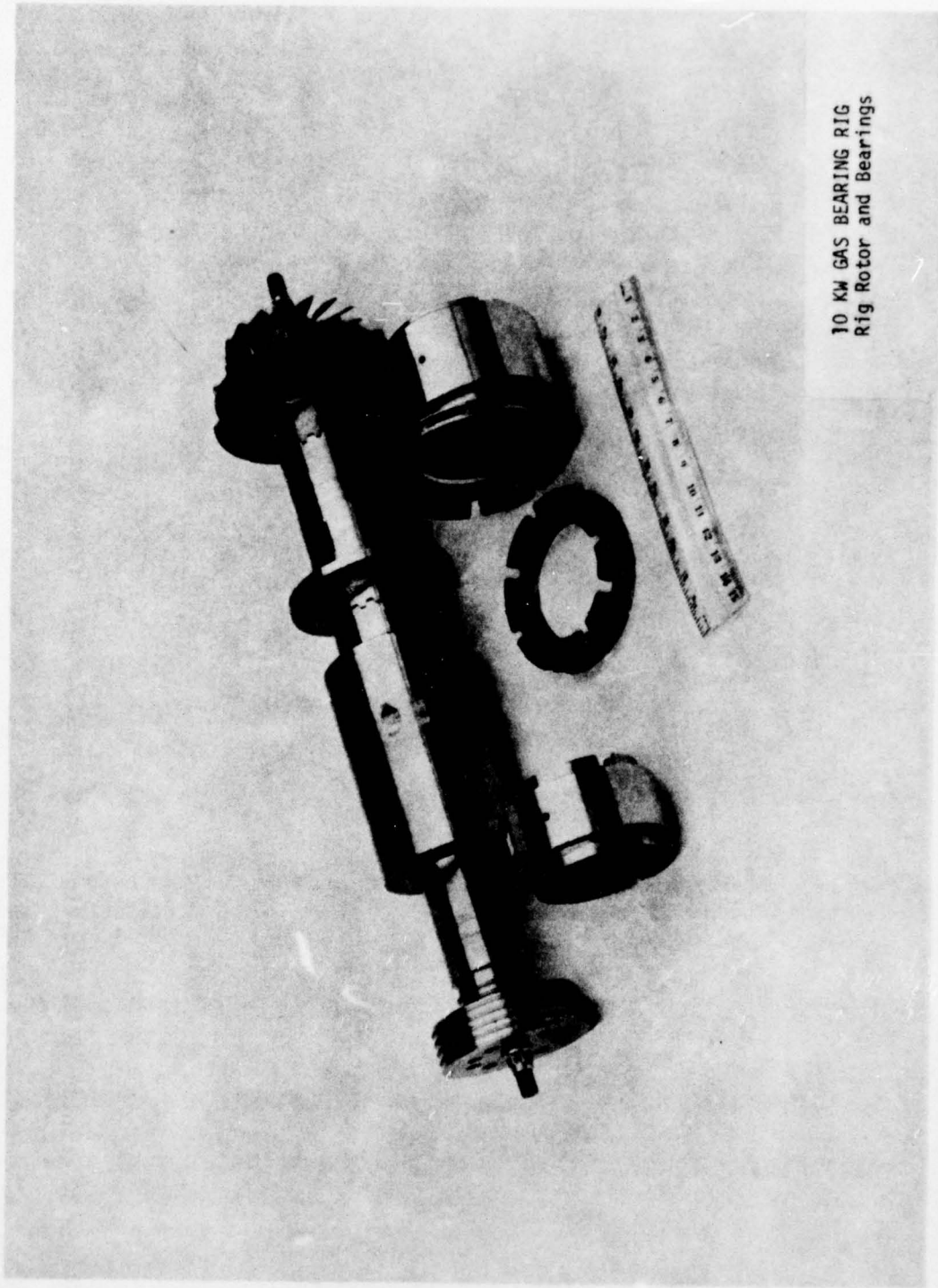


Figure 28. Solar Simulator Crosssection and Cooling Passages



10 KW GAS BEARING RIG
Rig Rotor and Bearings

Figure 29. Solar 10 KW Simulator Rotor and Gas Bearings

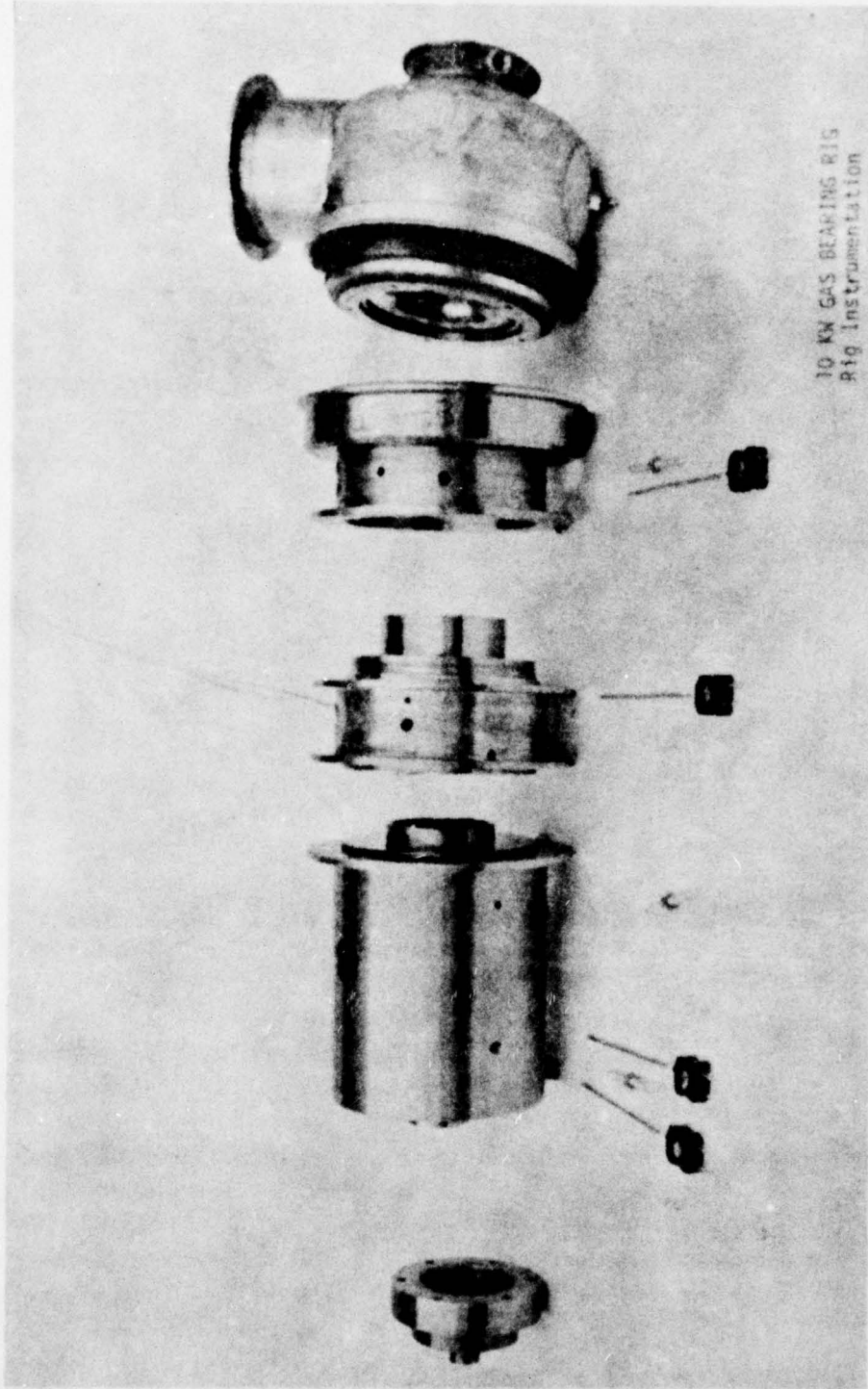


Figure 30. Solar 10 KW Simulator, Housing Components, Capacitance Probes and Thermocouples

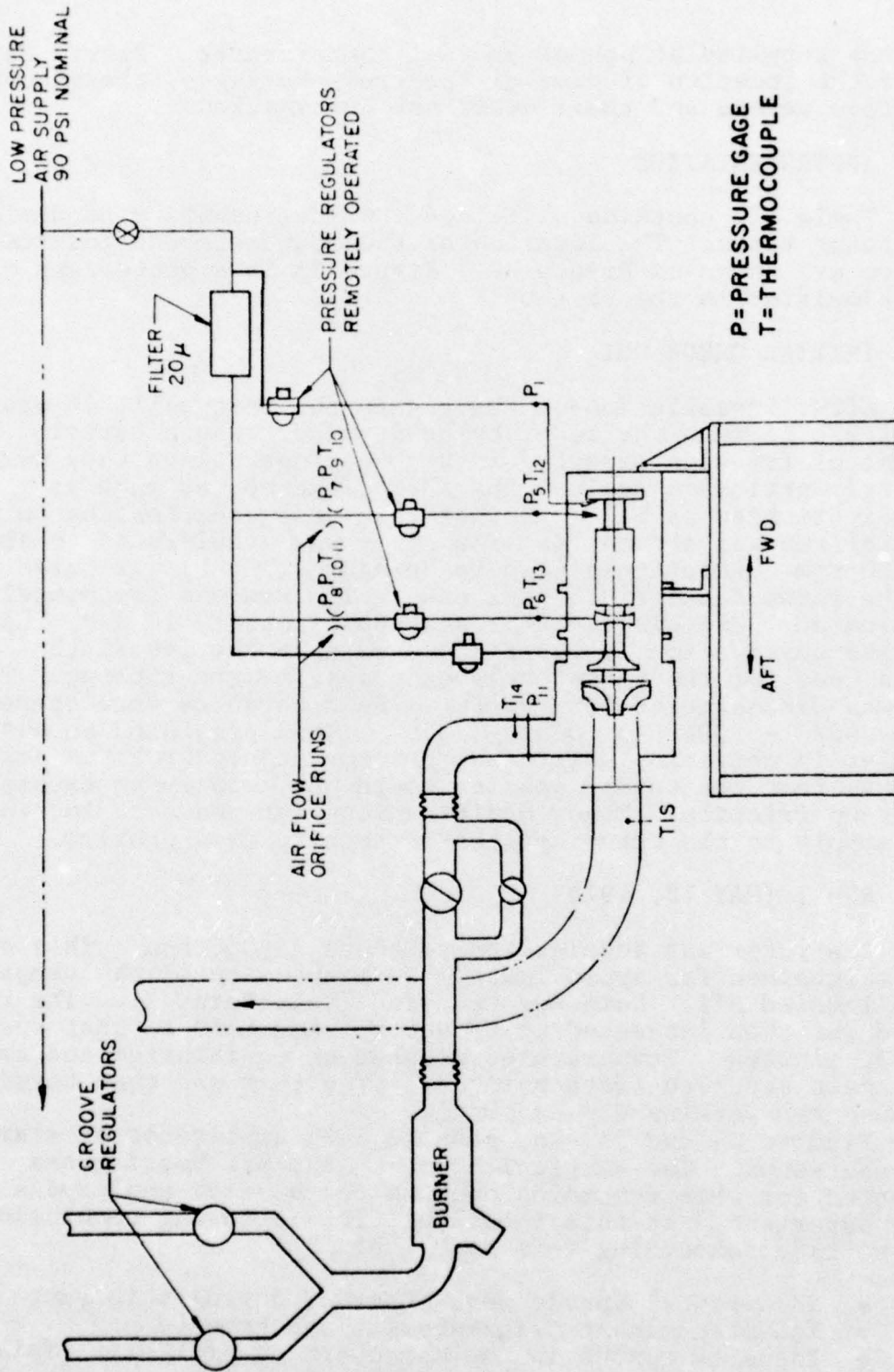


Figure 31. Schematic of Solar Test Loop

air was supplied at normal ambient temperatures. Figure 31 shows the location of some of the pressure gages, thermocouples and flow meters and their numerical designations.

7.3 INSTRUMENTATION

Table VII contains a list of the instruments used during simulator tests. The location of the most relevant instrumentation are shown on Figure 32. Figure 33 is a photograph of the simulator in the test cell.

7.4 INITIAL CHECK-OUT

After installation of the rig in the test cell, it was difficult to turn the rotor by hand. There was a certain amount of friction expected in the bearings, since they were slightly preloaded against the shaft, but not as much as was experienced at FIRL. Rather than delay the testing an initial run was attempted. The rotor was accelerated to about 30,000 rpm. Relatively high temperature (120°F) was noted in the forward labyrinth seal area. The run was immediately terminated. The elapsed time was approximately 20 sec. Upon further observation it was discovered that the labyrinth seals used for the thrust balancing system were rubbing. The rig was disassembled for rework. The clearances were opened from .002" - .004" to .020" - .030". This presented an additional problem in obtaining sufficient pressure to control the axial load so that the thrust bearing would not experience excessive start-up friction. Minor modifications were made to increase air supply to the thrust piston to rectify this problem.

7.5 RUN 1 (MAY 18, 1976)

The rotor was accelerated to about 35,000 rpm. This speed was maintained for approximately 10 minutes until the temperature leveled off. Data was recorded (Data Point 2). The rotor speed was then increased to 47,000 rpm and held at that speed for 30 minutes. Temperatures reached an equilibrium and data was again recorded (data point 3). The test was then terminated because the working day had ended.

Figures 34 and 35 show peak to peak amplitudes at start-up and shut-down. The vertical probe on the aft bearing was selected for this recording because the maximum amplitudes were experienced at this location. The following conclusions can be made concerning this test run:

- No critical speeds were observed during this run
- The predominant frequency was synchronous
- There is runout in the neighborhood of 1 mil. This was thought to be electrical. Therefore the actual amplitude is approximately .5 mils.

Table VII. Solar 10 KW Gas Bearing Test Rig - Instrumentation List

Item	Ident	Parameter	Instrumentation
1		radial displacement of rotor at planes 1, 2, and 3	6 proximity probes 2.5 L 6 proximitors Bently Nevada 3 oscilloscopes
2		Axial displacement of rotor	1 proximity probe (306L36) 1 proximitor Scope or RMS voltmeter
3		Motor speed	Magnetic pickup (3055A) AC-DC converter for O/S protection Frequency counter
4	P1	Static pressure on high pressure side of thrust piston	Mercury column/wall static tap
5	P2	Static pressure on LP side of thrust piston	Mercury column/wall static tap
6	P3	Forward thrust bearing air inlet static pressure	Water column/wall static tap
7	P4	Aft thrust bearing air inlet static pressure	Water column/wall static tap
8	P5	Fwd bearing cooling air rig inlet pressure	Water column/wall static tap
	P6	Aft bearing cooling air rig inlet pressure	Water column/wall static tap
10	P7	Fwd bearing flow measurement orifice upstream pressure	Mercury column/wall static tap
11	P8	Aft bearing flow measurement orifice upstream pressure	Mercury column/wall static tap
12	P9	Fwd bearing flow measurement orifice pressure drop	Water column/wall static taps
13	P10	Aft bearing flow measurement orifice pressure drop	Water column/wall static taps
14	P11	Turbine drive air - rig inlet pressure	Bourdon tube gage
15	T1A T1B	Forward radial bearing air inlet temperature	2 I/C thermocouples, P/N 110036-1
16	T2A T2B	Forward radial bearing air outlet temperature	2 I/C thermocouples, P/N 110036-1
17	T3A T3B	Forward thrust bearing air inlet temperature	2 bare bead I/C thermocouples mag pack
18	T4A T4B	Combined air outlet temperature for both thrust bearings	2 I/C thermocouples, P/N 110036-1
19	T5A T5B	Combined air inlet temperature for aft thrust & radial bearings	2 I/C thermocouples, P/N 110036-1
20	T6A T6B	Aft radial bearing air outlet temperature	2 I/C thermocouples, P/N 110036-1
21	T7	Combined temperature of housing for aft thrust & radial bearings	1 I/C thermocouple 'flexible wire' mag pack
22	T8	temperature	
23	T9	Forward radial bearing housing temperature	1 I/C thermocouple mag pack
24	T10	Forward bearing flow orifice air temperature	1 half shield I/C thermocouple P/N 110035-8
25	T11	Aft bearing flow orifice air temperature	1 half shield I/C thermocouple P/N 110035-8
26	T12	Forward bearing air, rig inlet temperature	1 I/C thermocouple, P/N 110035-8
26	T13	Aft bearing air, rig inlet temperature	1 I/C thermocouple, P/N 110035-8
27	T14	Turbine drive air, rig inlet temperature	1 I/C thermocouple, P/N 110036-1
28	T15	Turbine drive air, rig outlet temperature	1 I/C thermocouple, P/N 110036-1
29		Rig case vibration	Endevco accelerometer and charge amplifier

- NOTE: 1. A waveform harmonic analyzer and suitable recorders will be available for detail analysis of performance
2. Proximity probes monitoring radial displacement will be calibrated at predicted operating temperature prior to commencement of the test.
3. The following were added during Build 2

30	T7 1/2A T7 1/2B	Aft thrust bearing air temperature	2 bare bead I/C thermocouples
31	T8 1/2A T8 1/2B	Forward thrust bearing air temperature	2 bare bead I/C thermocouples

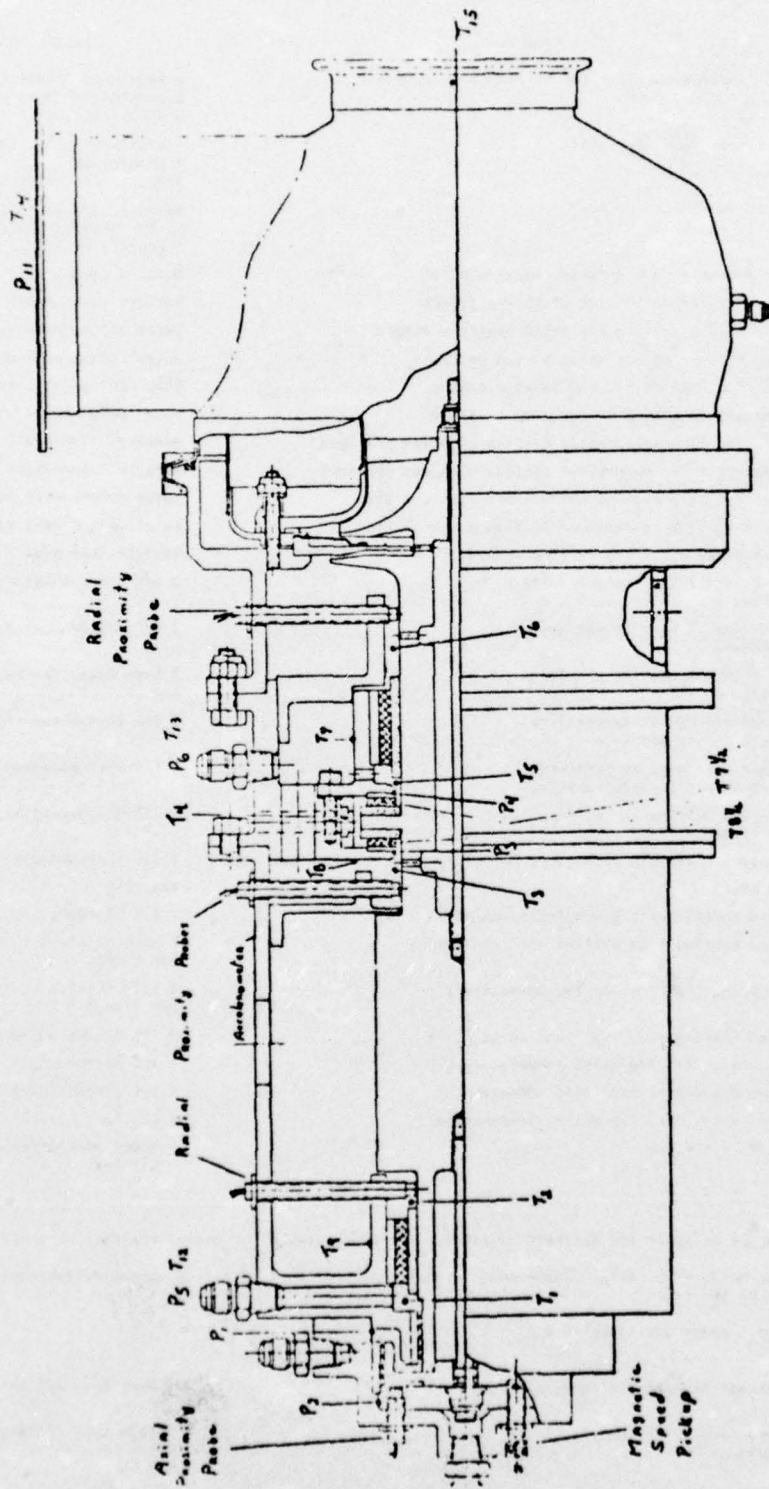
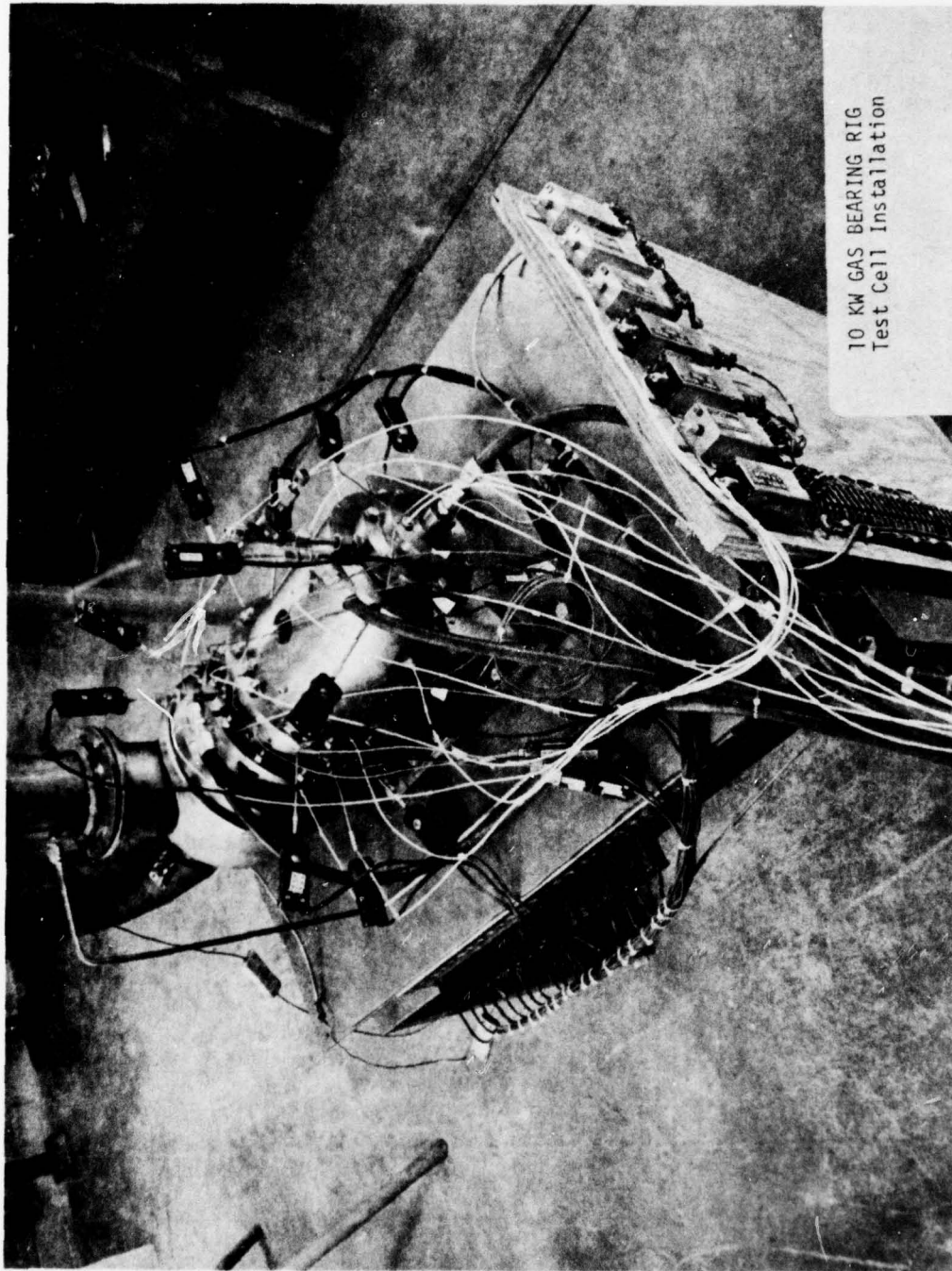


Figure 32. 10 KW Gas Bearing Test Rig Instrumentation



10 KW GAS BEARING RIG
Test Cell Installation

Figure 33. 10 KW Gas Bearing Rig - Test Cell Installation

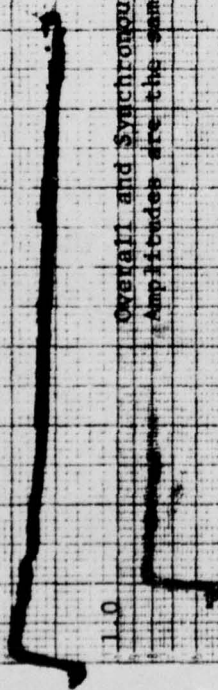
FRANKLIN INSTITUTE RESEARCH LABORATORIES
 COMPLIANT MOUNTED GAS BEARING TESTING
 1 KW SIMULATOR TESTING AT SOLAR

May 18, 1976 Testing (data points 2, 3)
 Inboard Vertical Probe location
 Amplitude vs Operating Speed

Start up

100% Speed = 94000 RPM

Overall and Synchronous
 Amplitudes are the same.



Peak-Peak Amplitude, Mile

Operating Speed, Percent

100%

90

80

70

60

50

40

30

20

10

Figure 34. Amplitude vs. Start-up Speed, Simulator Test, May 18, 1976

FRANKLIN INSTITUTE RESEARCH LABORATORIES
 COMPLIANT MOUNTED GAS BEARING TESTING
 10 KW SIMULATOR TESTING AT SOLAR

May 18, 1976 Testing (data points 2, 1)
 Inboard Vertical Probe Location
 Amplitude vs Operating Speed

Shut Down

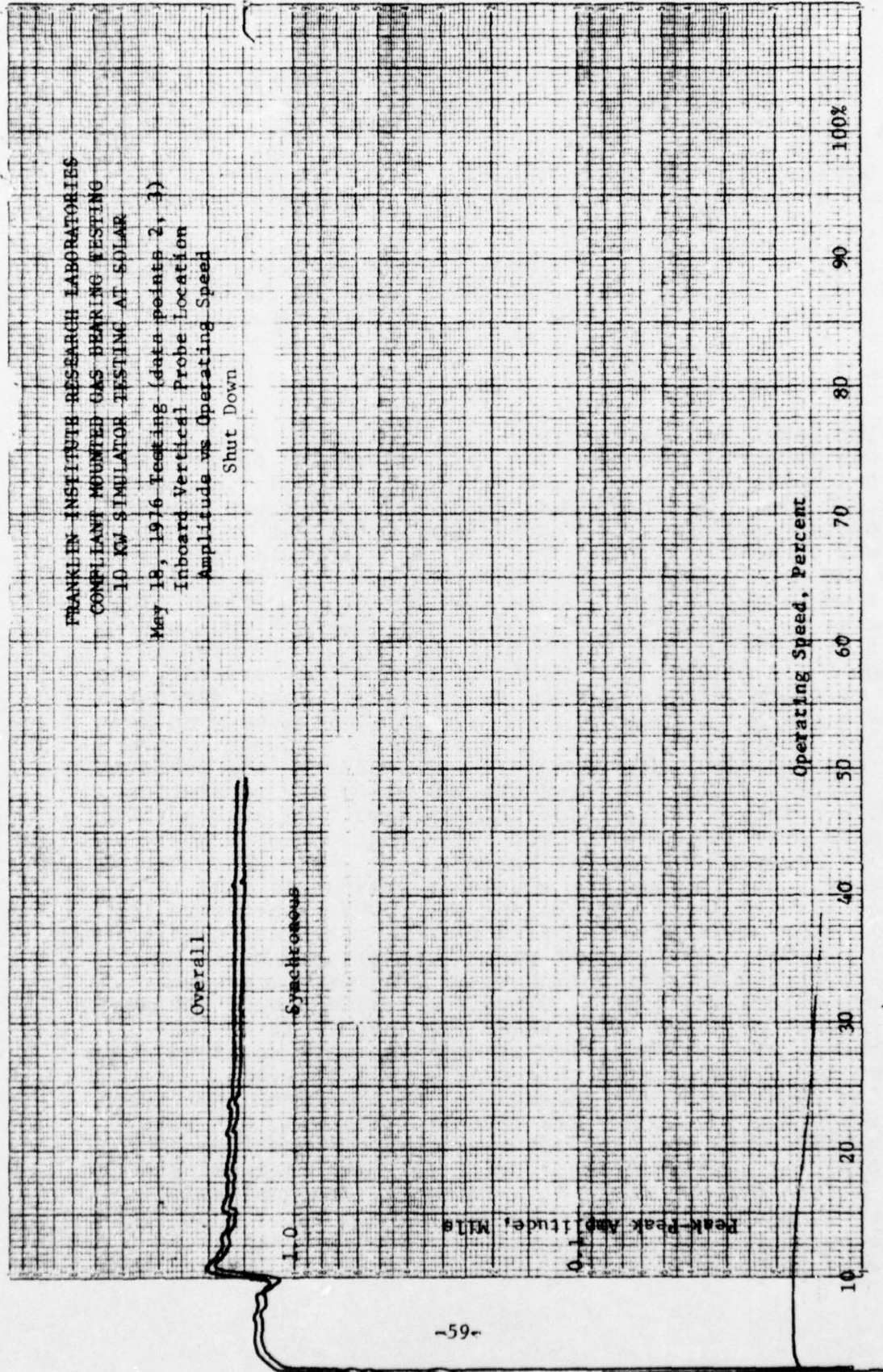


Figure 35. Amplitude vs. Shutdown Speed, Simulator Test, May 18, 1976

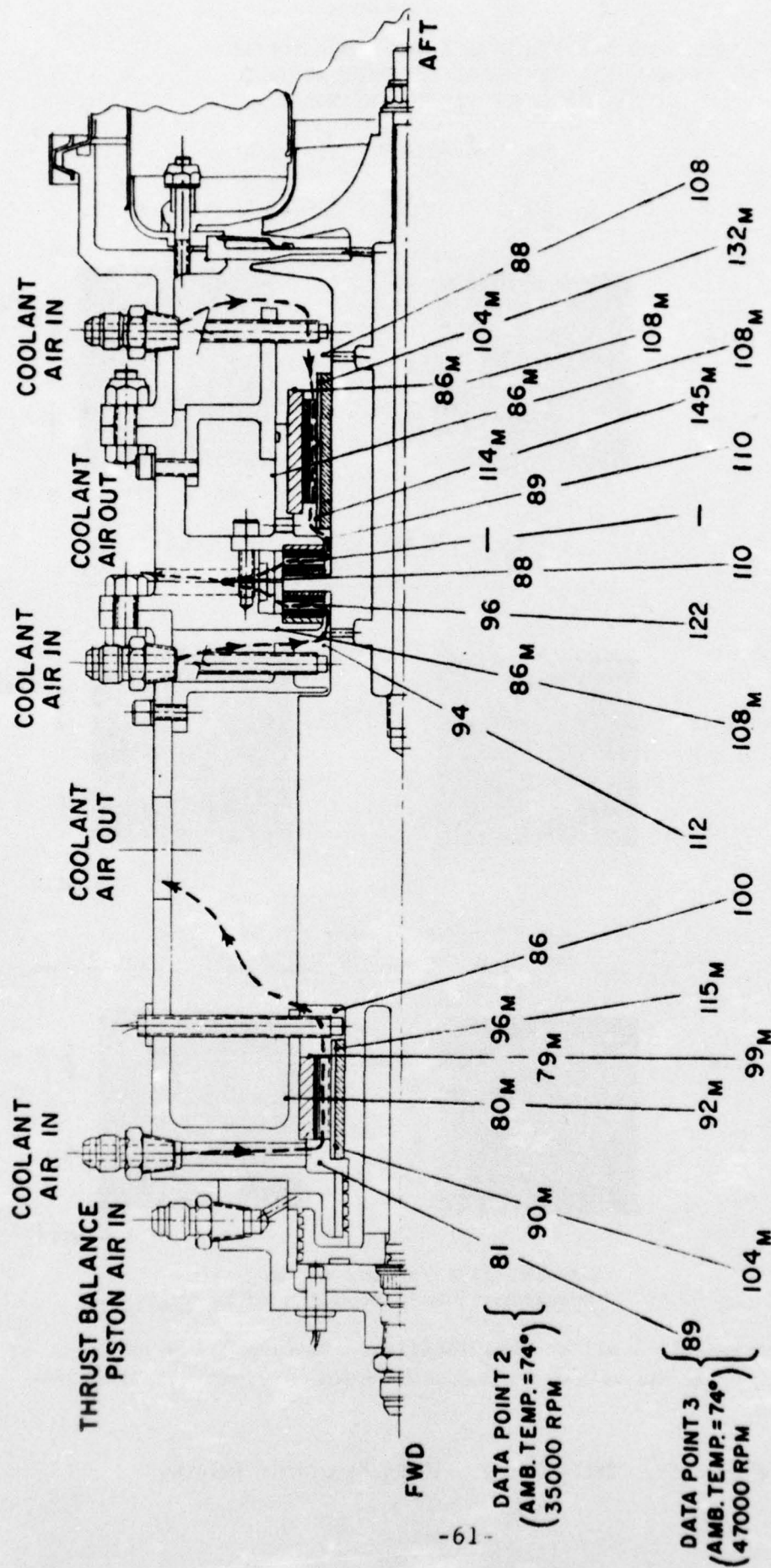
Figure 36 illustrates the temperatures recorded for this run. The maximum temperature (145°F) occurs at the carbon steel interface of the pad of the aft journal bearing. Since most of the heat is caused by the friction losses in the bearings, the thermocouple mounted on the bearing pads will have the highest temperature. These temperatures are well below design goals (250°F - 300°F).

Orbit traces are shown in Figure 37 for all the testing. The location of these displacement probes is shown on Figures 28 and 32. Note all the actual amplitudes for the May 18, 1976 testing are under a mil since the rotor experienced electrical runout of about 1 mil.

7.6 RUN 2 (MAY 19, 1976)

The rotor was accelerated to approximately 47,000 rpm. Data was recorded as data point 4, with similar results as data point 3. The rotor speed was then gradually increased to 62,600 rpm. This speed was maintained for approximately 15 minutes until the temperature leveled off, at which time data was taken (data point 5). Figure 37 contains the orbit plots for data point 5. At the higher speeds, the amplitudes increased, especially at the forward bearing location. The runout is not present in this picture. The peak amplitude is 1.6 mils as compared to .5 mils for run 1. Figures 38 through 43 illustrate the vibration frequencies present, and their relative importance, for the vertical probes for data points 4 and 5. Note that the predominant frequency is synchronous in all cases. The subsynchronous frequencies are less than 60 μ -in. Maximum amplitudes occur at the inboard (aft) probe. Figure 44 shows the temperature distribution for data points 4 and 5. The temperatures have substantially increased over the previous run. The highest temperature of 206°F occurred on the aft bearing pad. Note that the coolant air temperature through the wheel-end bearing is only 143°F and the bearing shell and housing are 140°F. Therefore the rubber temperature of this bearing still must remain relatively cool (< 200°F). The highest rubber temperature would have to occur in the thrust bearing where the maximum coolant air temperature was 196°F. Since the bearings were designed for temperature above 250°F these temperature levels are acceptable. The coolant flow at each entrance remained above recommended values during this run (\approx .025 lb/sec).

The rotor speed was increased. As the speed approached 65,000 rpm the amplitude grew rapidly, from 1.4 to 4 mils. The pad temperature on the aft bearing increased from 206°F to 220°F. At this point an attempt was made to terminate the run. Before the run could be terminated, the amplitude grew to such an extent that the bearing and rotor contacted. Pad temperature went off the scale (> 800°F). Amplitude increased above 12 mils. The rotor decelerated in less than 5 sec.

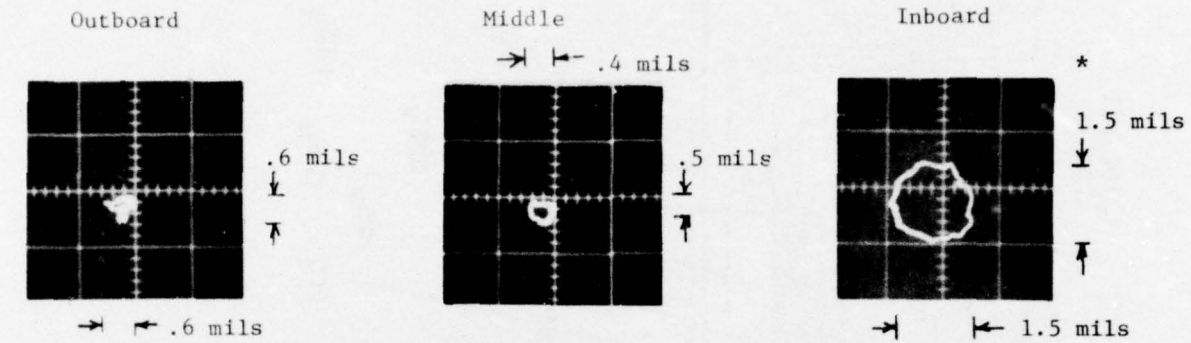


NOTE - M INDICATES METAL TEMPERATURE

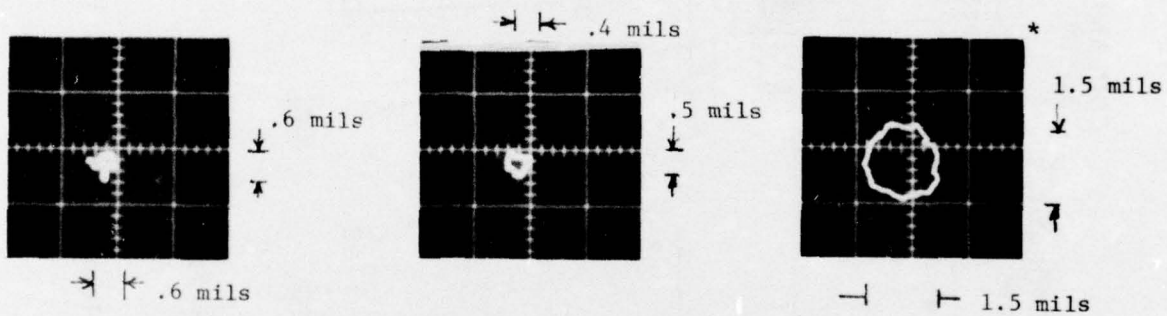
Figure 36. Recorded Temperatures, Run No. 1

FRANKLIN INSTITUTE RESEARCH LABORATORIES
 COMPLIANT MOUNTED GAS BEARING TESTING
 10 KW SIMULATOR TESTING AT SOLAR

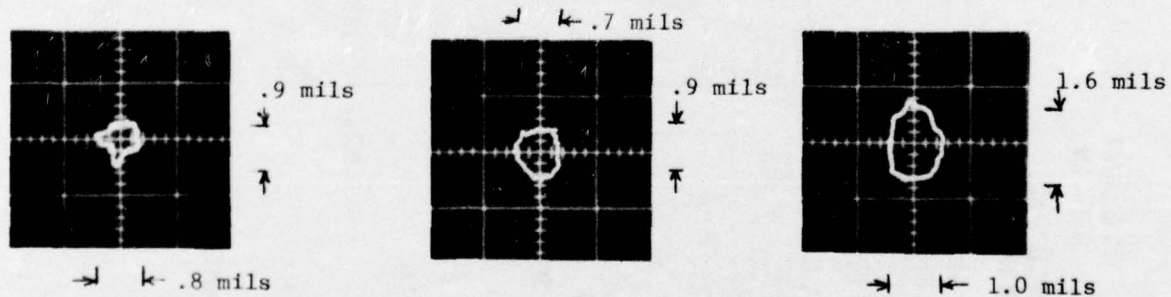
ORBIT ANALYSIS



May 18, 1976 Testing (10 min. run)
 Operating Speed 35000 RPM (data point 2)



May 18, 1976 Testing (30 min. run)
 Operating speed 47000 RPM (data point 3)



May 19, 1976 Testing (15 min. run)
 Operating speed 62600 RPM (data point 5)

* The runout is approximately 1 mil at this location. Therefore 1.0 mils should be subtracted from the values indicated to obtain the actual amplitude.

Figure 37. Orbit Traces, 10 KW Simulator Testing

FRANKLIN INSTITUTE RESEARCH LABORATORIES
COMPLIANT MOUNTED GAS HEARING TESTING
10 KW SIMULATOR TESTING AT SOLAR

FREQUENCY SPECTRUM ANALYSIS
MAY 19, 1976 TESTING (Data Point 4)
Outboard Vertical Probe Location
Operating Speed 47,000 RPM

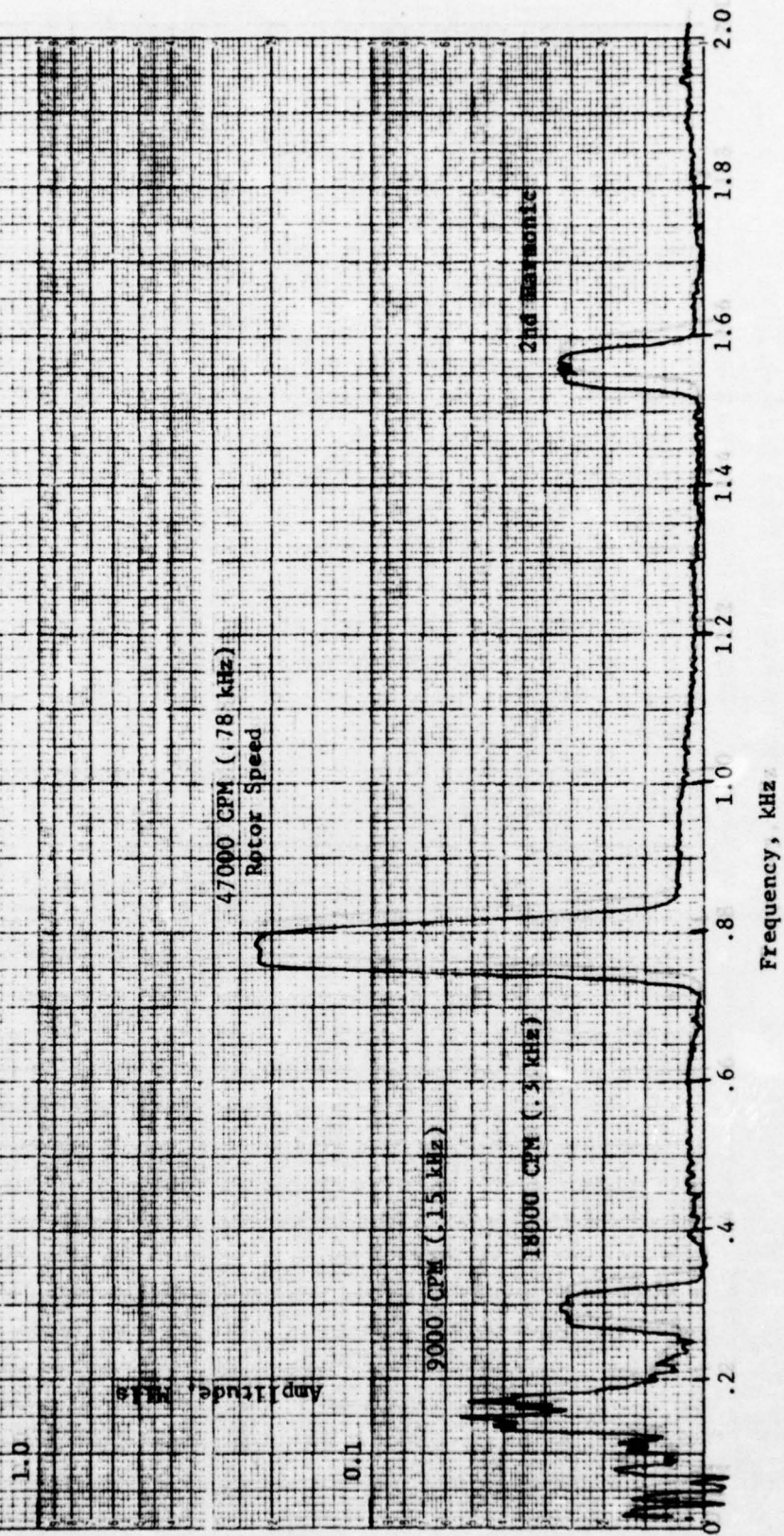


Figure 38. Amplitude vs. Frequency, Data Point 4, Outboard Vertical Probe

FRANKLIN INSTITUTE RESEARCH LABORATORIES
COMPLIANT MOUNTED GAS BEARING TESTING
10 KW SIMULATOR TESTING AT SOLAR

FREQUENCY SPECTRUM ANALYSIS
May 19, 1976 Testing (Data Point 4)
Middle Vertical Probe Location
Operating Speed 47000 RPM

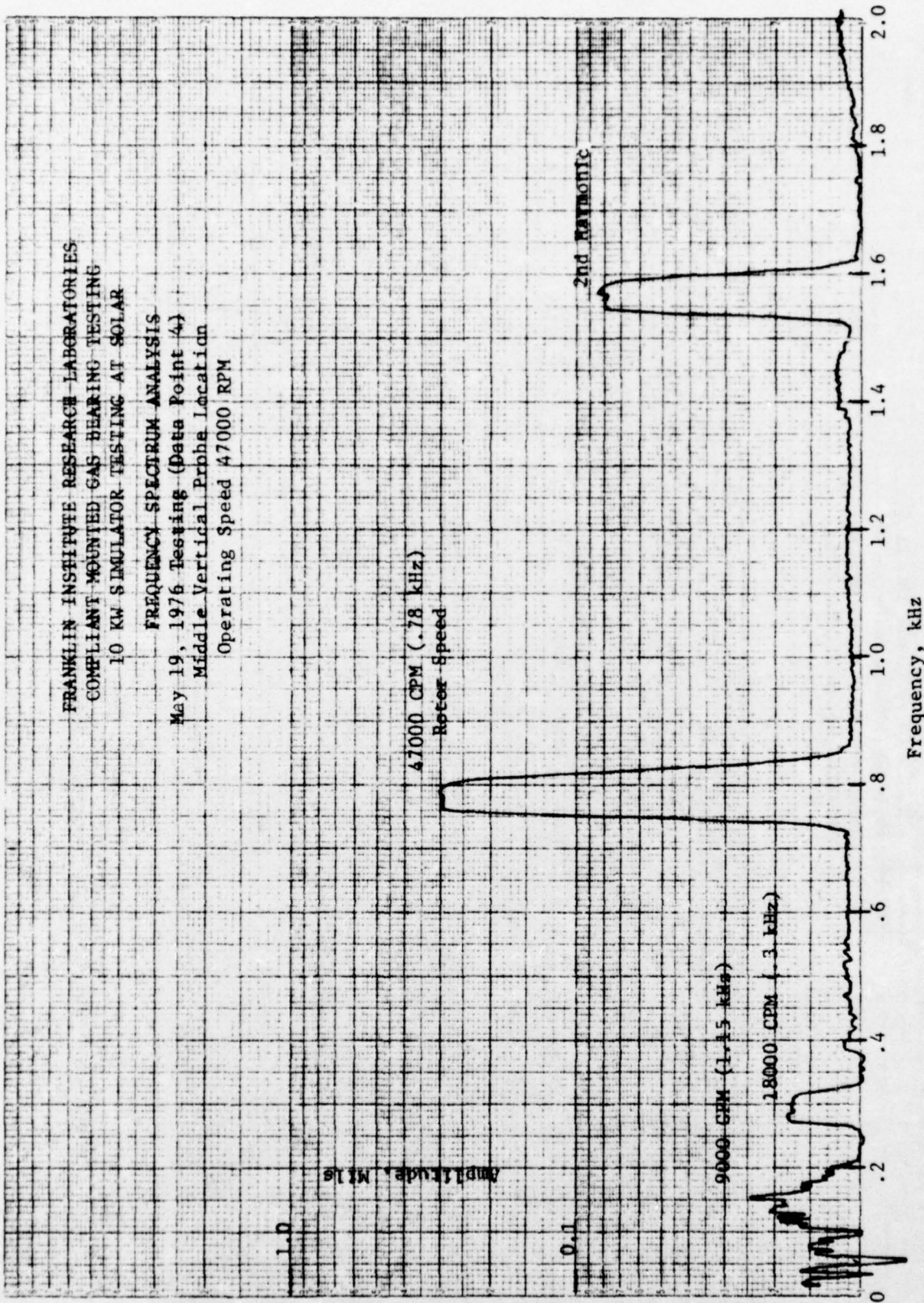


Figure 39. Amplitude vs. Frequency, Data Point 4, Middle Vertical Probe

FRANKLIN INSTITUTE RESEARCH LABORATORIES
 COMPLIANT MOUNTED GAS BEARING TESTING
 10 KW SIMULATOR TESTING AT SOLAR

FREQUENCY SPECTRUM ANALYSIS
 May 19, 1976 Testing (Data Point 4)
 Inboard Vertical Probe Location
 Operating Speed 47000 RPM

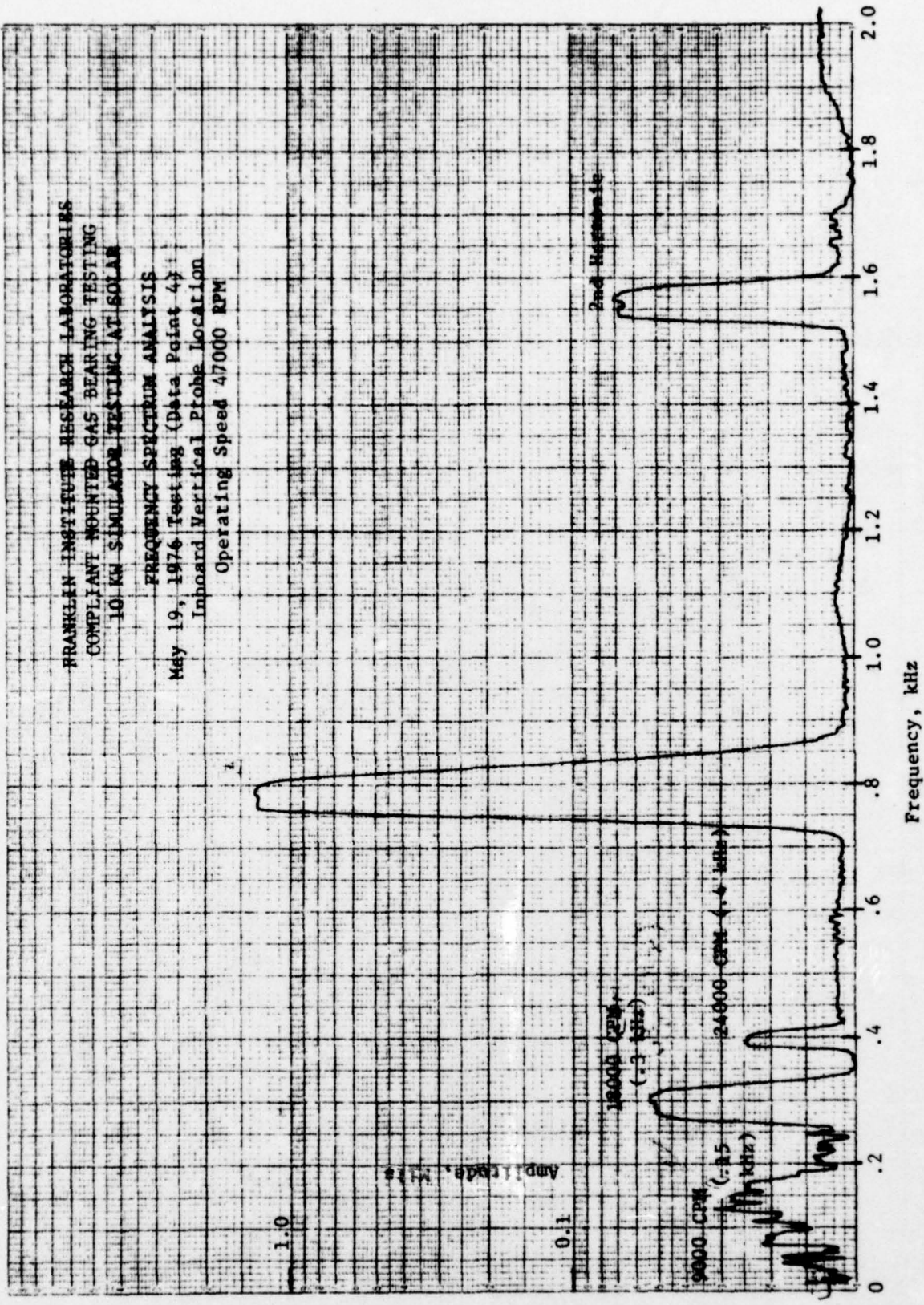


Figure 40. Amplitude vs. Frequency, Data Point 4, Inboard Vertical Probe

FRANKLIN INSTITUTE RESEARCH LABORATORIES
COMPLIANT MOUNTED GAS BEARING TESTING
10 KW SIMULATOR TESTING AT SOLAR

FREQUENCY SPECTRUM ANALYSIS
May 19, 1976 Testing (Data Point 5)
Outboard Vertical Probe Location
Operating Speed 62600 RPM

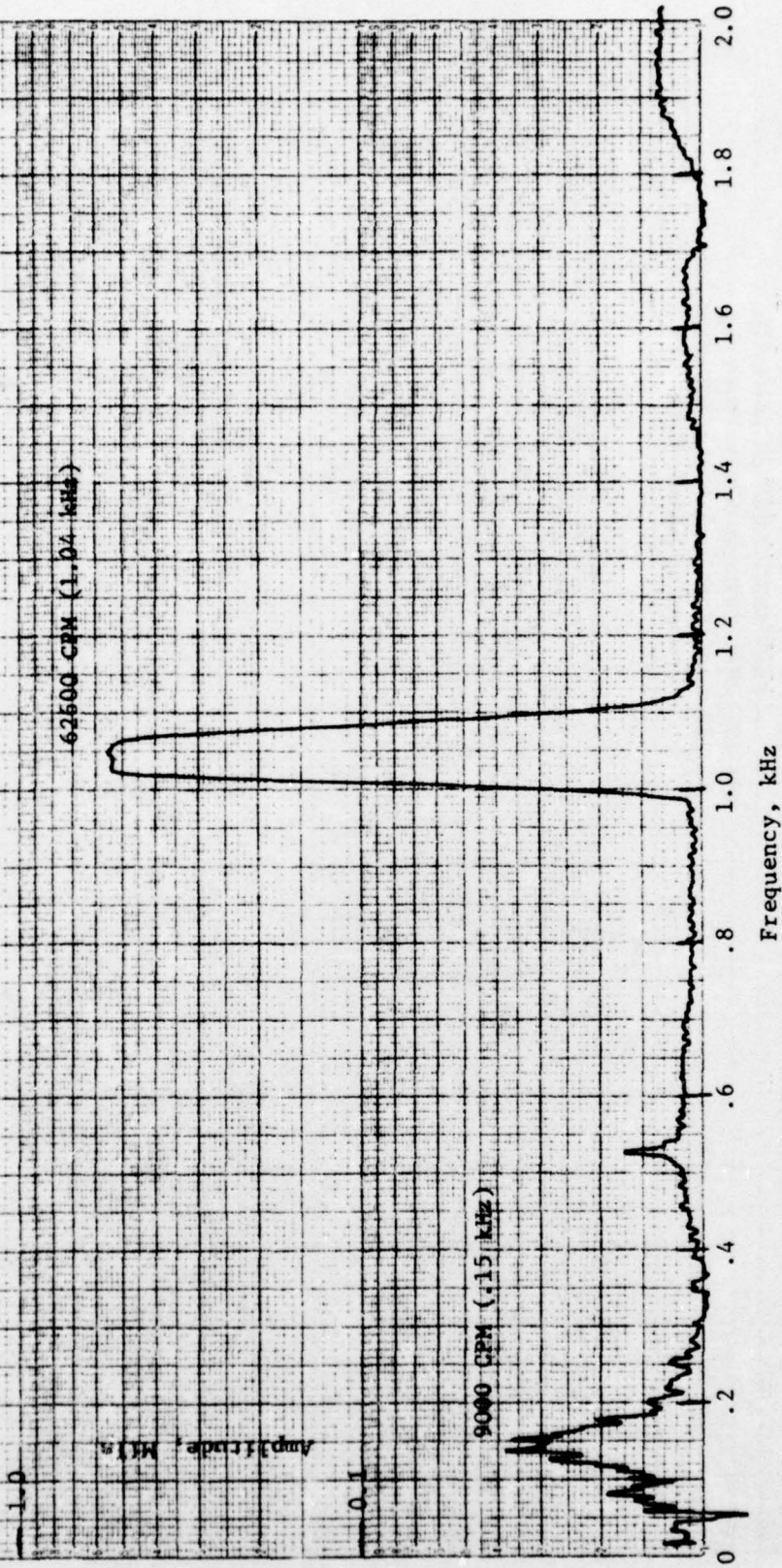


Figure 41. Amplitude vs. Frequency, Data Point 5, Outboard Vertical Probe

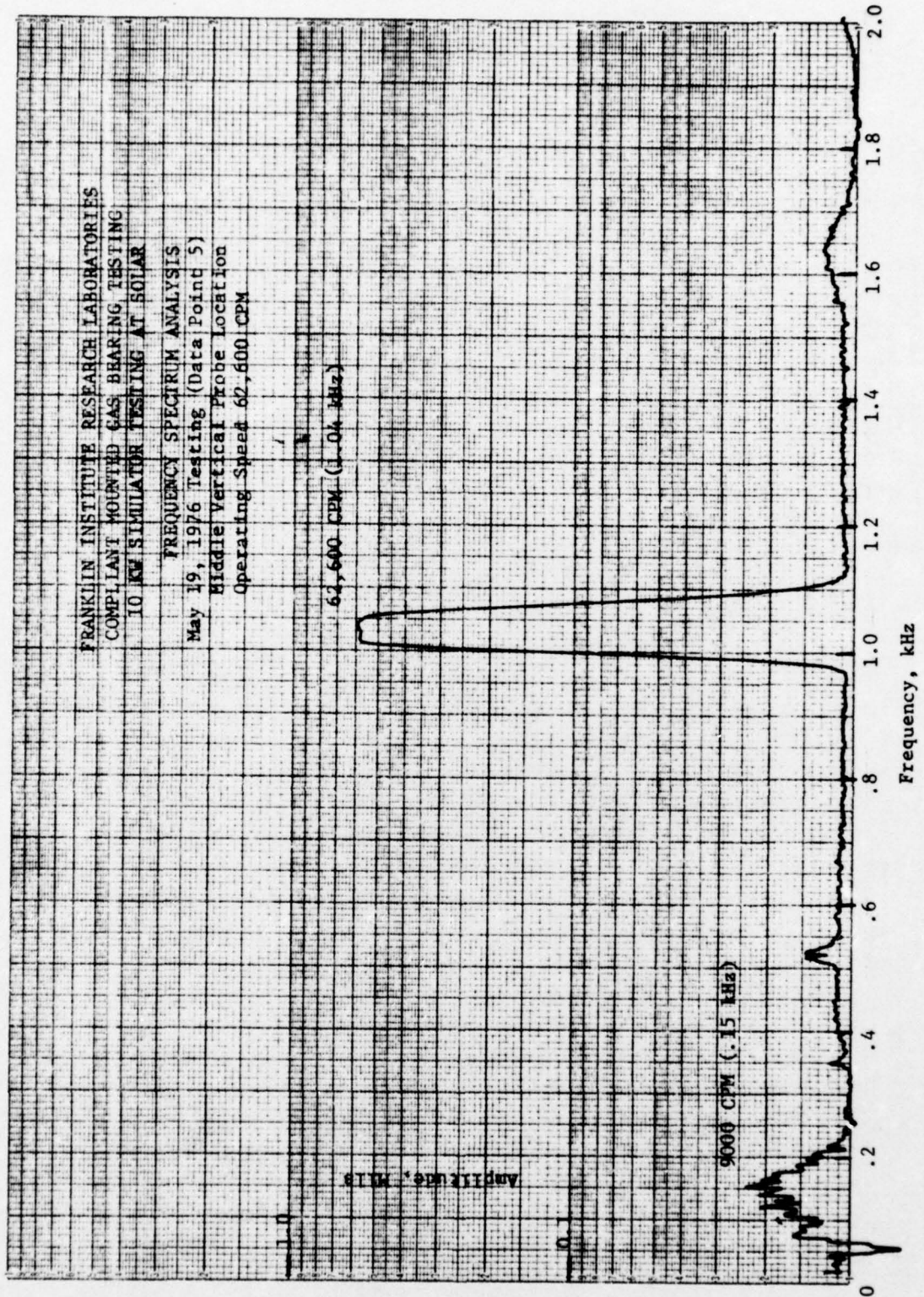


Figure 42. Amplitude vs. Frequency, Data Point 5, Middle Vertical Probe

FRANKLIN INSTITUTE RESEARCH LABORATORIES
COMPLIANT MOUNTED GAS BEARING TESTING
10 KW SIMULATOR TESTING AT SOLAR

FREQUENCY SPECTRUM ANALYSIS
May 19, 1976 Testing (Data Point 5)
Inboard Vertical Probe Location
Operating Speed 62,600 CPM

62,600 CPM (1.04 kHz)

9000 CPM (.15 kHz)

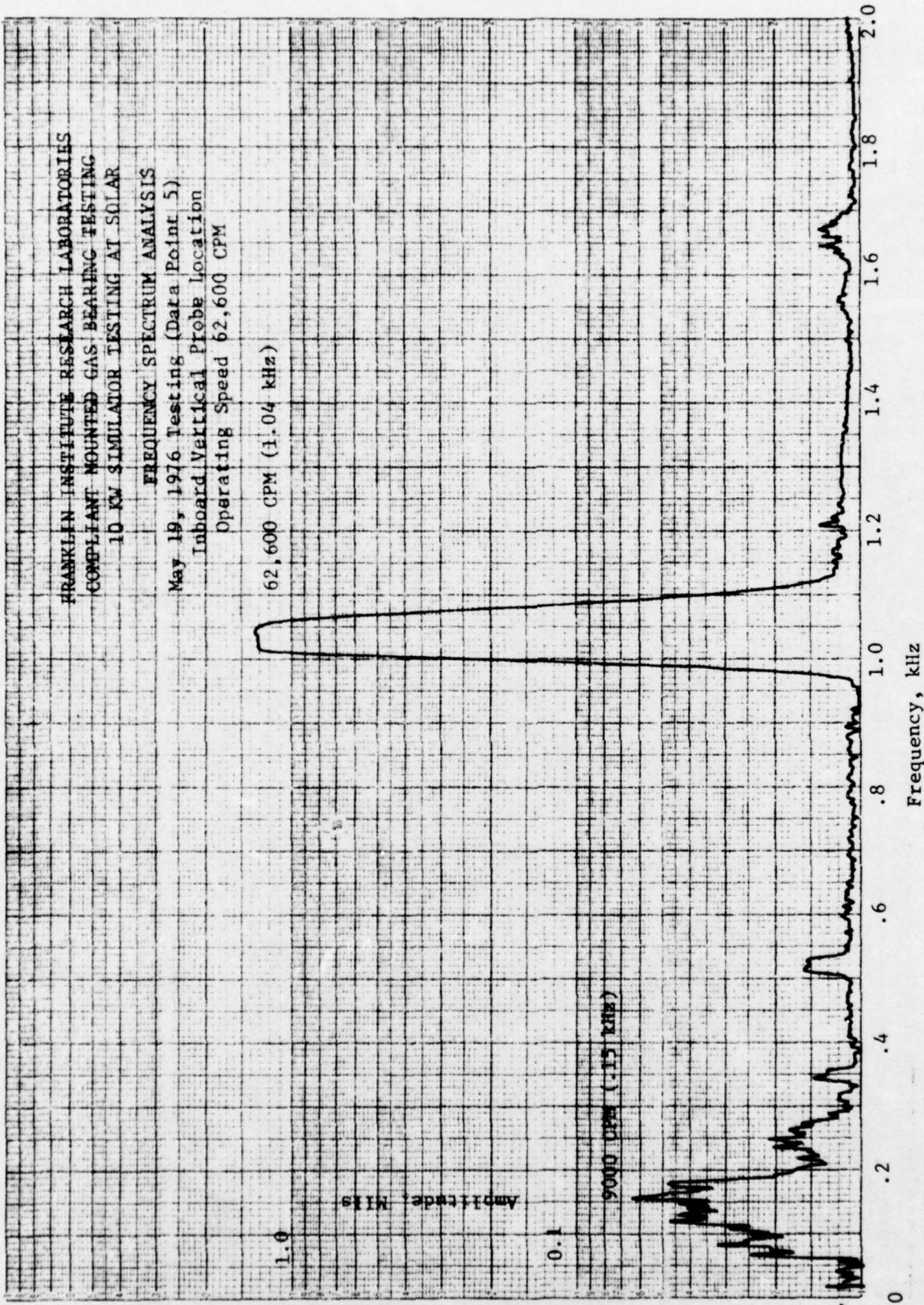
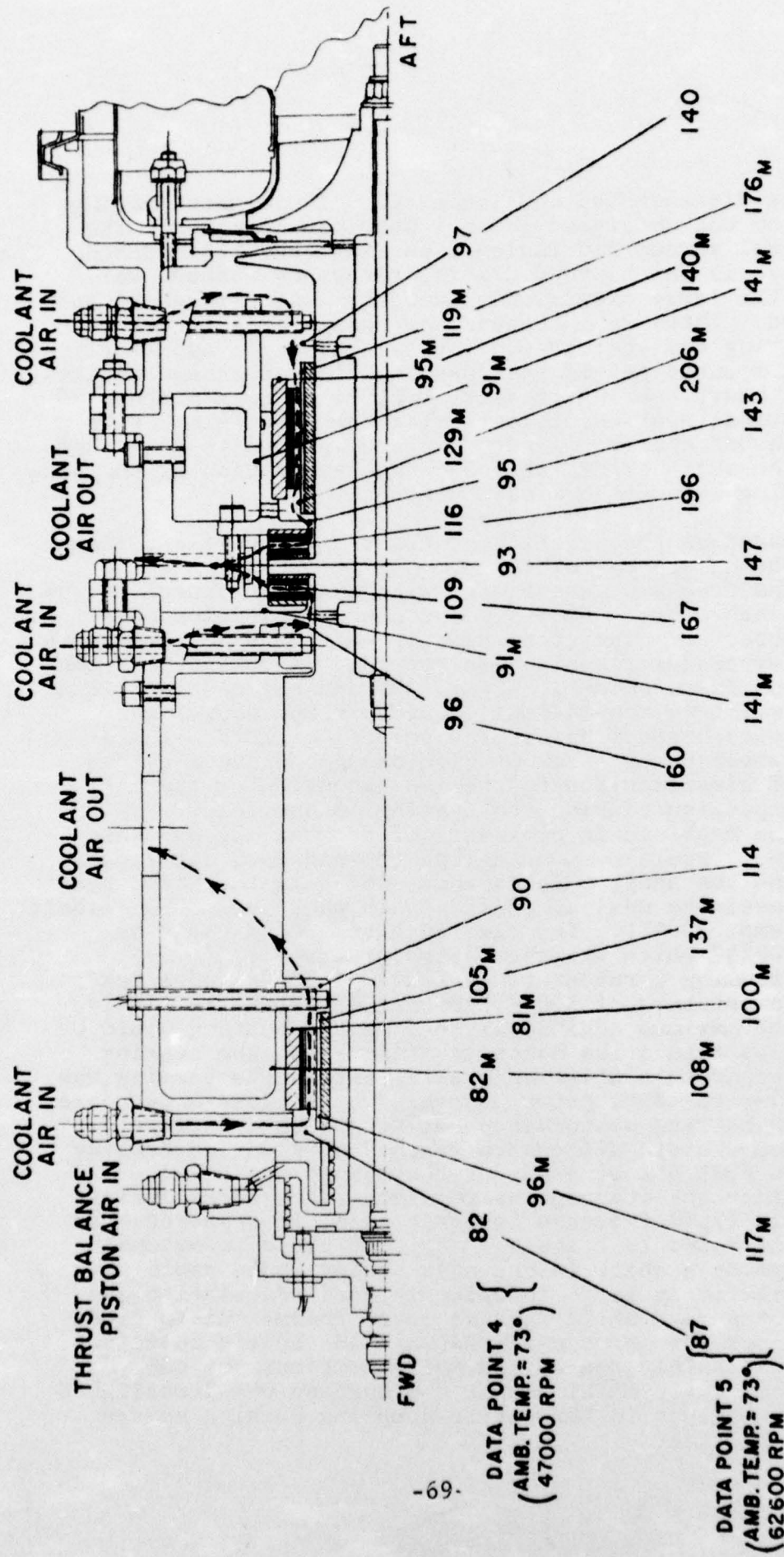


Figure 43. Amplitude vs. Frequency, Data Point 5, Inboard Vertical Probe



NOTE - M INDICATES METAL TEMPERATURE

Figure 44. Recorded Temperatures, Run No. 2

The rig was disassembled and inspected. There were bearing rub marks on the wheel-end journal bearing and rotor. The turbine wheel shroud had indications that they had touched. The labyrinth seals which had 0.020 in. clearance rubbed, which indicated the large excursions the rotor went through at the starter end. There was, however, no damage at all to the thrust bearing and starter-end journal bearing. Apparently the spring mounted pad of each bearing allowed enough movement to prevent heavy bearing contact. Figure 45 is a picture of the aft journal bearing, illustrating the rub marks. Note that the thrust bearing is not damaged. Figure 46 is a photograph of the shaft after the rub. Upon evaluation of the data the following observations were made:

- Based on the severity of the rub and past experience, the damage was minimal
- The frequency associated with the high vibration was synchronous. No subsynchronous frequencies were observed. Therefore bearing whirl was not the cause
- Temperature levels were recorded minutes before the rub (data point 5, Figure 44) and the pad temperature (which is the maximum recorded temperature) was noted seconds before the rub to be 220°F. These temperatures are not high enough to cause a loss of clearance due to thermal expansion or thermal expansion causing the bearing to overload. The machined-in clearance of the bearing pad was .004" radial. Considering the pad does not expand and the shaft only expands, which is the worst possible case, the maximum shaft growth would be .0015" (shaft temp. 300°F). The clearance remaining would be .0025" which was the design clearance. Assuming a rubber temperature of 200°F and a shaft temperature of 300°F, neither of which are likely, the maximum additional load on the bearing would be less than 3 lbs which is minimal for the bearing.
- Temperature difference axial across the bearing was 30°F for data point 5. This would cause a decrease in bearing performance but not cause a failure. Temperature difference reached 40°F during testing at FIRL but at a much reduced absolute value.
- Since the frequencies remained synchronous during the rapid increase in orbit size, it appeared that the rotor lost its balance. At these rotational speeds a shift in the mass center would cause a relatively large rotational load. Possibilities for a mass shift include rotor thermal distortions under the aft bearing between the curvic couplings. Or possibly due to thermal conditions, the dummy compressor wheel and/or the turbine wheel realigned themselves in the curvic coupling causing severe unbalance.

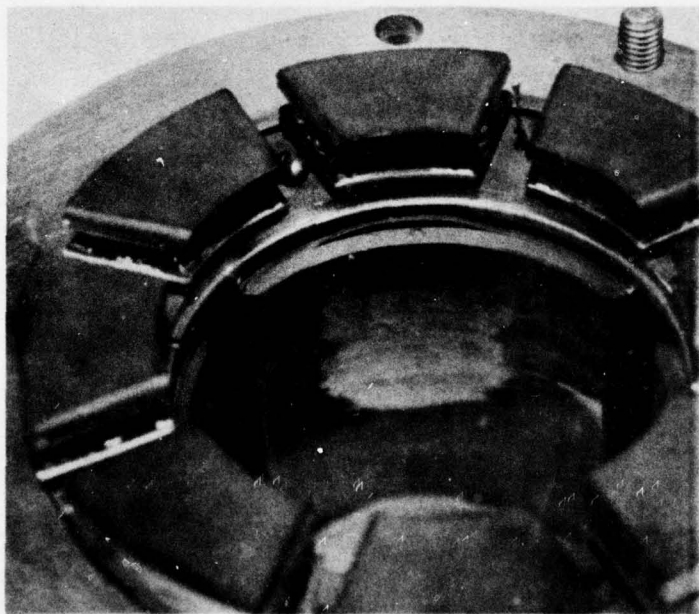


Figure 45. Photograph of Damaged Aft Journal Bearing

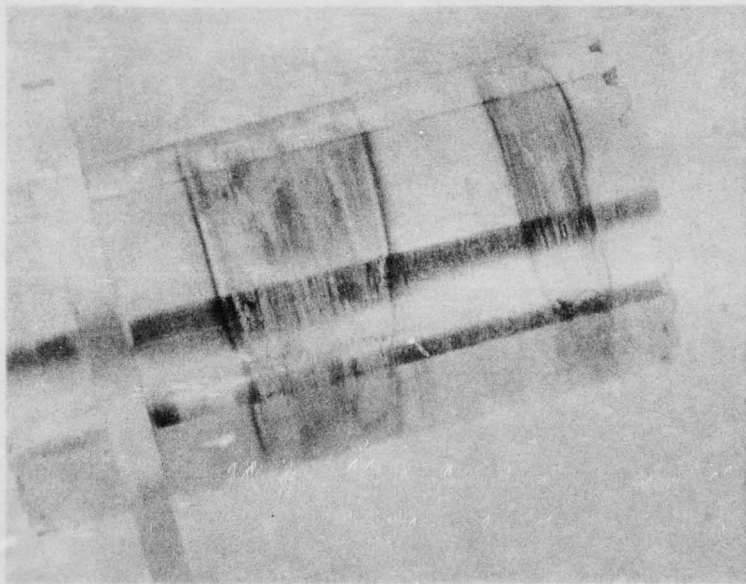


Figure 46. Photograph of Damaged Shaft Section

8. ORIGINAL COMPLIANT MOUNTED JOURNAL BEARING

8.1 CONFIGURATION

The original design concept of the compliant-mounted journal bearing is shown in Figure 47. This configuration is simple in construction and would be the most natural as a first try. The bearing consists of a bearing retainer and three 100° arc pads. Each pad is attached to the retainer by two circumferential strips of elastomer. The pads are made of carbon graphite surfaces backed by steel structures. Photographs of a journal bearing are shown on Figures 48 and 49. The critical dimensions of the journal bearing design are summarized as follows:

	<u>Wheel-end</u>	<u>Starter-end</u>
Configuration	=	3-pad compliantly mounted bearing
Journal Diameter	=	1.8 in. 1.4 in.
Length	=	1.8 in. 1.4 in.
Pad angle	=	100° 100°
Machined-in clearance	=	0.0029 in. 0.0022 in.
Pad surface material	=	Pure Carbon P6452 graphite
Elastomer mounts		
Shape	=	rectangular, 2 pieces
Length	=	1.4 1.2 in.
Width	=	0.55 in. 0.45 in.
Thickness	=	0.125 in. 0.125 in.
Material	=	Neoprene, 45 durometer
Radial Stiffness	=	14,000 lbs/in 8200 lbs/in
Rotational Stiffness	=	1500 - 2500 750 - 1250 in-lbs/rad in-lbs/rad

The major differences between the new and old bearing are as follows:

- The new design has one of the three pads supported by a mechanical spring. This was done to more accurately account for the effects of thermal expansion.
- The pitch inertia of the pads of the redesigned bearing is approximately 50% smaller than that of the original design.
- The compliant-mount stiffness in the pitch direction is an order of magnitude smaller for the redesigned bearings.
- The elastomer thickness in the radial direction, for the redesigned bearings, is 1/2 of the original bearings.

8.2 HIGH-SPEED COMPONENT RIG TESTING (APRIL, 1976)

Using the high speed component rig described in Section 6, testing was conducted using a set of the original design bearings.

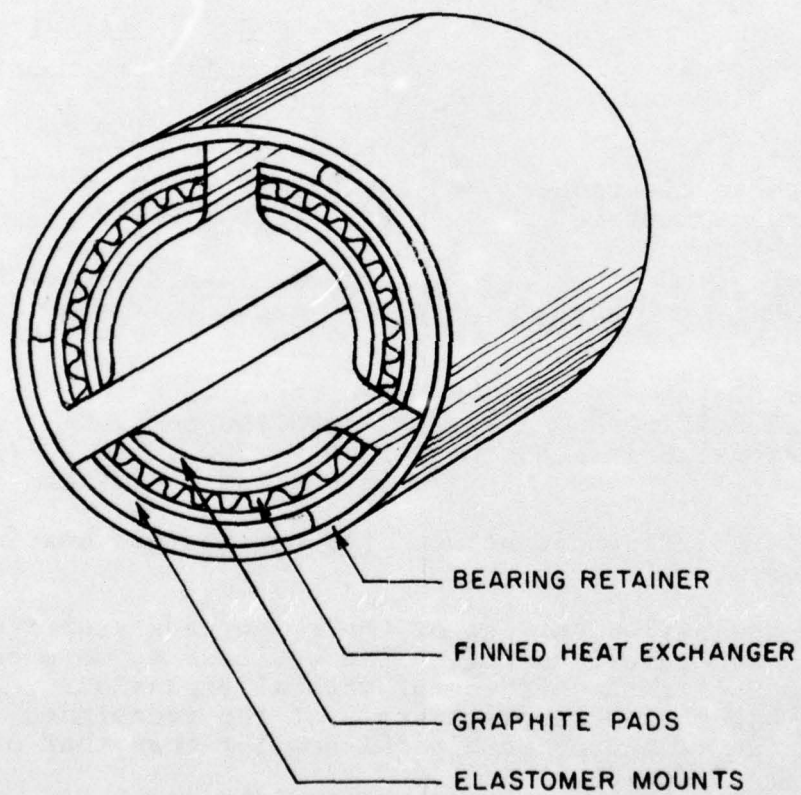


Figure 47. Configuration of Original Journal Bearing

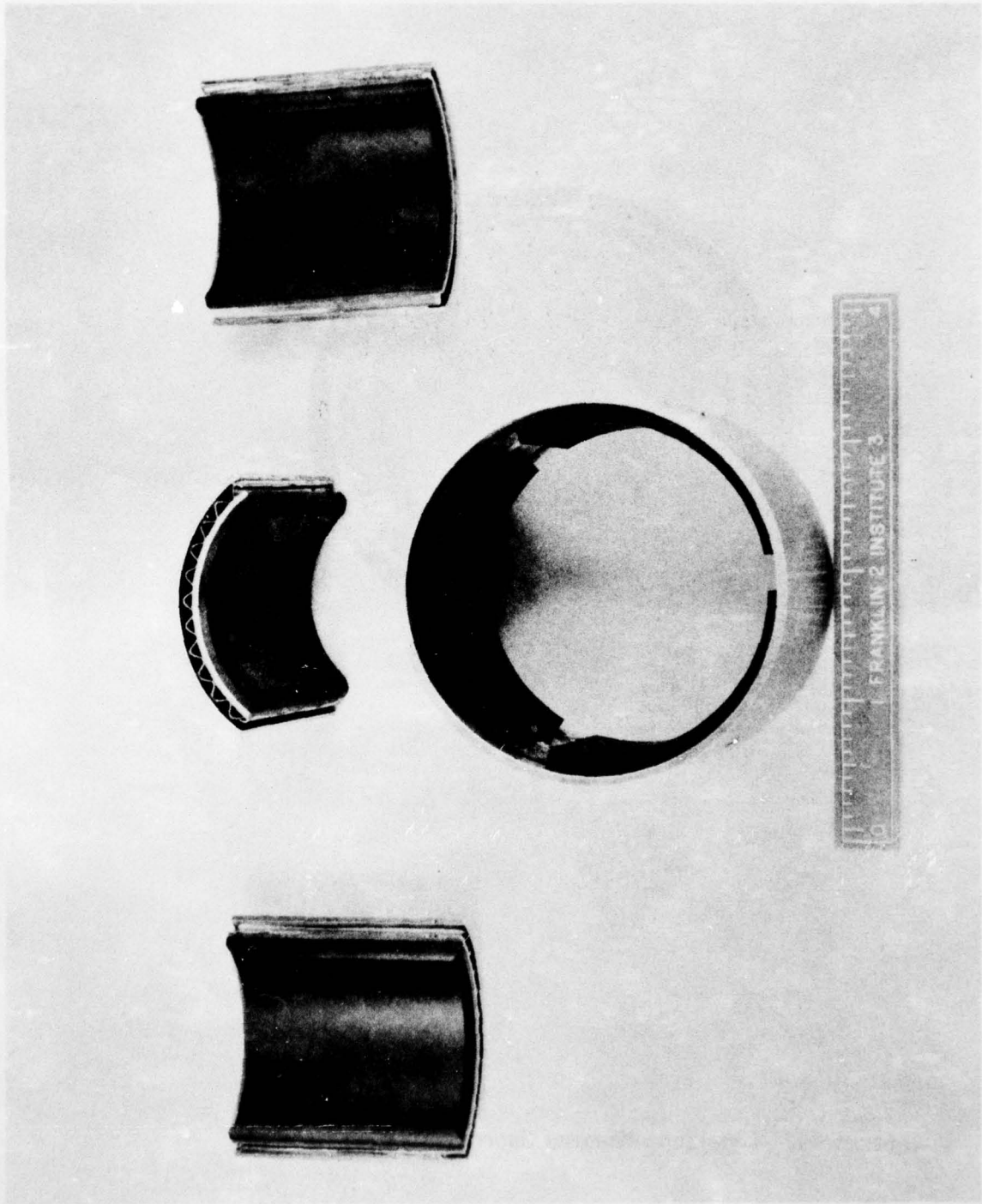


Figure 48. Compliant-Mounted Journal Bearing Components

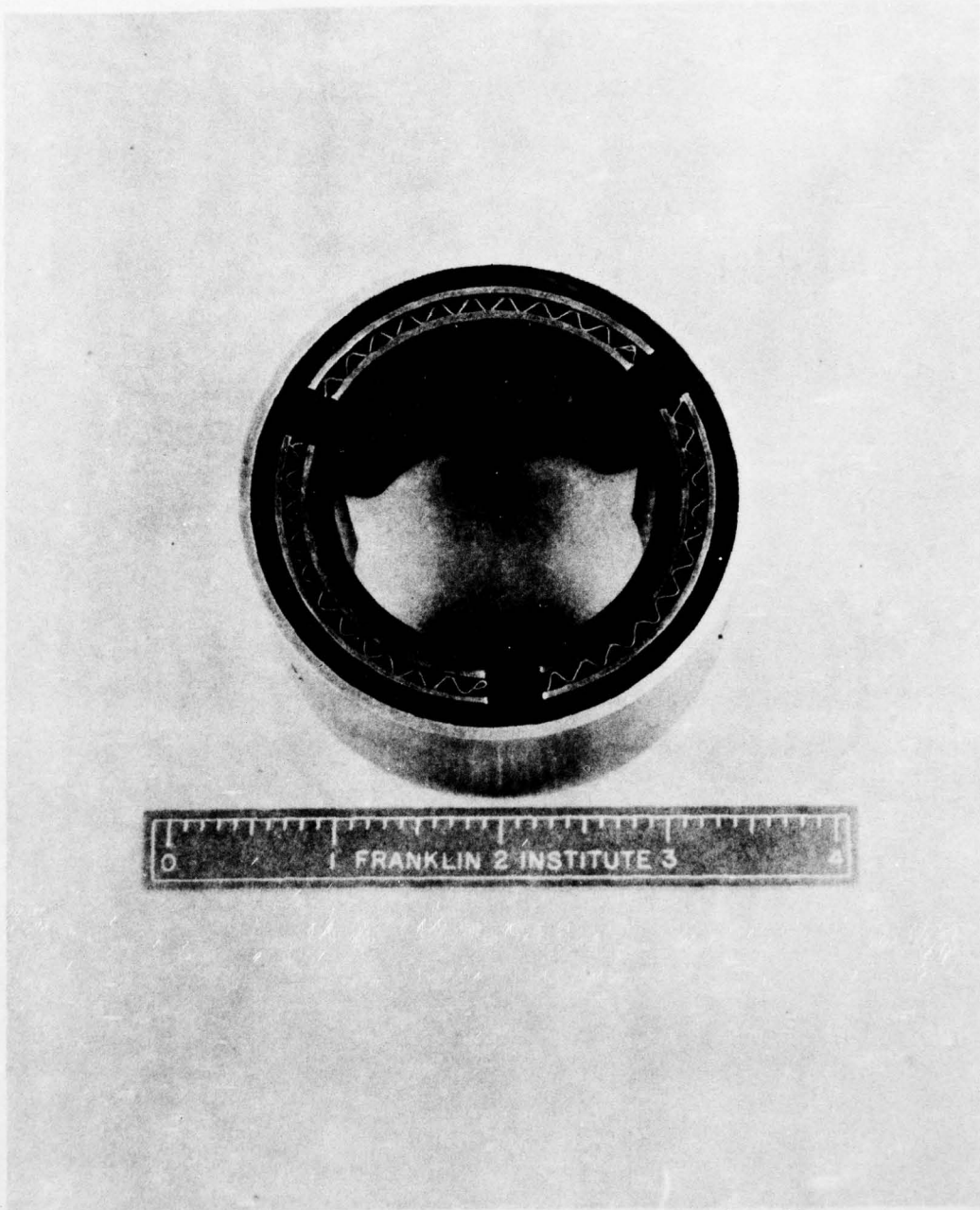


Figure 49. Compliant-Mounted Journal Bearing Assembly

After start-up, the rotational speed was slowly increased to about 64,000 rpm. At that speed the orbits increased dramatically in size. The test was immediately terminated and the bearings were examined. The bearings had slightly wiped the rotor but no serious damage was evident. Figure 50 shows the orbit traces before and after the increase in amplitude. The increase in amplitude was due to bearing whirl instability. It is self-excited and the whirl orbit frequencies are below the operating speed. Figures 51 and 52 are frequency traces for the probes located at both the inboard and outboard side of the rotor respectively. Before whirl (60,000 rpm) there is very little evidence of a subsynchronous frequency at 13,500 cpm. The predominant frequency is synchronous. After whirl (64,000 rpm) the predominant frequency is subsynchronous (13,500 cpm). Figure 53 shows the horizontal probes for the low frequency at the same speeds. The amplitude associated with the 13,500 cpm increased dramatically at the onset of whirl.

This test was repeated several times with similar results. The onset of whirl occurred between 50,000 rpm to 65,000 rpm.

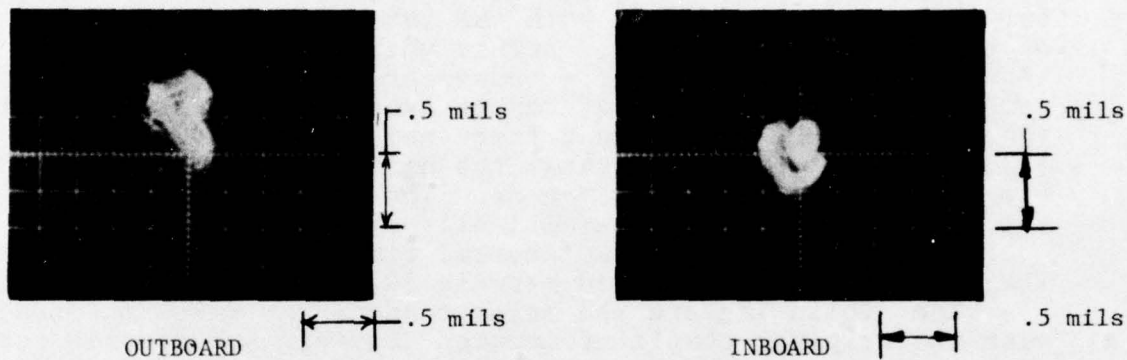
The following are the major reasons why whirl occurred with the original compliant-mounted bearings and did not occur with the spring mounted design:

- The pad compliant mount (rubber) stiffness in the pitch direction was 10 times stiffer with the original design as compared with the spring design. This caused the bearing to act more like a rigid bearing which is less stable than a bearing with flexibility in the pitch direction. This was the main reason for the instability.
- The pitch inertia is approximately twice as high with the original design as compared with the spring design. The higher the pitch inertia the less stable the bearing.

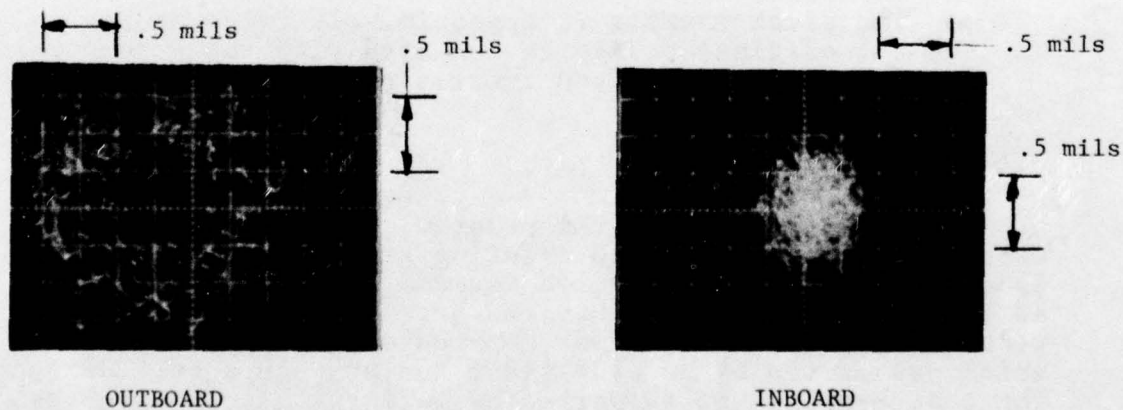
8.3 SLOW-SPEED COMPONENT TESTS

In an early part of the program, preliminary bearing tests were conducted on an existing single bearing, slow-speed test rig (Figure 54) to determine characteristics such as load capacity, power loss and break-away torque. The test journal (or runner) was mounted on a precision spindle which was driven by an electric motor through a belt drive. The test bearing was supported by an externally pressurized thrust bearing. Thus, the support was practically frictionless so that the recorded torque represented bearing drag. Loading of the journal bearing was accomplished by use of a spring scale connected to the side of the bearing (Figure 54). Thrust load was applied by pressing the bearing against the runner (Figure 55). The magnitude of the thrust load was determined from calibrations of load vs. displacement previously made of the externally pressurized support bearing. The displacement of the externally pressurized bearings was measured during testing.

FRANKLIN INSTITUTE RESEARCH LABORATORIES
COMPLIANT MOUNTED GAS BEARING COMPONENT TESTING
STIFF BEARINGS
ORBIT ANALYSIS



60,000 RPM
(Before whirl)

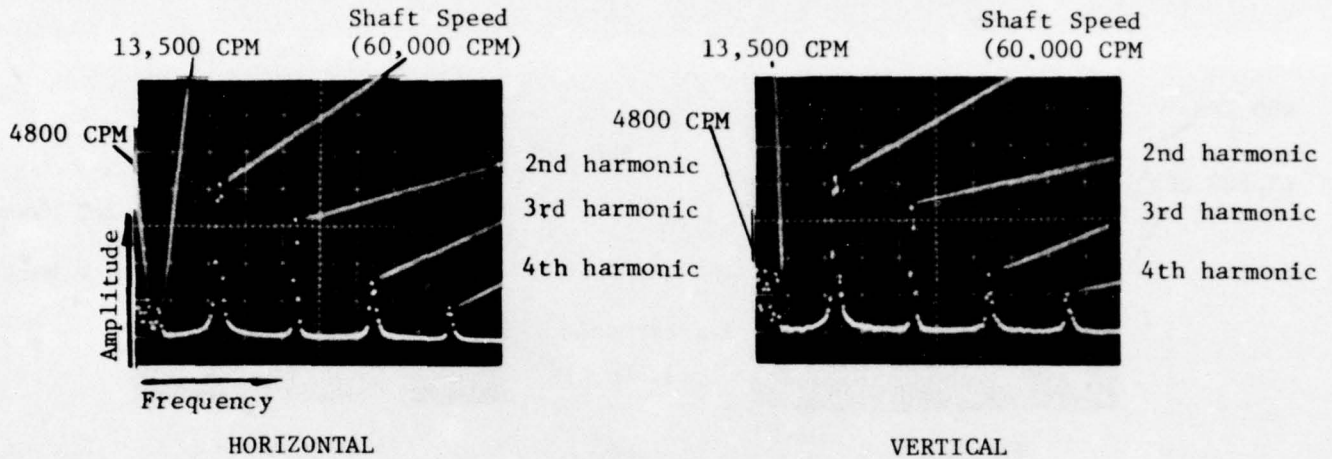


64,000 RPM
(Whirl)

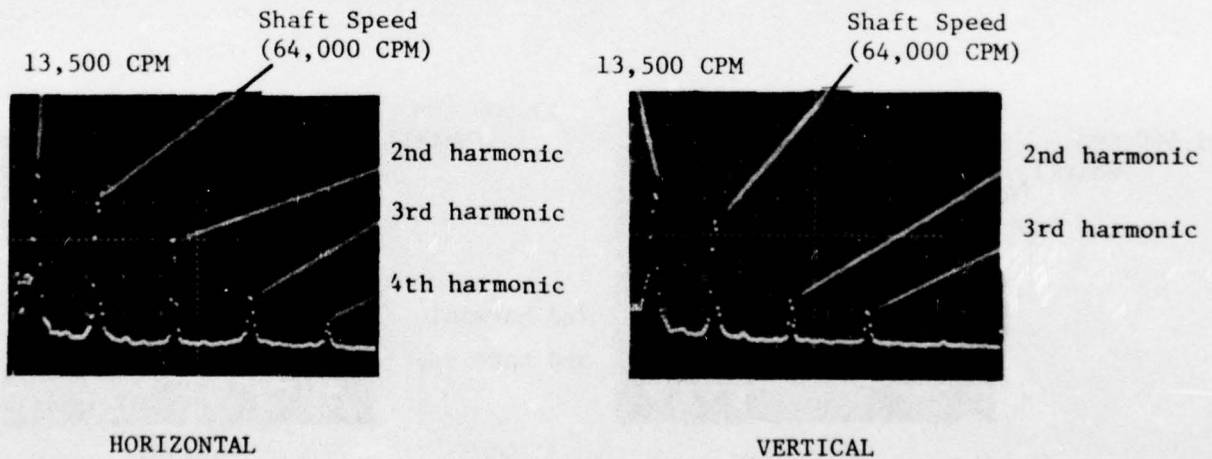
Figure 50. Orbit Traces - Original Bearing, High-Speed Component Test Rig

FRANKLIN INSTITUTE RESEARCH LABORATORIES
 COMPLIANT MOUNTED GAS BEARING COMPONENT TESTING
 FREQUENCY SPECTRUM ANALYSIS
 STIFF BEARINGS

INBOARD END



60,000 RPM
 (Before Whirl)



64,000 RPM
 (Whirl)

Figure 51. Frequency Spectrum, Original Bearings,
 Inboard End

FRANKLIN INSTITUTE RESEARCH LABORATORIES
 COMPLIANT MOUNTED GAS BEARING COMPONENT TESTING
 FREQUENCY SPECTRUM ANALYSIS
 STIFF BEARINGS

OUTBOARD END

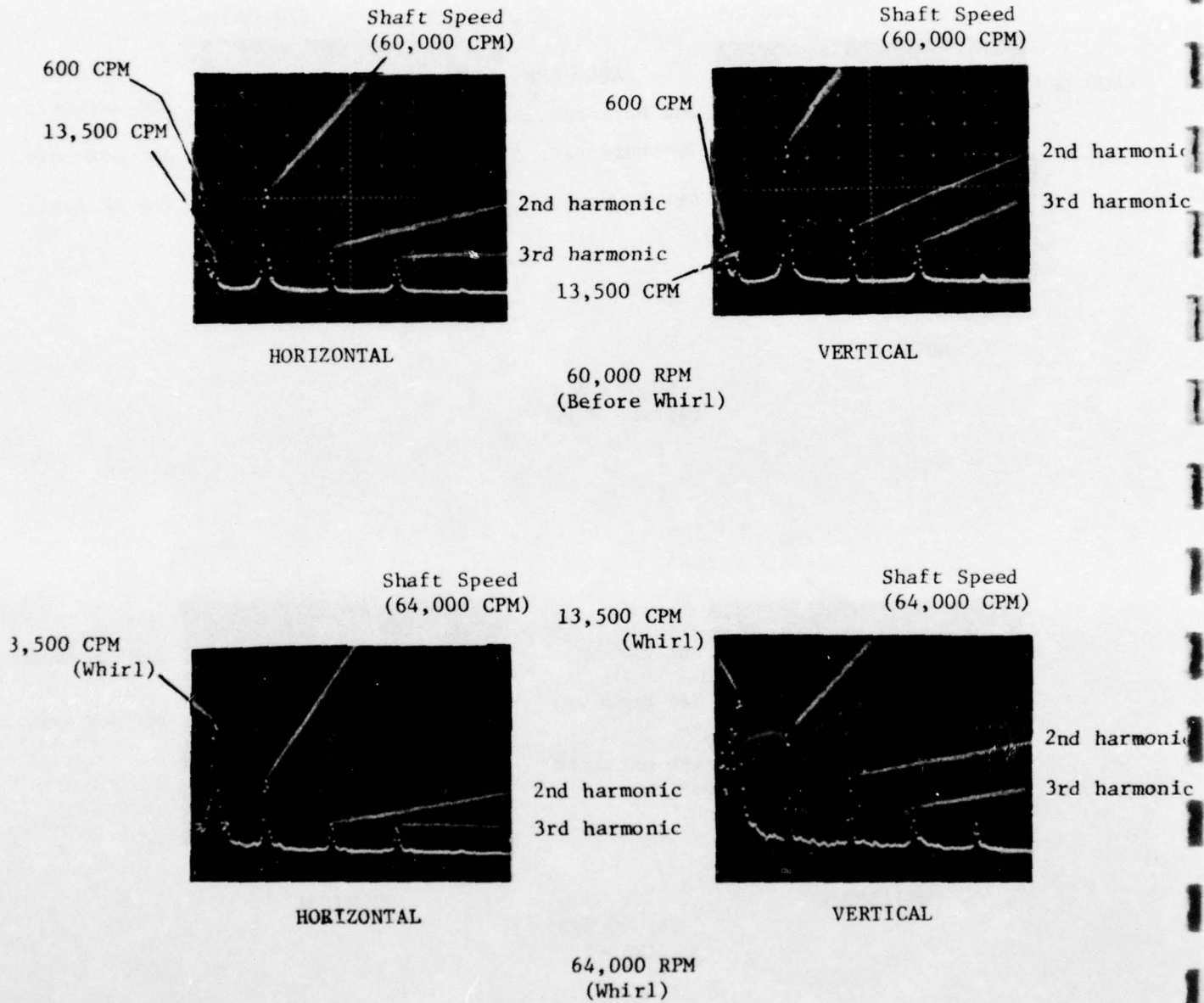


Figure 52. Frequency Spectrum, Original Bearings, Outboard End

FRANKLIN INSTITUTE RESEARCH LABORATORIES
COMPLIANT MOUNTED GAS BEARING COMPONENT TESTING
FREQUENCY SPECTRUM ANALYSIS
(LOW FREQUENCY RANGE)
STIFF BEARINGS
HORIZONTAL

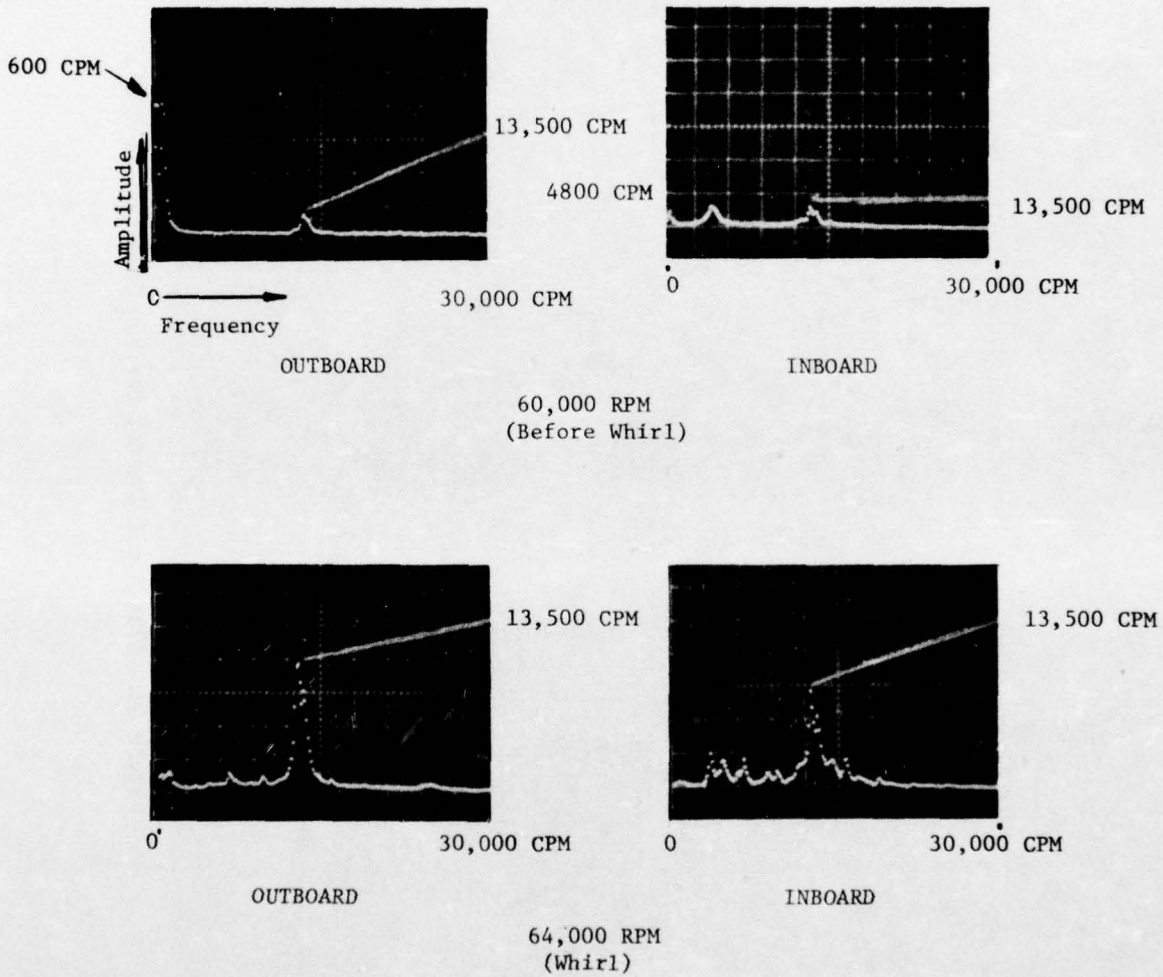


Figure 53. Frequency Spectrum, Original Bearings, Horizontal Probes

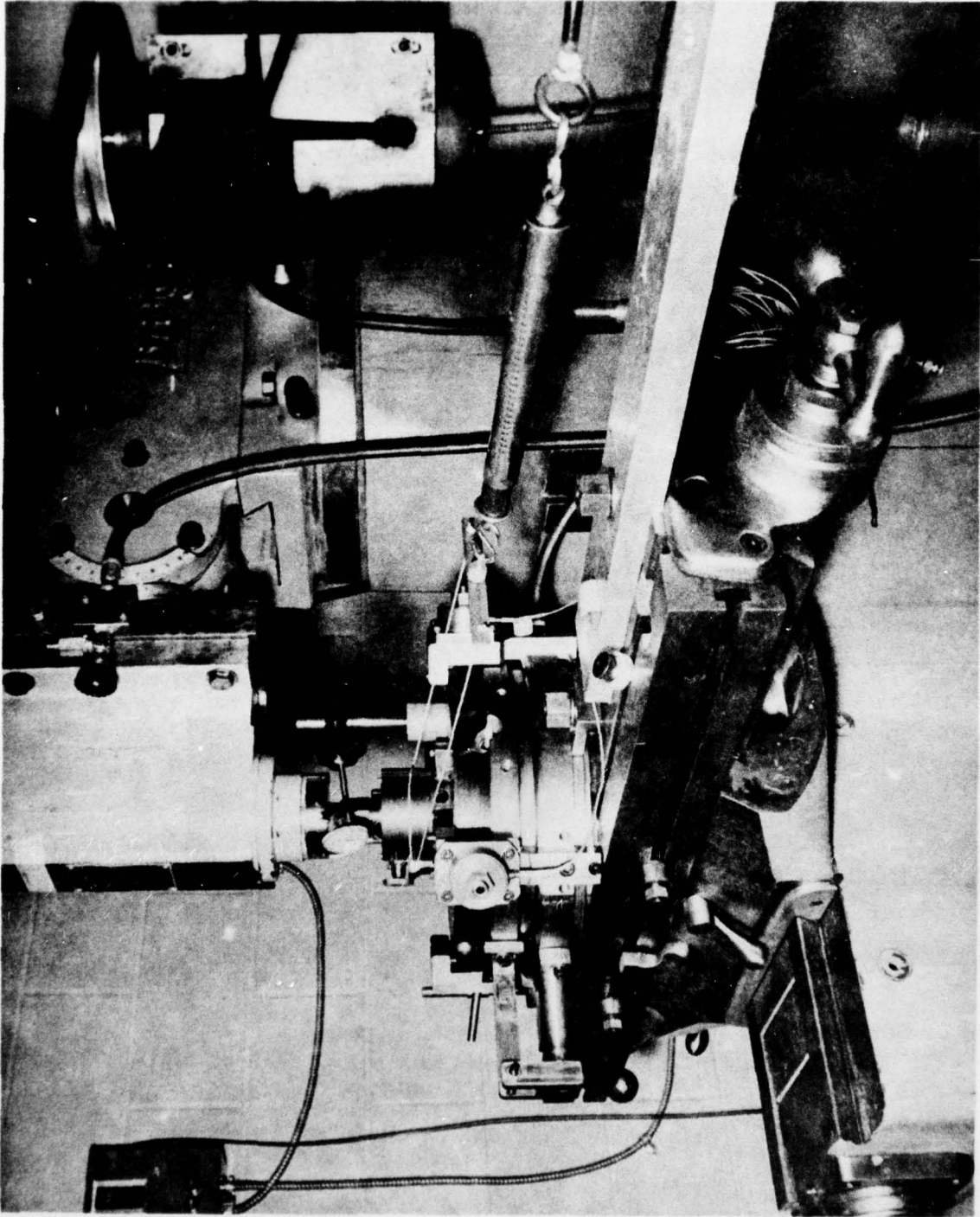


Figure 54. Slow-Speed Journal Bearing Component Test Rig

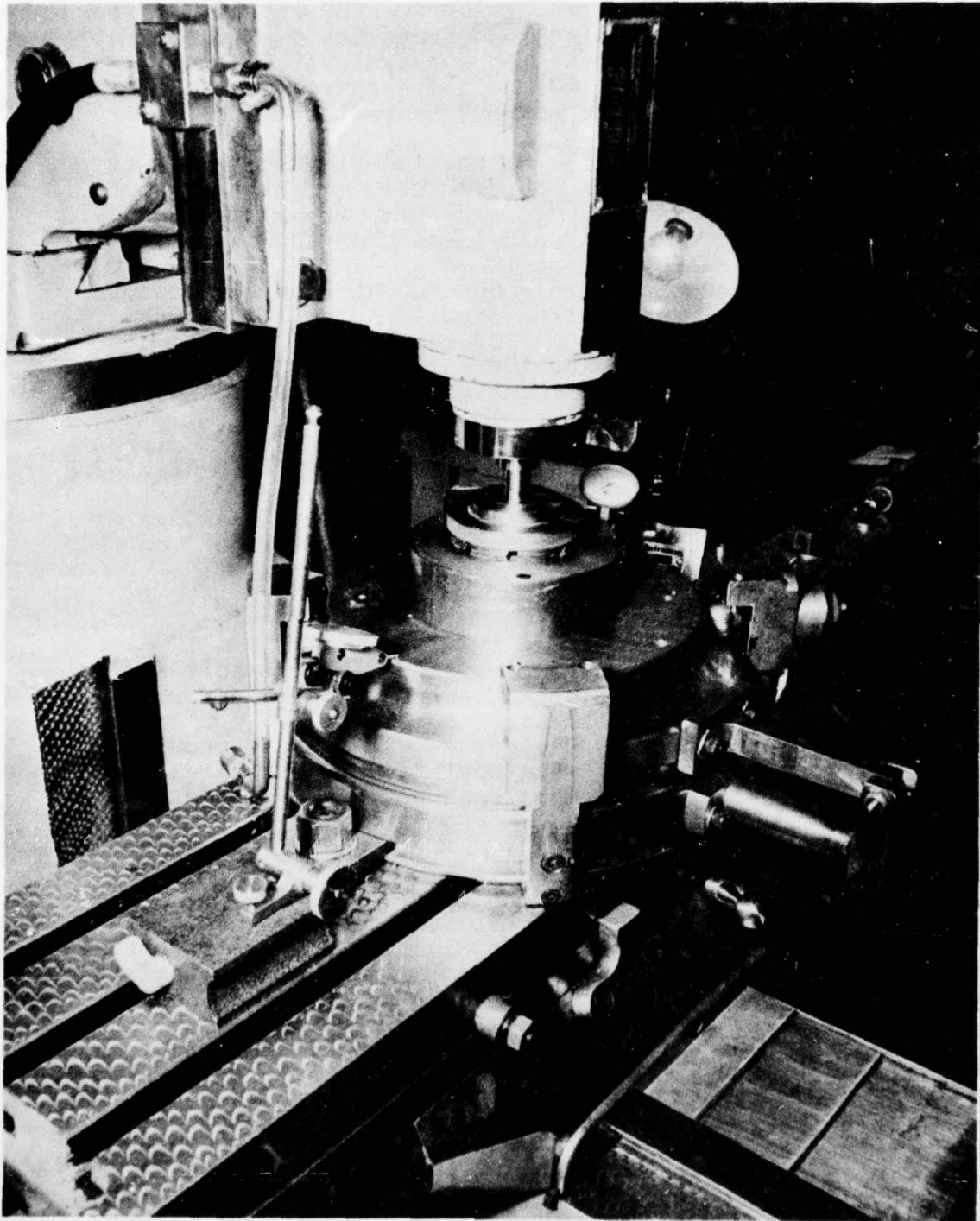


Figure 55. Slow-Speed Thrust Bearing Component Test Rig

Journal bearings were tested both at room temperature and at an elevated temperature of 200°F. The rotational speed was 13,000 rpm and the applied load range was 5 ~ 10 lbs. In all cases, the bearing operated successfully with no measurable torque and there was no temperature rise in the bearing after one hour of continuous operation. The film thickness was estimated to be 100 ~ 150 μ -in. A total of 40 start-stop runs were completed on each bearing under a unit load of 5 psi. Lift-off was achieved very quickly at about 400 ~ 700 rpm. The break-away torque was very small and could not be easily measured. Teardown inspection showed no bearing distress and negligible wear.

Thrust bearing tests were conducted at room temperature under applied loads ranging from 5 to 20 lb. The lift-off speed was estimated to be 500 ~ 700 rpm. At 13,000 rpm, the film thickness was found to be 100 ~ 150 μ -in. In addition, 40 start-stop runs with unit loads of 7 psi were accomplished and the bearing wear was negligible.

8.4 SIMULATOR TESTING OF ORIGINAL COMPLIANT-MOUNTED BEARINGS

The simulator used for testing the original bearings was essentially the same rig as described in Section 7 of this report. Testing was conducted at Solar's facility.

8.4.1 Summary of Test Results

Initial simulator tests consisted of three builds and three test runs. Each run lasted several minutes and was terminated due to bearing failure. The first two failures were in the thrust bearings while the last failure occurred in the aft journal bearing. Rig operation observations and tear down inspection summary for each build are presented as follows:

Build No. 1

Diametral clearances at the starter end and wheel end journal bearings were set to be 0.005 and 0.004 in. respectively.

A total of four starts were accomplished with satisfactory running but with slightly increasing drive torque to obtain rotor break-away. Start up of the rig was accomplished by increasing air flow to the drive turbine until break-away was obtained. Rotation at break-away was first slow and then acceleration was rapid to a speed of approximately 20,000 rpm. During this start-up procedure the increasing flow to the drive turbine resulted also in an increasing thrust on the turbine and the thrust bearing which accounted for the initial slow rotation without the development of the hydrodynamic air film. Thrust load on the bearing was directly proportional to the turbine nozzle inlet pressure with the thrust load in pounds equal to the nozzle pressure in psi. Starting break-away torque required 25-30 psi by the fourth start-up.

On the fourth run, the rotor speed was increased to 59,000 rpm when thrust bearing failure occurred. The sequence of the failure events cannot be exactly determined from the test observations. In particular, the measurements of the bearing case temperature or the air temperature around the bearing gave no indication of the impending failure. Thus, in later test runs, additional thermocouples were mounted on the finned structures of the thrust bearings.

The test rig was disassembled and inspected. The only damage to the rotor components was a decrease in hardness of the thrust runner from RC 34/38 to RC 28. The damage to the thrust bearing was severe with carbon pads separated from their steel backings. Figures 56 and 57 illustrate the condition of these components.

Build No. 2

Following the repair of the rig, the rotor was assembled with 0.005 and 0.004 in diametrical clearances in the journal bearings and 0.0035 in axial clearance in the thrust bearing. The start-up procedure was modified to reduce the thrust load during break-away by energizing the thrust piston. The unit was quickly brought to 25,000 rpm with minimum thrust load. When 32,000 rpm was reached, a rapid rise in the air temperature near the thrust bearing support prompted termination of the run and teardown for inspection. Another failure occurred with evidence of overheating and separation of the carbon pads similar to the failure of the first run.

Build No. 3

All rig and bearing dimensions were carefully reviewed during rig repair and assembly for the third test run. Various modifications and adjustments were made to improve the bearing running condition. These modifications included a reduction in the diametral clearance of the journal bearings to .0015 and .002 in. and a removal of material from the face of the thrust pads at their outside diameters to obtain a flatness within .0001 inches. The thrust bearing support structure were improved to maintain thrust bearing flatness on final assembly. It was determined that the primary cause of thrust bearing failure was due to interference between the thrust bearing support structure and the O.D. of the bearing causing coning of the thrust bearing as it was attached to its support structure. This problem was eliminated by undercutting the corner of the support so that the bearing could be mounted flat against it and not contact the corner radius.

Rotor run up was accomplished with minimum thrust bearing load, and rotor operation was characterized by extreme smoothness of operation. A stable orbit within .001 inches was obtained with some fractional whirl component in the speed range of from

AD-A031 950

FRANKLIN INST RESEARCH LABS PHILADELPHIA PA

F/G 13/9

DEVELOPMENT OF COMPLIANT-MOUNTED GAS-BEARINGS FOR A SMALL HIGH---ETC(U)

SEP 76 W SHAPIRO, R COLSHER

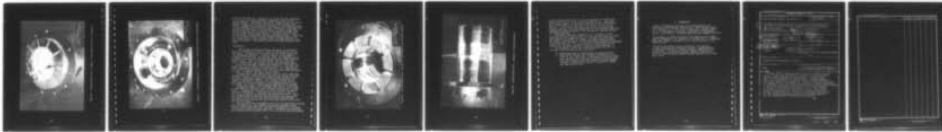
DAAK02-72-C-0571

UNCLASSIFIED

FIRL-I-C3425

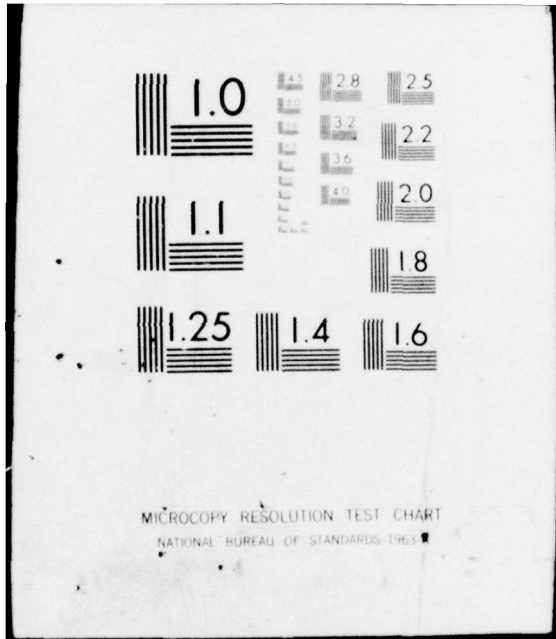
NL

2 OF 2
AD
A031950



END

DATE
FILMED
1-77



MICROCOPY RESOLUTION TEST CHART
NATIONAL BUREAU OF STANDARDS-1963-A

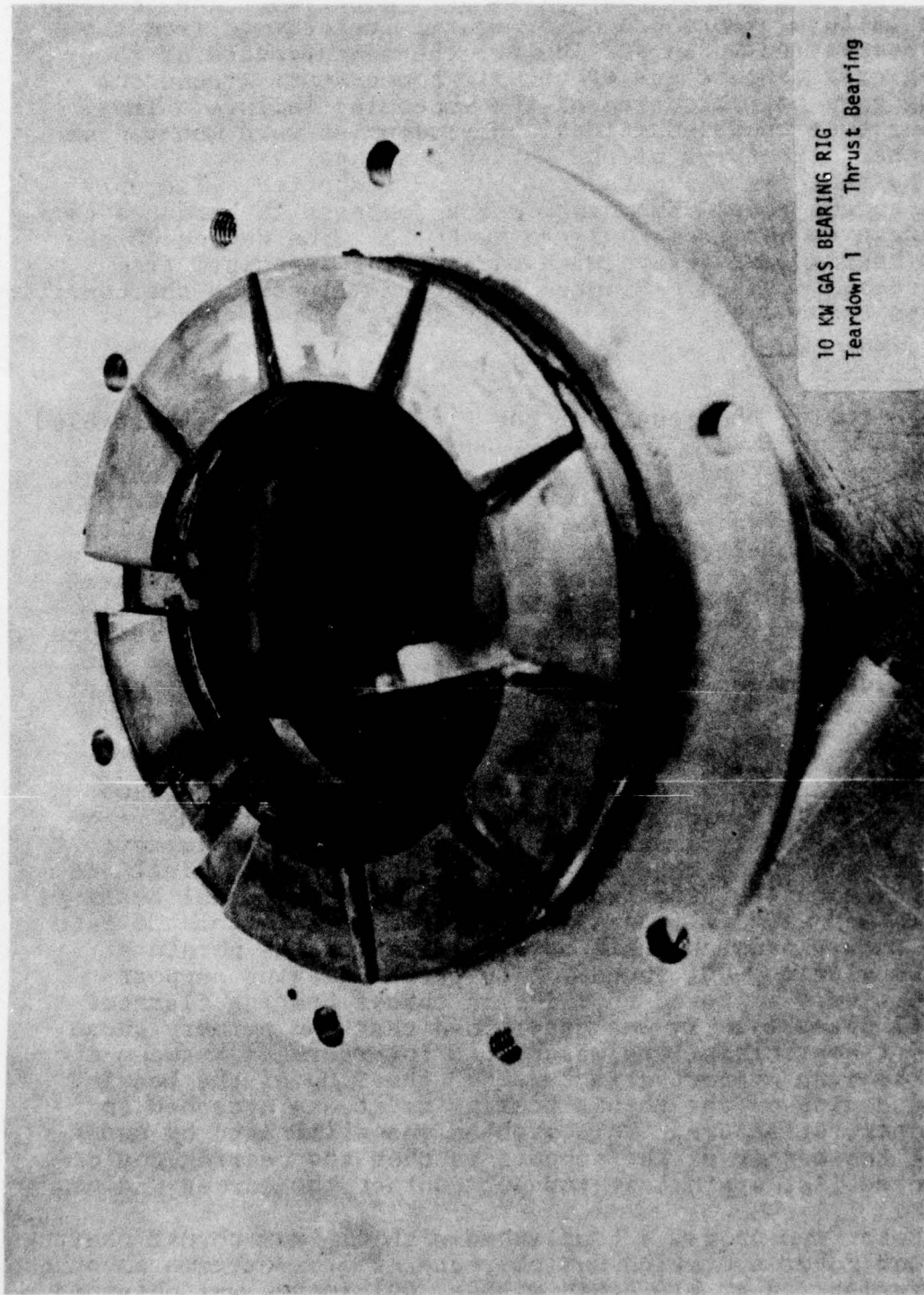
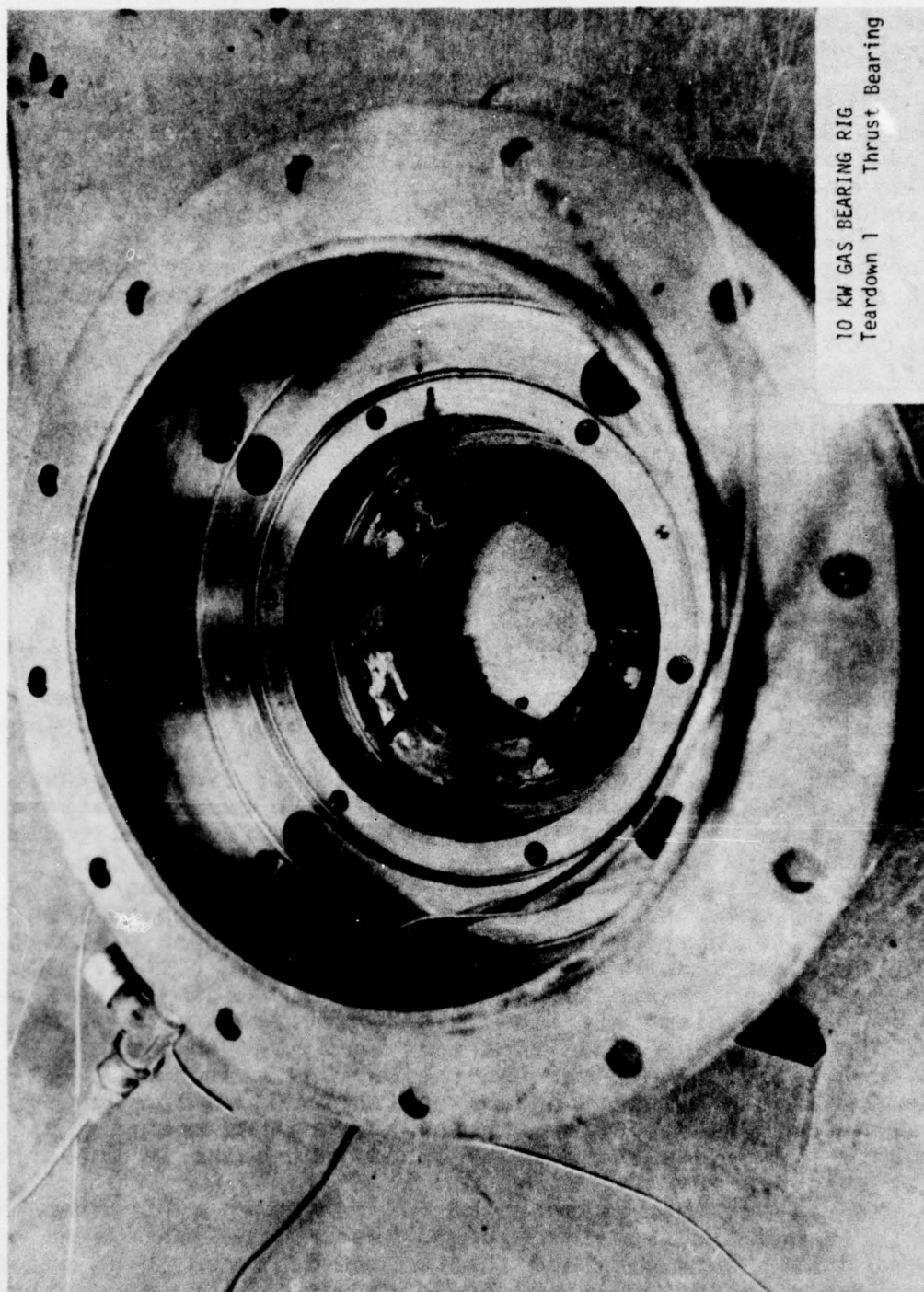


Figure 56. 10 KW Gas Bearing Rig - Teardown 1, Thrust Bearing Failure, Aft Bearing



10 KW GAS BEARING RIG
Teardown 1 Thrust Bearing

Figure 57. 10 KW Gas Bearing Rig - Teardown 1, Thrust Bearing Failure, Forward Bearing

30,000 to 50,000 rpm. Operation at 65,000 rpm was terminated by a rapidly increasing ambient temperature near the aft thrust bearing. Tear down inspection revealed that the thrust bearing showed no distress but the aft radial bearing had failed. Damage was principally confined to the central section of this bearing with sufficient heat generated to dislodge the carbon pads from their steel backings, to spall carbon from the pad surfaces and to overheat and oxidize the shaft very locally under the bearing failure. Figures 58 and 59 show the condition of the shaft and bearing respectively. Inspection of the forward journal bearing showed incipient failure of the carbon pads at their centers (both circumferentially and shaft axis-wise). The journal under these pads showed no distress.

Build No. 4

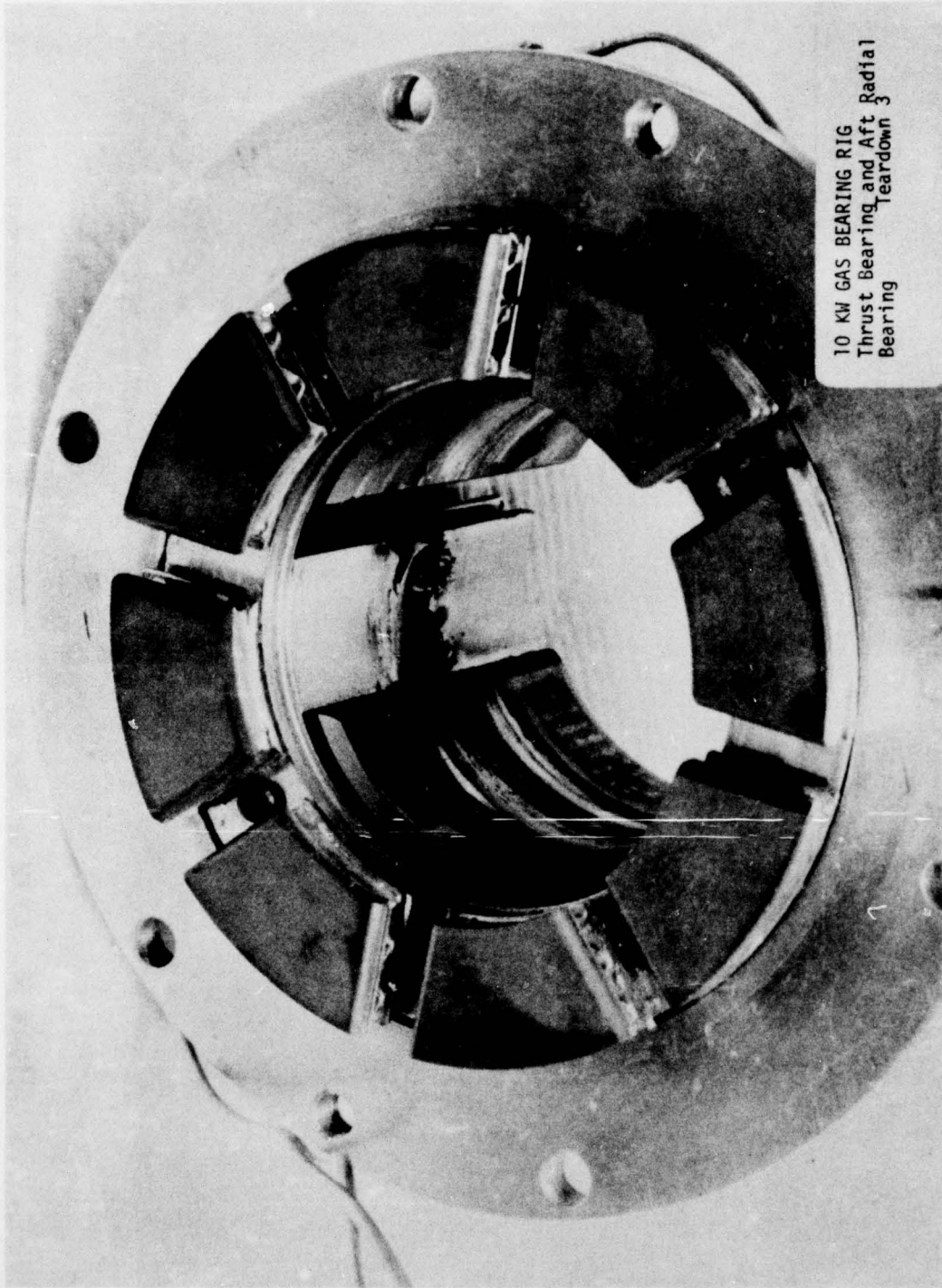
The journal bearing diametral clearance on the wheel end was increased to 0.003 in. and the rig installed in the test cell. The method of rig start-up was investigated and the procedures improved. A twenty minute run was made at a speed of 40,000 rpm. During this time, the temperature as measured in the air cavity nearest the active thrust bearing slowly rised. When it attained 200°F, the unit was shut down. During this test, shaft orbits were extremely small.

The thrust bearing assembly was modified to increase the axial play in the thrust bearing to 0.0135 in. The unit was then reassembled and run up to 60,000 rpm. The temperature in the air cavity adjacent to the active thrust pads continued to rise. At 200°F, the unit was shut down.

During both of the above tests, exit air flow, measured by physical feel, from the wheel end bearing casing discharge was low. Tear-down inspection revealed that the wheel end journal bearings had rubbed. The rub was located at the center of the pads, indicative of crowning of the journal. The cause of the rub appeared to be overheating due to lack of coolant air supply. Shaft damage appeared to be minimal.

Subsequent inspection indicated that the air inlet flow to the wheel end bearing cavity had been blocked by a thermo-couple. Insufficient air flow to this cavity was the prime cause of overheating. Modifications were made to improve the flow of cooling air through the bearing structure. This was accomplished by removing the obstruction and increasing the area for flow out of the thrust bearing pad mounting structure and by sealing off the other vent holes in the drive end of the casing.

The rig was then reassembled and run in an exploratory manner with increased air flow through the bearing cooling system. Several starts were made and instruments adjusted in an effort to correct a defective speed read-out. The shaft was operating very smoothly with minimum orbits at the radial bearing locations.



10 KW GAS BEARING RIG
Thrust Bearing and Aft Radial
Bearing
Teardown 3

Figure 59. 10 KW Gas Bearing Rig - Teardown 3, Thrust Bearing and Aft Radial Bearing

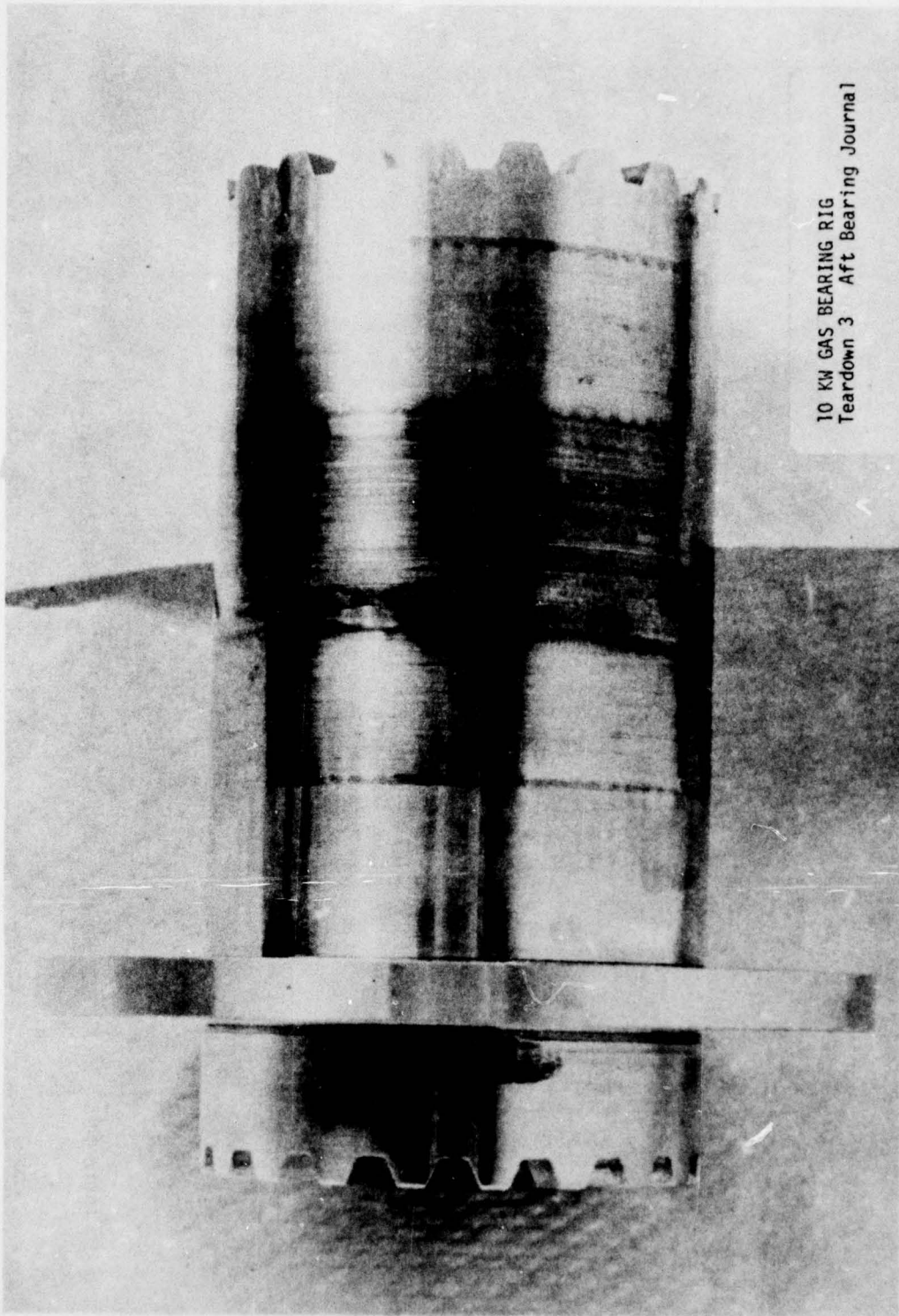


Figure 58. 10 KW Gas Bearing Rig - Teardown 3, Aft Bearing Journal

A start-up was made and the rotor accelerated to 60,000 rpm. Large orbits and a bearing rub were experienced. Rig tear-down showed damage to the radial bearing at the turbine drive end of the rotor with peeling of the chrome on the journal surface. It peeled in the same area as the rub during the initial testing. The rub during the initial testing could have weakened the chrome bonding, thus causing the peeling during the latest testing.

Subsequent detailed examination of the thrust collar, wheel-end journal bearing shaft section revealed that the shaft was cracked in a number of places. Attempts to grind down the shaft to eliminate the cracks were unsuccessful because the cracks were too deep. It was therefore necessary to purchase a new shaft section. It was decided to concentrate further efforts on the spring mounted, compliant-pivot bearings.

In retrospect, there are several possibilities for the failures that occurred during this build:

- 1) Overheating due to insufficient cooling-air flow
- 2) Rotor whirl because the original bearings were too stiff in the pitch mode. Subsequent testing of these type bearings with the FIRL high-speed rig indicated that the original compliant-mounted bearings showed evidence of whirling in speeds in excess of 60,000 rpm (See Section 8.2).

9. REFERENCES

1. "Design, Fabrication and Test of an Experimental Air-Lubricated, Hydrodynamic Bearing Rig", FIRL Interim Report, by W. Shapiro, T. Y. Chu and F. Kramberger, January, 1974 for U.S. Army Mobility Equipment Research and Development Center, Fort Belvoir, Virginia under Contract DAAK02-72-6-0571.
2. "Development of Compliant-Mounted Gas Bearings for a High-Speed Turbomachine", W. Shapiro, R. Colsher and F. Kramberger, SAE Paper 715071, published in 1975 SAE Transactions, pp. 2989 to 3003.
3. "Analysis and Design of Gas-Lubricated, Tilting-Pad Journal Bearings for Miniature Cryogenic Turbomachinery", W. Shapiro, R. Colsher, Technical Report AFFDL-TR-70-99, August 1970, for Air Force Flight Dynamics Laboratory, U.S. Air Force Systems Command, Wright-Patterson Air Force Base, Ohio.

DOCUMENT CONTROL DATA - R & D

Security Classification of title, body of abstract and indexing annotation must be entered when the overall report is classified

1. ORIGINATING ACTIVITY (Corporate author) Franklin Institute Research Laboratories ✓		2a. REPORT SECURITY CLASSIFICATION Unclassified	
		2b. GROUP	
3. REPORT TITLE 6 Development of Compliant-Mounted Gas-Bearings for a Small High-Speed, 10KW Turboalternator			
4. DESCRIPTIVE NOTES (Type of report and inclusive dates) 9 Final rept.			
5. AUTHOR(S) (First name, middle initial, last name) 10 Wilbur/Shapiro Richard/Colsher			
6. REPORT DATE September, 1976		7a. TOTAL NO. OF PAGES 11 Sep 76	7b. NO. OF REFS 12 102 p.
8. CONTRACT OR GRANT NO. 15 DAAK02-72-C-0571		9a. ORIGINATOR'S REPORT NUMBER(S) 14 FIRL-I-C3425 ✓	
9. PROJECT NO. I-C3425		9b. OTHER REPORT NO(S) (Any other numbers that may be assigned this report) None	
10. DISTRIBUTION STATEMENT Distribution of this report is unlimited.			
11. SUPPLEMENTARY NOTES None		12. SPONSORING MILITARY ACTIVITY U.S. Army Mobility Equipment Research and Development Command, Ft. Belvoir, VA	
13. ABSTRACT Several types of compliant-mounted bearings were developed for application to a Solar 10KW Turboalternator Simulator. The most successful journal bearing incorporated one spring-mounted, pad and two fixed pads, all of which pivoted on a compliant-mount. Component testing of these journal bearings were successfully completed to 76,000 RPM which was the limiting speed of the component rig. Simulator testing was accomplished to 65,000 RPM at which time a journal bearing failure occurred. There is evidence to support the conclusion that the failure was not bearing originated but was due to other factors concerned with the rig. After initial installation difficulties were resolved, the compliant mounted thrust bearings performed very well. The results of the program indicated that the final bearing configurations demonstrated encouraging potential for their implementation to high-speed turbomachinery.			

142 925 mt

